

From the Department of Internal Medicine II of the Department of Medicine of
the Justus-Liebig-University Gießen

Director: Prof. Dr. Werner Seeger

The role of viral and host factors in alveolar fluid clearance during Influenza A virus- induced lung injury

Inaugural Dissertation

submitted to the Faculty of Medicine
in partial fulfillment of the requirements for the Doctor in Philosophy (PhD)

by

Christin Becker

born in Attendorn, Germany

Gießen, 2015

1. Supervisor and Committee Member: PD Dr. med. Susanne Herold, PhD
 2. Supervisor and Committee Member: Prof. Dr. rer. nat. Albrecht Bindereif
- Committee Member (Chair):
- Committee Member:

Date of Doctoral Defense:

Table Of Contents

1.	INTRODUCTION	6
1.1.	Acute Respiratory Distress Syndrome	6
1.2.	Microanatomy And Physiology Of The Lung	7
1.2.1.	The Alveolar Mononuclear Phagocyte System	8
1.2.2.	Epithelium	10
1.3.	Sodium-Potassium Adenosine Triphosphatase (Na, K-ATPase)	12
1.3.1.	Structure	12
1.3.2.	Function	13
1.3.3.	Regulation	14
1.4.	Influenza A Virus	16
1.4.1.	Taxonomy	16
1.4.2.	Structure	16
1.4.3.	Replication	17
1.4.4.	Epidemiology	19
1.5.	Interactions At The Host-Virus Interface	20
1.5.1.	Interferon Signaling	21
1.5.2.	TNF-Related Apoptosis Inducing Ligand (TRAIL)	22
2.	AIM OF THIS WORK	24
3.	METHODS	25
3.1.	Mouse Strains	25
3.2.	Human Material	25
3.3.	Cell Culture	25
3.4.	Primary Murine Alveolar Epithelial Cells	26
3.5.	Primary Human Alveolar Epithelial Cells	27
3.6.	Primary Alveolar and Bone Marrow-Derived Macrophages	27
3.7.	Virus Strains	28
3.8.	Influenza A Virus Propagation And Titration	28

3.9. In Vivo Experiments And Preparation Of Animal Materials	29
3.9.1. Intratracheal Intubation	29
3.9.1. Adoptive Transfer	30
3.9.2. Alveolar Fluid Clearance	30
3.9.3. Blood Gas Analysis	31
3.9.4. Preparation Of Lung Homogenate For Flow Cytometry	31
3.10. In Vitro Experiments	31
3.10.1. Influenza A Infection Of Cultured Cells	31
3.10.2. Adenoviral Transduction Of A549 Cells	31
3.10.3. Transfection Of A549 Cells	32
3.10.4. Vectorial Water Transport	32
3.11. Analysis Of Gene Expression	33
3.11.1. RNA Isolation	33
3.11.2. cDNA Synthesis	33
3.11.3. Quantitative Real-Time Polymerase Chain Reaction (qRT-PCR)	33
3.12. Analysis Of Protein Expression	34
3.12.1. SDS-PAGE And Western Blotting	34
3.12.2. Surface Biotinylation	35
3.12.3. Co-Immunoprecipitation	36
3.12.4. Enzyme Linked Immunosorbent Assay (ELISA)	36
3.12.5. Cytometric Bead Array (CBA)	37
3.12.6. Flow Cytometry	37
3.13. Microscopy	38
3.13.1. Fixation And Preparation Of Lung Tissue For Histology	38
3.13.2. Fixation Of Cell Cultures For Immunofluorescence Microscopy	38
3.13.3. Fixation Of Lung Tissue For Immunofluorescence Microscopy	38
3.13.4. Antibody Staining and Fluorescent Laser-Scanning Microscopy	39
3.13.5. Live Cell Imaging	39
3.14. Statistics	39
4. RESULTS	39
4.1. Impaired alveolar fluid clearance after IAV infection is associated with decreased expression of Na₊/K⁺-ATPase α1 subunit on alveolar epithelial cells	40
4.2. A paracrine epithelial-macrophage crosstalk via epithelial type I IFN and IFN-dependent macrophage TRAIL reduces NKAα1 surface expression on AEC	44

4.3.	IAV-induced reduction of NKA α 1 in AEC is mediated by the kinases CaMKK β and AMPK	49
4.4.	IAV-induced paracrine reduction of plasma membrane NKA α 1 protein and AFC capacity require the presence of IFNAR and TRAIL and macrophage recruitment <i>in vivo</i> .	52
4.5.	Na,K-ATPase activity is necessary for efficient IAV replication	53
4.6.	Na,K-ATPase is relocalized to the apical cell membrane in IAV-infected epithelial cells	54
4.7.	Na,K-ATPase apical relocalization is caused by interaction with IAV matrix protein 2	57
5.	DISCUSSION	60
6.	SUMMARY	65
7.	ZUSAMMENFASSUNG	66
8.	REFERENCES	68
9.	SUPPLEMENT	89
9.1.	List of Figures	89
9.2.	Materials	90
9.2.1.	Chemicals And Consumables	90
9.2.2.	Enzymes, Recombinant Proteins And Inhibitors	92
9.2.3.	Antibodies	93
9.2.4.	ELISA and CBA Kits	94
9.2.	List of Abbreviations	94
9.3.	Curriculum Vitae	Fehler! Textmarke nicht definiert.
9.4.	Acknowledgements – Danksagung	Fehler! Textmarke nicht definiert.
9.5.	Affirmation - Eidesstattliche Erklärung	98

1. Introduction

1.1. Acute Respiratory Distress Syndrome

The Acute Respiratory Distress Syndrome (ARDS) is a severe disease characterized by a widespread inflammation within the lungs, extensive flooding of the alveolar airspace with protein-rich exudate fluid and impaired gas exchange capacities, leading to respiratory failure and resulting in mortality rates of 40-58% (1, 2).

ARDS, as defined by the Berlin definition from 2012, includes an acute onset of disease, radiological finding of bilateral infiltrates due to non-cardiogenic reasons and impaired oxygenation of $\text{PaO}_2/\text{FiO}_2$ (partial pressure of oxygen/ fraction of inspired oxygen) $\leq 300\text{mmHg}$ (3). ARDS can be subdivided according to the degree of hypoxemia into mild (200-300mmHg, matching the former definition of Acute Lung Injury, *ALI*), moderate (100-200mmHg) and severe ARDS ($\leq 100\text{mmHg}$). ARDS can be triggered either by direct lung injuries, e.g. pneumonia, toxic inhalation or near drowning, or by indirect systemic injuries, e.g. sepsis, pancreatitis or burn. Pneumonia caused by viral or bacterial infection is the most frequent underlying condition (4).

Disease progression of ARDS can be separated into three phases (2, 5). First, in the acute phase (Fig. 1.1), ARDS presents with extensive interstitial and alveolar flooding (edema) that leads to severely reduced oxygen uptake (hypoxemia) and carbon dioxide excretion from the blood (hypercapnia). Neutrophil, macrophage and red blood cell infiltrates are found in the alveoli, a diffuse injury to both endothelium and epithelium is present and the formation of hyaline membranes can be detected. During this first phase of ARDS, high levels of inflammatory mediators, proteases and oxygen radicals are found in the alveolus, and inactivation of surfactant leads to microatelectasis. Resolution of edema is usually delayed as the injury to the endo-epithelial barrier prevents adequate removal of alveolar edema fluid. Importantly, mortality in ARDS patients has repeatedly been found to correlate with persistence of alveolar edema (2, 5-8). The acute phase is followed by a subacute phase of ARDS (day 7-14), where fibroblasts infiltrate the lung and epithelial type II cells proliferate, promoting the repair of the alveolar epithelial barrier. A third chronic phase is characterized by the resolution of neutrophilic infiltrates by mononuclear phagocytes and alveolar macrophages but also a vast fibroproliferative response, which is not found in all ARDS patients and can progress into pulmonary fibrosis.

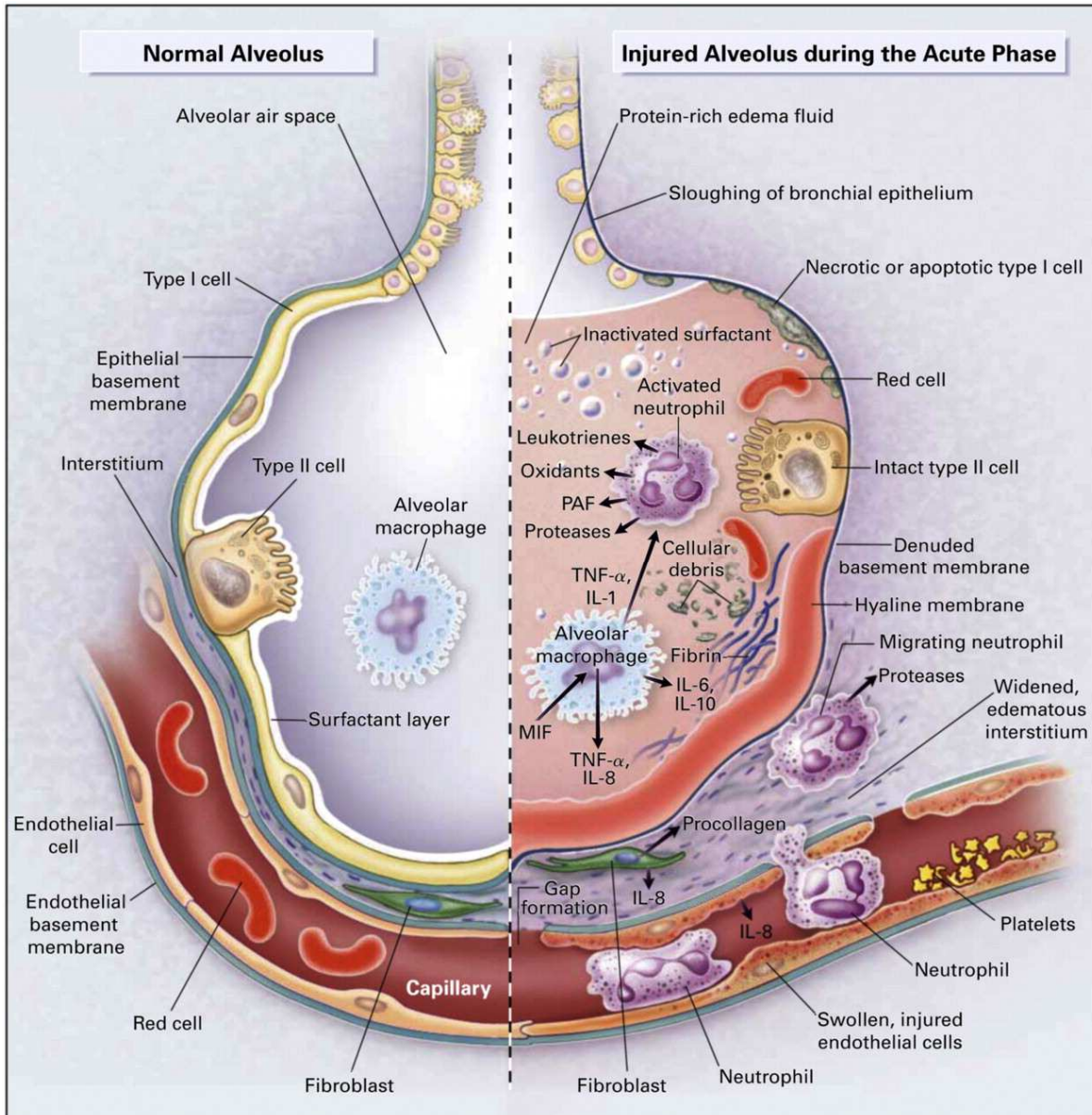


Figure 1-1 Schematic overview of pathological changes to the alveolar compartment during the acute phase of ARDS, adapted from Matthay and Zeman, 2011 (2). Depicted is on the left-hand side a healthy alveolus with an intact epithelial barrier consisting of type I and type II epithelial cells. After injury (right-hand side), leukocytes and red blood cells intravasate into the alveolar airspace. Disruption of the endothelial and epithelial barrier leads to edema formation.

1.2. Microanatomy And Physiology Of The Lung

The primary function of the lung is to provide an interface for gas exchange of inhaled, atmospheric oxygen and carbon dioxide carried in by the bloodstream. The lung therefore comprises of a thin but large surface area, which also renders the alveolo-capillary barrier a vast and important site for initial pathogen-host interactions (9, 10). Epithelial but also endothelial cells maintain barrier integrity (9) thus preventing edema formation and are also important for the primary induction of innate immune responses. Resident alveolar

macrophages, dendritic cells and stimulus-dependent recruited neutrophils, monocytes and lymphocytes play a crucial role in alveolar defense strategies but also in resolution of inflammation (10–13).

1.2.1. The Alveolar Mononuclear Phagocyte System

Resident and recruited cells of the mononuclear phagocyte system play a key role in the activation and regulation of innate and adaptive immune responses towards invading pathogens. Resident alveolar macrophages (AM) originate from fetal monocytes that initially colonize the lung during embryonic development (14). These fetal monocytes, in turn, derive from a hematopoietic stem cell (HSC) that during embryonic development populates the fetal liver and later on the bone marrow and gives rise to a common monocyte/dendritic cell (DC)-precursor (MDP) (15–17). The MDP can further differentiate into a common monocyte precursor (cMoP) (18) and, successively, monocytes that enter the blood stream and finally extravasate into the lung tissue (Figure 1-2).

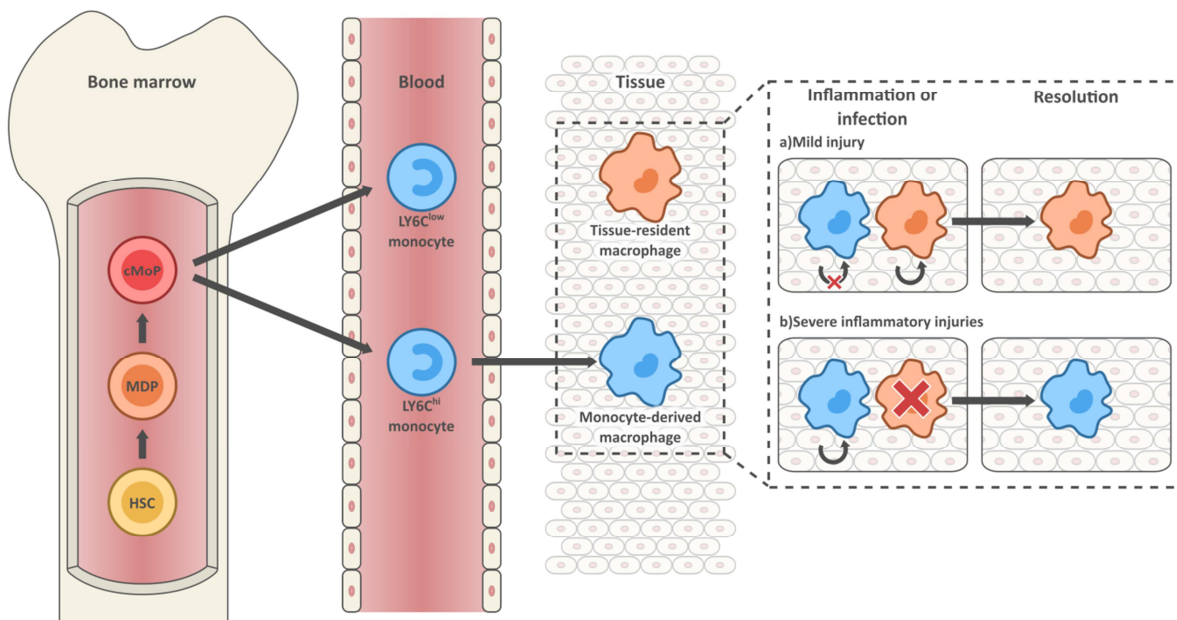


Figure 1-2 Origin and dynamics of murine macrophages, adapted from Hussel and Bell, 2014 (19). In the adult murine system, blood circulating monocytes derive from a hematopoietic stem cell (HSC) that gives rise to a common monocyte/dendritic cell (DC)-precursor (MDP) and subsequently to a common monocyte precursor (cMoP) intermediate. The cMoP can differentiate into Ly6C^{low} monocytes patrolling the endothelial luminal surface and Ly6C^{high} monocytes that are recruited to inflamed tissues. Within their niche, tissue-resident macrophages tolerate mild injuries by proliferation and self-renewal, but are supplemented with monocyte-derived macrophages upon severe injuries and depletion.

Under steady-state conditions, the resident AM is a long-lived cell capable of self-renewal and thus sustaining the AM population (20–22). It can be identified by the markers F4/80⁺

GR1^{low} $\text{CD11c}^{\text{high}}$ $\text{SiglecF}^{\text{high}}$ $\text{MHCII}^{\text{low}}$ and remains sessile in close connection to the alveolar epithelial cells (23, 24). Their role is to elicit immediate innate immune responses towards invading pathogens, but at the same time they need to remain relatively inactive towards innocuous stimuli (19). Therefore the AM inflammatory response is dampened by a number of epithelial expressed blocking agents such as CD200, SIRPa (signal-regulatory protein alpha), MARCO (macrophage receptor with collagenous structure) and surfactant proteins A and D, and also by macrophage autocrine anti-inflammatory signaling elicited by TGF- β (transforming growth factor beta) and IL-10 (interleukin-10) (19, 25–30). The conversion of resident AM to pro-inflammatory active cells is triggered by a loss of epithelial regulatory ligands, presence of necrotic cells and signaling by diverse pattern recognition receptors (PRR) (13, 31). PRR expressed by AM are various toll-like receptors (TLR) (32, 33), nucleotide oligomerization domain (NOD)-like receptors (34, 35), and intracellular helicases like retinoic acid inducible gene I (RIG-I) (36, 37) or protein kinase R (PKR) (38, 39) recognizing several pathogen-associated molecular patterns (PAMP). In response, AM produce a range of inflammatory cytokines (e.g. type I interferons) that further perpetuate the innate immune response and lead to the recruitment of additional inflammatory cells, such as neutrophils, exudate macrophages or lymphocytes, to the alveolar compartment (13, 40, 41).

In general, the more pro-inflammatory, classically activated macrophages are termed M1 macrophages and are associated with activation of the pro-inflammatory transcription factor IRF-5 (interferon regulatory factor 5) and production of mediators like TNF- α (tumor necrosis factor alpha), IFN- γ (interferon gamma), IL-1 β , IL-6 or IL-12 (42, 43), and antimicrobial agents such as nitric oxide or L-arginine (44). Yet it is well described that macrophages can also differentiate into an anti-inflammatory, regenerative phenotype termed M2. Factors inducing differentiation into the M2 phenotype include IL-4, IL-10, IL-13, IL-1ra (IL-1 receptor antagonist), T-helper cell 2 released IL-25 and IL-33, Lipoxin A₄ and phagocytosis of apoptotic neutrophils (43, 45–47). M2 macrophages then produce the anti-inflammatory cytokines IL-1ra, IL-10, and TGF- β (46, 48). They are involved in the resolution of inflammation by promoting the cessation of monocyte and neutrophil migration, the removal of apoptotic granulocytes, the initiation of repair processes and their own maturation to resident alveolar macrophages (49). Macrophages show a broad plasticity in their capability to flexibly change phenotype in response to different environmental stimuli (43).

Even if normally long-lived and self-renewable, the resident AM might be driven into cell death in severe inflammatory conditions, e.g. influenza A infection (14, 50). An above-average depletion of this cellular subset in the adult lung leads to the recruitment of circulating blood Ly6C^{high} monocytes to the alveolar lumen to replenish the local macrophage pool (51) (Figure 1-2). These monocytes can be further characterized as CD11c^{low} CD11b^{high}, but change to a CD11c^{high} CD11b^{negative} phenotype as they achieve a sessile macrophage phenotype (52). Experimentally, these so-called “exudate” macrophages can be studied by using bone marrow-derived macrophages (BMM) cultured *ex vivo* in presence of GM-CSF (granulocyte-macrophage colony-stimulating factor) that approximate an exudate M1-like phenotype with the F4/80^{high} CD11c^{low} CD11b^{high} signature and expression of M1-associated cytokines such as TNF- α , IL-6 or IL-1 β (53).

In vivo, the recruitment of blood-circulating monocytes into the alveolar compartment crucially depends on the monocyte expression of CCR2 (C-C chemokine receptor type 2) and its interaction with its major ligand CCL2 (C-C chemokine ligand 2). Lack of CCR2 inhibits migration of bone marrow monocytes into the blood stream as well as monocyte extravasation from the blood stream to the site of inflammation (54, 55).

1.2.2. Epithelium

The proximal airways are lined by columnar goblet cells or cuboidal Club cells, secreting mucus, thus preventing desiccation of the airway but also trapping incoming particles, and ciliated cells that serve to transport foreign particles out of the lung. In the distal lung compartment, the alveolar epithelium provides the initial barrier to environmental influences. More than 95% of the alveolar surface consists of flat, squamous type I pneumocytes (alveolar epithelial cells I, AEC I). Their primary function is to enable gas exchange by limiting the diffusion distance between inhaled air and the pulmonary, capillary blood vessels (56). Due to their large surface, AEC I are prone to damage by environmental and mechanical stress. Loss of AEC I is compensated by proliferation and differentiation of type II pneumocytes (AEC II) to AEC I, that in addition to their regenerative potential produce surfactant – a mixture made of amphiphilic phospholipids and specific proteins that prevents the alveoli from collapsing during exhalation (57). Moreover, AEC II play a role in recognition of pathogens and initiation of innate immune responses, in ion conductance as well as fluid homeostasis in the lung (58).

Both AEC I and AEC II are well-polarized and tightly interconnected cells (Fig. 1-3), thus providing a structural and functional barrier tightly regulating alveolar fluid homeostasis as well as transport of proteins and solutes in the lung (outlined below). Within this cellular network, adherens junctions provide the physical anchorage in cell-cell adhesion by strong interaction of the extracellular domains of neighboring cells as well as by being linked to the intracellular actin cytoskeleton (59). In the alveolar epithelium, they are formed by E-Cadherin and proteins of the Catenin family (59, 60). By limiting the movement of membrane-integral proteins, adherens junctions are important for the establishment of cell polarity. The tight junctions are an apically located multiprotein complexes consisting of claudins, occludins, junctional adhesion molecules (JAM) and scaffolding proteins such as zona-occludens protein 1 (ZO-1), that in concert form a continuous circumferential ring. Tight junctions are therefore essential in limiting paracellular transport and as well maintenance of cell polarity (61). Desmosomes are additional adhesive molecules found in the alveolar epithelium and they provide resistance to mechanical stress by being closely connected to the intermediate filament network (62).

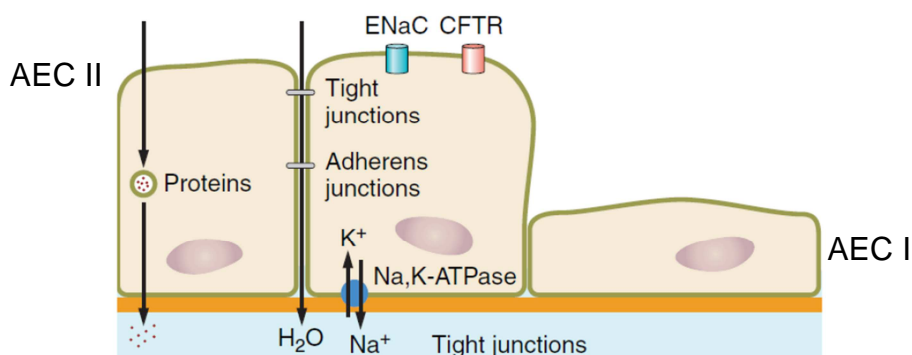


Figure 1-3 Schematic presentation of the alveolar barrier, adapted from (63). Flat AEC I and squamous AEC II build the epithelial barrier. AEC are connected by tight and adherens junctions, thus allowing for vectorial sodium transport into the interstitium by apical ENaC and basolateral Na,K-ATPase, accompanied by paracellular water transport.

The structural integrity of the alveolar epithelium results in low paracellular permeability to solutes. This promotes - in combination with its polarity providing an asymmetric distribution of ion transporters - the accumulation of sodium ions in the underlying interstitium. Sodium ions are taken up by the alveolar epithelial cells by the apically expressed amiloride-sensitive epithelial sodium channels (ENaC) as well as via the amiloride-insensitive sodium channels (9, 64, 65), accompanied by transport of chloride ions through CFTR (cystic fibrosis transmembrane conductance regulator) (66). The primary

driving force of sodium accumulation in the interstitial space is the basolaterally expressed ion transporter Na,K-ATPase, that exchanges intracellular sodium ions against extracellular potassium ions at a ratio of 3:2 under consumption of ATP (64, 67, 68). The interstitial accumulation of sodium ions creates an osmotic force that passively drains excessive water out of the alveolar airspace to the interstitial space and successively, to the lung lymphatic vessels and the pulmonary microcirculation, a process vital for alveolar fluid homeostasis (69–72). Interestingly, the Na,K-ATPase does not only play a crucial role in alveolar epithelial barrier function, but is also involved in the formation of junctional integrity (73). Of note, it has been shown that the integrity of the epithelial layer is dominant over the endothelial barrier in limiting formation and persistence of alveolar edema, as the disruption of the endothelial barrier alone has been reported to have no influence on epithelial permeability and formation of alveolar edema (74, 75).

1.3. Sodium-Potassium Adenosine Triphosphatase (Na, K-ATPase)

1.3.1. Structure

The Sodium-Potassium Adenosine Triphosphatase (Na,K-ATPase) is an ion transporter belonging to the family of P-type ATPases, consisting of more than 500 ion and lipid pumps characterized by the ability to catalyze their own autophosphorylation at conserved aspartate residues (76). As typical for most P-type ATPases, the Na,K-ATPase oscillates between two conformational states E1 and E2. In E1, three sodium ions and consequently a molecule of ATP bind to the protein complex. Hydrolysis of ATP to adenosine diphosphate and autophosphorylation of the Na,K-ATPase lead to a conformational change to E2, where sodium (Na) is released into the extracellular space and two potassium (K) ions are bound.

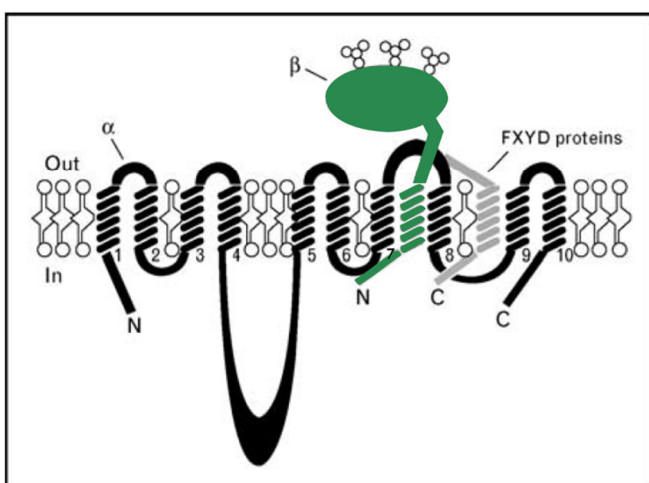


Figure 1-4 Schematic presentation of Na,K-ATPase protein, adapted from Geering, 2008 (77). The catalytic α -subunit (black) is composed of 10 membrane spanning domains. The extracellular loop between α -helices 7 and 8 interacts with the β -subunit extracellular domain (green). The β -subunit consists of a short intracellular N-terminus, a single membrane spanning domain and a highly glycosylated extracellular domain. The FXYD subunit (light grey) interacts with α -helix 9 as well as the intracellular domain of the α -subunit.

Dephosphorylation of the pump reverts it to E1, accompanied by release of the K ions into the intracellular compartment. The Na,K-ATPase is built of a heterodimer consisting of a catalytic α -subunit and a largely extracellular β -subunit, but is often found to be complexed with a third regulatory subunit called γ -subunit or FXYD.

There are four known isoforms of the α -subunit, showing a specific tissue- and developmental distribution, with the $\alpha 1$ isoform being the most ubiquitously expressed isoform (78). The different isoforms are transcribed from different loci instead of being produced by alternate splicing, and form integral membrane proteins with 10 membrane spanning domains of approximately 100-110kDa. The α -subunit harbors the binding domains for both Na and K ions as well as for ATP, phosphate and the Na,K-ATPase inhibitor ouabain. The β -subunit is a type II glycoprotein, expressed in 5 known isoforms, with $\beta 1$ being the most frequently expressed isoform (79). The β -subunit core consists of 32kDa protein with a short membrane-spanning domain and a large extracellular domain. The mature protein is usually highly glycosylated and thus can be found in sizes varying between 42 and 55kDa. The β -subunit acts as chaperone for correct α -subunit folding, induces correct transport of the α/β -complex to the cellular basolateral membrane, has influence on the affinity of the α -subunit to Na/K ions and is involved in intercellular junction formation (73, 80, 81).

The regulatory FXYD subunit is a small type I membrane protein. It is found to interact with the α/β -heterodimer at the α -helix 9 as well as at the intracellular domain of the α subunit, and may also interact with the β -subunit (82, 83). Seven isoforms are known in mammals, all shown to modulate Na,K-ATPase maximal ion conductance, affinity to Na or K ions, or ATP (77).

1.3.2. Function

The Na,K-ATPase is an ubiquitously expressed protein and is essential to cellular survival. It does not only control intracellular concentration of ions, thus regulating cellular osmotic properties and preventing swelling as well as maintaining membrane potential necessary for neuronal signaling; it is also indispensable for the transport of solutes such as amino acids, glucose or phosphates, that rely on the ion gradient produced by the Na,K-ATPase (77). It is also crucial in the regulation of osmotically driven, paracellular water transport, thus enabling renal reabsorption but importantly also fluid homeostasis in the alveolar airspace, which ensures normal gas exchange in the alveolar compartment (79, 84). Na,K-ATPase is

commonly found to be deregulated in ARDS, which greatly impacts on formation and persistence of edema and consequently, on the survival of the patient (85).

Independent of its ion pumping activity, the Na,K-ATPase has also been found to be involved in the formation and maintenance of cell-cell adhesions (73, 86). The β -subunit has been shown to colocalize with adherens junctions, playing an essential role in junctional formation and polarization in canine kidney epithelium (MDCK cells) (87, 88).

Additionally, it has become more and more apparent that Na,K-ATPase is involved in a number of signal transduction events. Several studies revealed that the non-receptor tyrosine kinase Src is bound to the Na,K-ATPase $\alpha 1$ -subunit in an inactive state (89–91). Src can be released and thus activated by low nanomolar concentrations of ouabain and is involved in the activation of MAP kinase signaling by EGFR (epidermal growth factor receptor) and Ras-GTP, in phospholipase C γ (PLC γ) and PI3K (Phosphatidylinositol-4,5-bisphosphate 3-kinase) mediated Akt signaling (92–95). Accordingly, Na,K-ATPase as signaling molecule is currently thought to be involved in cellular proliferation, differentiation and metabolic regulation (78).

1.3.3. Regulation

As described above, the Na,K-ATPase is vital for cellular function and survival, but is also making up to 50% of cell total energy consumption (96, 97). Thus, its expression and activity levels need to be tightly regulated. This is in part accomplished by the tissue-specific distribution of different isoforms for the α - and β -subunit and the regulatory influence of different FXYD proteins (77). Additionally, up to 70% of Na,K-ATPase is stored in intracellular pools, from which additional proteins can quickly be recruited to the cell membrane and consequently allow the cell to respond to environmental stimuli (98, 99). Further short-term regulations include variations of ion affinity and the catalytic rate of the Na,K-ATPase, as well as ubiquitin-dependent degradation of membrane-located ion pump (71, 100). Long-term changes are regulated by transcriptional and post-transcriptional events, and have recently been shown to be influenced by histone deacetylase 2 (HDAC2)-dependent epigenetic changes of the β -subunit gene locus (101, 102).

A deregulation of Na,K-ATPase cellular homeostasis has been widely described in lung injury as response mechanism to hyperoxia, hypercapnia, ventilator-, endotoxin-, oleic acid- and alcohol-induced lung injury, causing elevated levels of alveolar edema (100). The significance of Na,K-ATPase expression in edema formation in lung injury was underlined

by studies showing that overexpression of Na,K-ATPase by electroporation-based methods or adenoviral transfer increased alveolar fluid clearance and could even protect from LPS-induced injury (103–106).

Upstream signaling events and molecules leading to the decrease in plasma membrane expressed Na,K-ATPase include nitric oxide (107), oxidant generation (108–110), coagulation factors (111) and also hormonal signals (112–114). The decrease of plasma membrane located Na,K-ATPase caused by hyperoxia or hypercapnia has been studied in detail and was shown to rely on the PURED (phosphorylation - ubiquitination - recognition - endocytosis - degradation) pathway (100, 115).

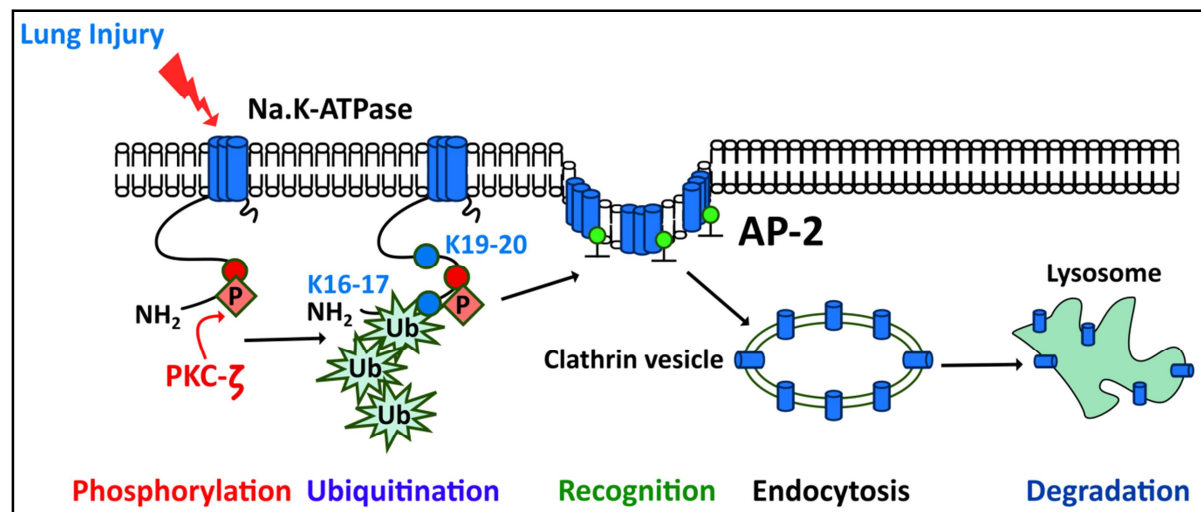


Figure 1-5 PURED pathway mediated degradation of plasma membrane Na,K-ATPase, adapted from Lecuona, Trejo and Sznajder, 2007 (100). Na,K-ATPase α1-subunit is phosphorylated at Serin 18 by PKC-ζ, followed by ubiquitination of N-terminal lysine residues. Ubiquitinated Na,K-ATPase is endocytosed by an AP2-/ clathrin-dependent mechanism, transported to the endosome and degraded in the lysosome.

It was established that hypoxia results in formation of mitochondrial reactive oxygen species (ROS) that can activate the cellular energy sensor and stress kinase adenosine-monophosphate (AMP)-activated kinase (AMPK) (108). AMPK is a heterotrimeric serine/threonine kinase consisting of a catalytic α-subunit and two regulatory subunits β and γ with a central role in cellular energy metabolism. It senses energy shortages by binding of AMP, antagonized by presence of ATP, that renders it sensitive to phosphorylation and thus activation by its upstream kinases, the liver kinase B1 (LKB1), the Calcium/Calmodulin-sensitive kinase kinase beta (CaMKKβ), and TGF-β-activated kinase 1 (TAK1) (116). AMPK activation generally increases the availability of energy, e.g. by enhancing Glut4-dependent glucose uptake, and decreases energy consuming processes, e.g. protein synthesis or glycogen synthesis (117–119). Not only hypoxia, but also hypercapnia, induces an

AMPK-dependent degradation of the Na,K-ATPase (120). Besides ROS, adrenergic or dopaminergic receptor signaling mediated by MAPK and ERK activation has been described to reduce plasma membrane located Na,K-ATPase (121). Mediators known to upregulate Na,K-ATPase ion transport activity include catecholamines (98, 122) and the growth factors KGF (keratinocyte growth factor) and EGF (epidermal growth factor) (123–125).

1.4. Influenza A Virus

Influenza A viruses (IAV) cause a respiratory disease in humans that can progress to lung injury with fatal outcome. They transmit by respiratory droplets and primarily infect the epithelia of the proximal as well as the distal respiratory tract and result in a primary viral pneumonia causing severe damage to the alveolar compartment, the acute respiratory distress syndrome (ARDS) (126–128). IAV infections lead to substantial morbidity and mortality worldwide (129, 130). Often, additional secondary superinfections with *Streptococcus pneumonia*, *Staphylococcus aureus* and *Haemophilus influenzae* induce a secondary, bacterial pneumonia worsening outcome substantially (131, 132).

1.4.1. Taxonomy

Influenza A viruses belong, together with influenza B, influenza C, thogoto- and isaviruses, to the family of *Orthomyxoviridae* that are characterized by a single stranded, negative oriented and segmented RNA genome. They are coated by a host cell-derived lipid membrane. The genera can be differentiated by the molecular and serological characteristics of the viral matrix and nucleoproteins and have different amounts of gene segments (133), of which influenza A viruses possess eight. IAV are further separated into subtypes by antigenic characteristics displayed by their hemagglutinin (HA) and neuraminidase (NA) proteins, of which we currently know 16 and 9 subtypes, respectively, found circulating in wild birds and waterfowl (134), as well as a unique HA-NA combination found recently in bats (H17N10) (135). IAV are named by genus, host species (if not human), place of isolation, number of the isolate, year of isolation and its subtype (for example: A/Puerto Rico/8/34 (H1N1)).

1.4.2. Structure

IAV form pleiomorph particles of 80-120nm diameter. Inside, the viral RNA is complexed with the viral nucleoprotein NP and the polymerase complex, generating the viral ribonucleoprotein (RNP). The viral RNA consists of 13,6k basepairs and is - due to its

negative orientation - *per se* not infectious (136). It encodes for 11 viral proteins: non-structural proteins NS1 and NS2, important for regulation of host innate immune responses and export of viral RNA from the nucleus, respectively; the matrix proteins M1 and M2, the neuraminidase (NA), nucleoprotein (NP), hemagglutinin (HA), the polymerase subunits PA, PB1 and PB2 and PB1-F2. The viral protein pairs PB1 and PB1-F2, M1 and M2, NS1 and NS2 are each generated by alternative splicing from one RNA segment, whereas the other RNA segments encode for one viral protein each (137–139). The flanking 3' and 5' ends of each segment contain a non-coding region serving as promoter and bind the viral polymerase complex. The viral matrix protein M1 lines the viral envelope that derives from the host outer cell membrane from the inside. Embedded into the viral membrane are the viral proteins M2, the viral transmembrane proton channel, HA, that is relevant for adsorption and fusion of host and virus membrane, and NA, the viral sialidase (Fig.1-6). Viral proteins that cannot or only in scarce amounts be found in the viral particle are NS1, NS2 and PB1-F2.

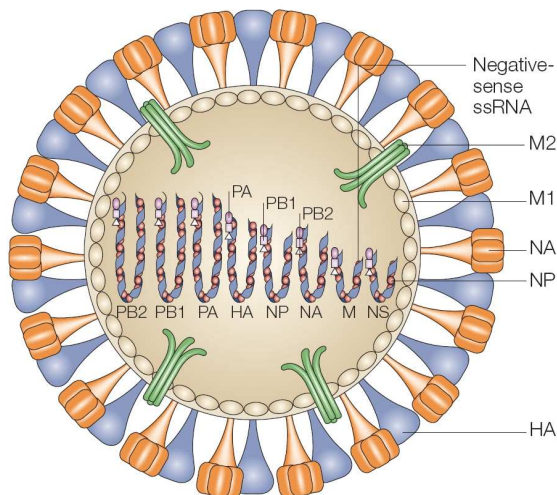


Figure 1-6 Schematic depiction of an influenza A virus particle, taken from Subbarao and Joseph, 2007 (140). Eight gene negative oriented, single stranded (ss) RNA segments are associated with the nucleoprotein and the polymerase subunits PA, PB1, PB2. The matrix protein M1 is lining the lipid membrane, in which the ion channel M2, hemagglutinin (HA) and neuraminidase (NA) are embedded.

1.4.3. Replication

For efficient replication (Fig. 1-7), IAV attach to a host cell via interaction of HA with cellular N-acetyl sialic acids (SA). Avian influenza strains show a preference for α 2,3-linked SA prominently expressed in the avian intestinal tract, whereas human IAV prefer α 2,6-linked SA (141). Virions are then endocytosed and trafficked to the endosome where the acidification of the surrounding medium triggers a conformational change in the viral HA leading to the fusion of viral and endosomal membrane (142). Additional activation of M2 ion conductance minimizes interactions between NP and M1, promoting the release of

the RNP into the cytoplasm (143, 144). RNPs are then imported into the nucleus through cellular importin- α and transcribed into viral mRNA (145, 146). HA, NA and M2 are translated in the endoplasmatic reticulum and enter the exocytic pathway. The remaining mRNAs are translated in the cytoplasm (147). Polymerase proteins, NP and M1 are transported back into the nucleus, triggering synthesis of negative-oriented viral RNA, form new RNPs and are transported out of the nucleus by an NS2- and cellular Crm1-mediated mechanism (148). Viral proteins are then transported to the apical cell membrane, accumulating at lipid-raft domains (149). Budding of new virions is facilitated by clustering of M1 monomers, and pinching off has been proposed to involve the small RAS-like GTPase Rab11 (150). Also, the viral NA is crucial for efficient viral replication, as its sialidase activity prevents the newly formed virions from sticking to the host cells and forming immobile virus-aggregates (151).

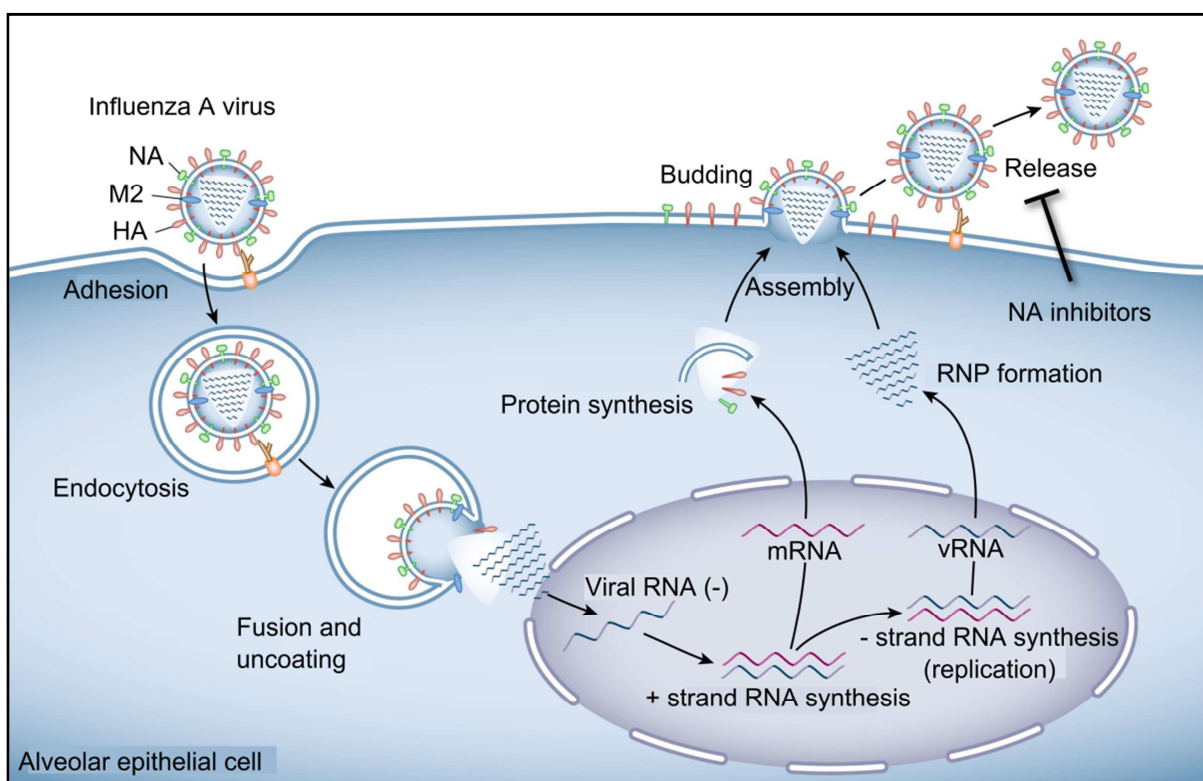


Figure 1-7 Influenza A virus replication cycle (152). The virion adsorbs to the host cell via interaction between HA and sialic acids and is endocytosed. Viral and endosomal membrane fuse and released vRNA is transported into the nucleus, where it is transcribed to positive sense mRNA. Translation of viral proteins takes place in the cytoplasm and endoplasmatic reticulum. New virions containing newly synthesized, negative sense RNA assemble and bud from the apical host cell membrane and are released from the cell by action of NA.

1.4.4. Epidemiology

Seasonal influenza epidemics typically occur during the cold season in temperate regions and are caused by virus subtypes that are proposed to persist and evolve in a virus reservoir in the East and Southeast human population where influenza is less seasonal as well as by dynamic migration between Northern and Southern hemispheres (153–155). As the viral polymerase lacks a proof-reading function present in mammalian DNA polymerases, IAV exhibit a mutation rate of 10^{-5} mutations per nucleotide (156). This results in a large pool of genetically and antigenetically different IAV strains and a high adaptive flexibility towards selective pressure deriving from the host innate and adaptive immunity, leading to a gradual but constant change in antigen properties (*antigenic drift*). Seasonal IAV display a substantial morbidity with an incidence of influenza-associated acute respiratory failure of 2.7 per 100.000 persons per year (157). Pandemic influenza events are preceded by introduction of new virus subtypes into the human population by *antigenic shift*, the event of reassortment or exchange of virus RNA segments between different virus strains. Typically reassortment between an avian and human virus strains results in the introduction of an antigenetically altered virus strain into an immunologically naïve human population. The introduction of reassortant IAV strains into the human population is characterized by a succession of pandemic waves with increased mortality (158), a higher transmissibility than seasonal influenza (159) and a dramatic increase in mortality in younger populations (159–162). The 1918 H1N1 pandemic was caused by a virus of avian origin (163) and caused an estimated 40 million deaths worldwide (164). Further reassortment events of the circulating human virus strains with avian viruses led to the emergence of the 1957 H2N2 and 1968 H3N2 influenza pandemics (165), and multiple reassortments between avian, swine and human viruses resulted in the 2009 H1N1 pandemic influenza strain (166). Since 1997, recurring infections of humans with avian viruses of the subtypes H5N1, H7N7, H9N2, H7N2 and H7N9 partly displaying high mortality rates of 34–60% (167–171) cause concern about high pathogenic avian viruses crossing the species barrier and gaining pandemic potential. Avian influenza viruses are restricted in their replication in humans but can adapt to the mammalian host by introducing changes in the HA, NA and the polymerase proteins (172–177).

Inhibitors of viral NA protein activity, Oseltamivir, Zanamivir, Laninamivir and Peramivir, are used to control seasonal or pandemic influenza, but an increasing prevalence of resistant influenza strains leads to a limited efficacy of these antivirals (178). A better understanding

of influenza pathophysiology is therefore of utmost importance as it might provide cellular targets for new treatment options.

1.5. Interactions At The Host-Virus Interface

Replication of IAV in a host cell greatly impacts on cellular function and structure. First of all, it leads to impaired protein biosynthesis of cellular proteins, as components of the transcriptional and translational machinery are recruited for viral RNA processing (179, 180). IAV infection also impacts on the functional integrity of the alveolar epithelium. It directly affects tight junction stability, through the action of NS1. Its carboxylterminus domain contains a PDZ-ligand binding motif that can interact with host factors scribble and Dlg1 (Disks large homolog 1), leading to tight junction disruption accompanied by lower transepithelial resistance and higher protein diffusion rates of the epithelial cell layer (181). HA binding to the cell surface leads to rapid activation of Src, phospholipase C and protein kinase C (PKC) that decrease the activity of the apical epithelial sodium channel ENaC (182, 183). M2 also affects ENaC as M2 expression leads to enhanced levels of reactive oxygen species (ROS) formation, subsequent PKC activation and proteosomal degradation of ENaC (184). M2 further has been demonstrated to affect the chloride channel CFTR, driving it to ubiquitin-mediated degradation by M2-mediated changes in secretory organelle pH (185).

The cellular recognition of pathogen-/danger- associated molecular patterns (PAMPs/ DAMPs) by diverse pattern recognition receptors induces the activation of inflammatory, anti-viral signal cascades (Fig. 1-8). Detection of uncapped 5'-triphosphorylated RNA by RIG-I (RNA helicases retinoic acid inducible gene-I) and subsequent interaction with MAVS (mitochondria-associated antiviral signaling protein) and TRIM25 (Tripartite motif-containing protein 25) and IPS-1 (Interferon-beta Promotor Stimulator-1) leads to an IRF-3 and IRF-7 (interferon regulatory factor)-dependent transcription and translation of type I interferons (IFN) (36, 186). Furthermore, recognition of viral patterns by protein kinase R (PKR) activates NF-κB (nuclear factor 'kappa-light-chain-enhancer' of activated B-cells) translocation to the nucleus and transcriptional activation of pro-inflammatory, pro-apoptotic and anti-viral gene clusters (187–189). Besides RIG-I and PKR, the NLRP3 (NOD-like receptor family, pyrin domain containing 3) inflammasome, but also endosomally located TLR3 and TLR7 (190–192) are able to sense IAV infection. Activation of NLRP3 induces caspase-1 dependent release of pro-inflammatory IL-1 β and IL-18 (193),

whereas TLR3/TLR7 act via IRF-3, IRF-7 and NF- κ B, again triggering the induction of the IFN and pro-inflammatory cytokine response (194).

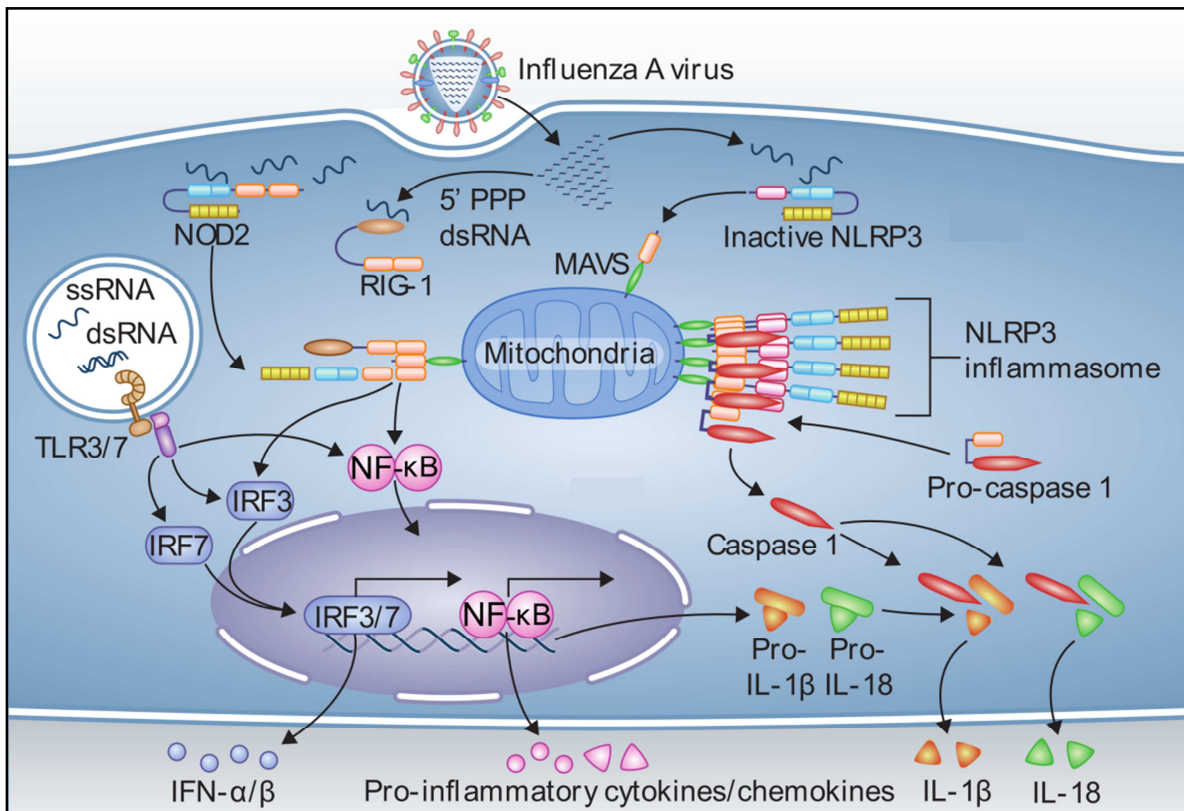


Figure 1-8 Host immune responses to IAV infection, adapted from (152). Presence of intracellular viral RNA activates TLR3/7 signaling via IRF3, IRF7 and NF κ B, inducing of transcription type I interferons and pro-inflammatory mediators. RIG-I responds to 5' uncapped dsRNA, interacts with MAVS and NOD-2 to activate IRF3 and NF κ B. Also the NLRP3 inflammasome responds to IAV infection by scission and activation of caspase-1, resulting in release of IL-1 β and IL-18.

In addition, IAV infection leads to a high release of pro-inflammatory mediators by both tissue-resident and monocyte-derived recruited alveolar macrophages that amplify lung injury after IAV-infection, as shown for highly pathogenic avian influenza H5N1 or the pandemic 2009 H1N1 (195–198). In particular, exuberant production of IFN and IFN-dependent tumor necrosis factor (TNF)-related apoptosis-inducing ligand (TRAIL) have been demonstrated to impact on the epithelial barrier integrity, severity of lung injury and mortality and also hamper resolution of inflammation (45, 126, 199–201).

1.5.1. Interferon Signaling

IFN are antiviral cytokines that can be divided into three groups, type I, II and III IFN. Type I IFN are mainly produced by AM, AEC and DC after IAV infection (201–203) and consist of IFN- α , - β and the less known IFN- ω , - κ and - τ , whereas IFN- γ and IFN- λ are assigned to

the type II and III IFN, respectively (204, 205). IAV infection primarily triggers the production and secretion of type I and III IFN in response to PRR signaling (206). Type I IFN secreted by infected cells bind to their respective receptors, termed IFN- α - β receptor (IFNAR), on surrounding cells to induce a specific signaling program establishing an antiviral state in these cells. Receptor binding of IFN to IFNAR results in activation of ISRE (interferon-sensitive response elements) promotor elements (204–206). These ISRE elements are found upstream of more than 100 different genes, the transcription of which they regulate, termed interferon stimulated genes (ISG). Of note, type I IFN have not only been ascribed antiviral activity in IAV infection, but have also been shown to add to IAV-induced pathogenesis by promoting TRAIL-mediated apoptosis of the alveolar epithelial cells (201, 207).

1.5.2. TNF-Related Apoptosis Inducing Ligand (TRAIL)

Together with Fas ligand and TNF- α , TRAIL (or Apo2L) belongs to the superfamily of TNF ligands, consisting of mostly homotrimeric type II transmembrane proteins whose extracellular domains can be cleaved by specific metalloproteinases to generate soluble cytokines (208). In the human system, five different binding partners for TRAIL are present: the membrane-bound death receptors DR4 and DR5 that both induce a pro-apoptotic signaling cascade, the as well membrane-bound anti-apoptotic decoy receptors DcR1 and DcR2 and the soluble interaction partner osteoprotegerin (OPG) (209). In the murine system, only DR5 has been identified to ligate TRAIL (210). Ligand-binding to DR4 and DR5 results in the cleavage and activation of the effector caspase-3 that affects a large variety of substrates and drives the cell into apoptosis (211).

In IAV infection, TRAIL is specifically released from infected alveolar macrophages depending on an autocrine signaling loop (Figure 1-9). Upon infection, NF κ B translocates to the nucleus due to PKR activation and induces transcription of IFN- β . Binding of IFN- β to macrophage-expressed IFNAR activates a JAK/STAT-dependent release of TRAIL, which then acts through its receptor DR5 on the alveolar epithelial cells thereby inducing apoptosis and affecting structural barrier integrity, with significant impact on morbidity and mortality (45, 201).

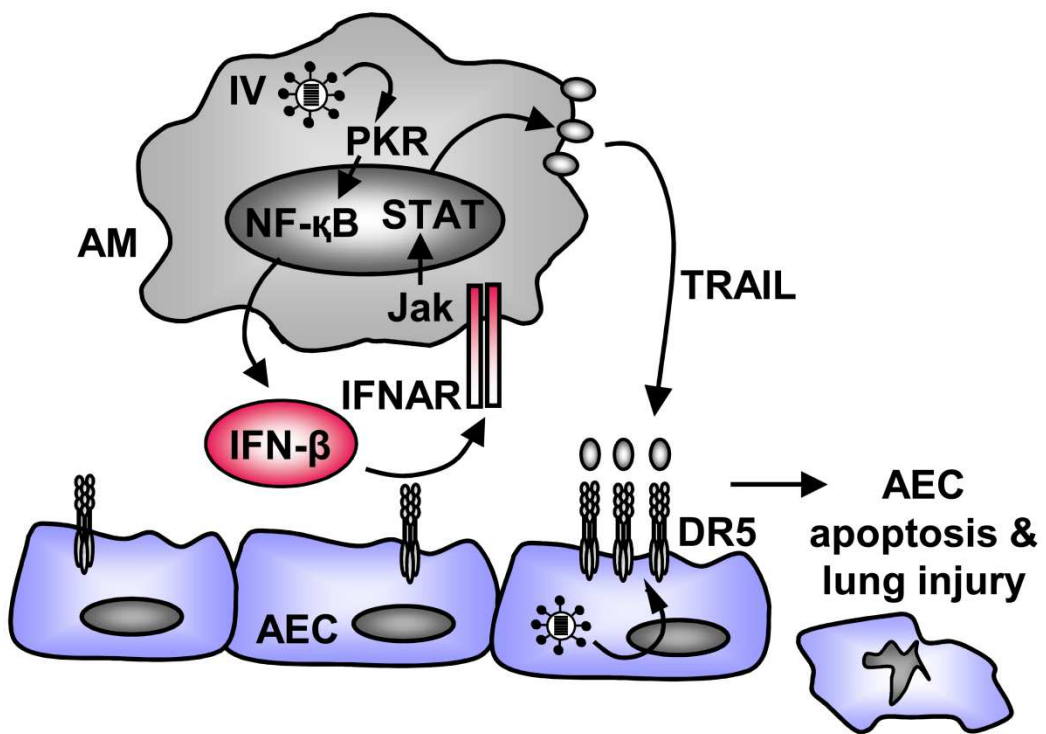


Figure 1-9 IFN- β dependent TRAIL-mediated pro-apoptotic AM-AEC cross-talk in IAV-induced lung injury (201).
 Upon IAV infection of AM, PKR is activated and NF κ B translocates to the nucleus. This results in IFN- β formation and release. IFN- β binds in autocrine fashion to AM-expressed IFNAR, inducing STAT-dependent production and release of TRAIL, which in turn acts on AEC. Ligation of TRAIL to DR5 induces an apoptotic signaling cascade promoting lung injury by structural barrier disruption.

2. Aim Of This Work

The aim of the presented work was to address if and by which signaling events Na,K-ATPase was deregulated after IAV-infection, as - despite its prominent function in sodium ion conductance and therefore in fluid homeostasis - the particular role of Na,K-ATPase in the clearance of IAV-induced alveolar edema has not been addressed so far.

Therefore, a potential deregulation of Na,K-ATPase $\alpha 1$ subunit was analysed on mRNA and protein level in primary isolated murine or human alveolar epithelial cells after *ex vivo* and *in vivo* IAV infection. Furthermore, it was addressed in a co-culture model of primary alveolar epithelial cells with resident alveolar or bone marrow-derived macrophages if presence of IAV-infected mononuclear phagocytes would further impact on Na,K-ATPase regulation.

To study if any underlying host- or virus-induced molecular mechanisms leading to a deregulation of Na,K-ATPase were amenable to manipulation and thus could provide possible targets to improve alveolar fluid clearance after IAV infection, Na,K-ATPase expression was determined after IAV infection in presence of specific chemical inhibitors, adenoviral transfer of dominant-negative protein constructs and in lung epithelial cells of respective knockout mouse lines.

Additionally, the impact of those signaling mechanisms on epithelial fluid transport was analysed *in vivo* after IAV infection of wildtype or knockout mice as well as after *in vivo* application of adenoviral over-expression constructs.

Moreover, this work also aimed to reveal if Na,K-ATPase subcellular localization and trafficking was affected by host or viral factors after IAV infection, as a correct basolateral membrane-insertion of Na,K-ATPase is crucial for efficient vectorial fluid transport and thus edema reabsorption.

Together, the ultimate aim of this study was to elucidate the cellular and molecular mechanisms of Na,K-ATPase deregulation during IAV pneumonia, to design novel therapeutics, to improve fluid clearance and outcome in patients with severe virus-induced ARDS.

3. Methods

3.1. Mouse Strains

Wildtype C57BL/6 mice (wt) were purchased from Charles River Laboratories. wt, *trail*^{-/-} mice (212), *ifnar*^{-/-} mice (213), *dr5*^{-/-} mice (214) and *ccr2*^{-/-} mice (215) were housed under specific pathogen-free conditions (SPF) and transferred to IVC conditions upon treatment and monitored 1-3 times per day. Animal experiments were performed at the Northwestern University of Chicago, Department of Pulmonary and Critical Care Medicine within the framework of the IRTG1062 graduate program, and partially at the Justus-Liebig University of Giessen.

3.2. Human Material

Human lung tissue was obtained from patients who underwent lobectomy after informed written consent (Departments of Pathology and Surgery, Justus-Liebig-University, Giessen). Use of human lung tissue samples was approved by the University of Giessen Ethics Committee (Az. 10/06).

3.3. Cell Culture

Cell lines were cultured in cell culture flasks in adequate media at 37°C and 5% CO₂. For passage, cells were detached and singularized with Trypsin-EDTA after washing with PBS. For experiments, cells were passaged on 6-, 12-well or 12-well permeable transwell supports 24h prior to further treatment.

cells	origin	media composition
A549	human adenocarcinoma lung epithelial cell line	HAM F-10, 10% FCS, 1% Amphotericin, 1% Penicillin/Streptomycin, 1% L-Glutamine
MDCK II	canine kidney epithelial cell line (clonal)	DMEM, 10% FCS, 1% Penicillin/Streptomycin, 1% L-Glutamine, 2.5% HEPES
MLE-12	mouse lung epithelial cell line (SV40 transformed)	DMEM, 10% FCS, 1% Penicillin/Streptomycin, 1% L-Glutamine, 2.5% HEPES

DMEM and HAM F-10 were purchased from Gibco/Life Technologies, Carlsbad (USA).

3.4. Primary Murine Alveolar Epithelial Cells

Murine alveolar epithelial cells (AEC) were isolated based on the protocol developed by Corti et al (216). Mice were sacrificed by cervical dislocation. The chest cavity was opened and lungs were perfused with steril HBSS via the right ventricle. To insert dispase into the lung, a small incision was made into the trachea to insert a shortened 21-gauge cannula. This cannula was fixed and 1.5ml of sterile dispase followed by 500 μ l of prewarmed low-melting agarose (1% in PBS) was administered into the lungs to allow enzymatic separation of distal but not proximal epithelial cells. After agarose jellied at room temperature (RT) lungs and trachea were removed, washed in PBS and placed in dispase for 40min at RT. Next, heart, trachea and large airways were removed and the remaining lung tissue was dissected in DMEM/2,5% HEPES plus 0.01% DNase in C tubes using the gentleMACS Dissociator. (Milteny Biotec). Cells were filtered through 70, 40 and 20 μ m cell filters, washed, resuspended in DMEM/2,5% HEPES and counted. Then cells were incubated with biotinylated anti-mouse CD31, CD16/32 and CD45 antibodies for 30 min at 37°C to remove remaining endothelial and lymphoid cells. Antibody amounts were calculated by following equations:

$$\text{number cells}/1,000,000 *0,9 = \mu\text{l of CD45 antibody}$$

$$\text{number cells}/1,000,000 *0,675= \mu\text{l of CD16/32 antibody}$$

$$\text{number cells}/1,000,000 *0,4 = \mu\text{l of CD31 antibody}$$

After incubation, cells were washed and streptavidin-linked magnetic beads (washed thrice with 1ml PBS) were added for 30 min at room temperature with gentle rocking. Amounts of magnetic beads were calculated by following equation:

$$\text{number cells}/1,000,000 /3*50\mu\text{l} = \mu\text{l of magnetic beads}$$

After incubation, magnetic separation was performed for 15 min and remaining cells were washed and resuspended in mAEC medium. The purity of freshly isolated mAEC was assessed by flow cytometry for murine EpCAM (staining epithelial cells) and pro-surfactant protein C (staining type II AEC). Cell suspensions with a purity $\geq 90\%$ were used for further experiments. Cell viability was examined by trypan blue staining and was $\geq 95\%$. Murine AEC were plated at a density of 120-150,000 cells/cm² and grown for 3 days to confluence prior to further treatment.

3.5. Primary Human Alveolar Epithelial Cells

Fresh tissue samples were sheared with forceps and scissors and extensively washed with hAEC medium and filtered through a 100 μ m cell filter. The lung tissue was then stored in hAEC medium at 4°C until further digestion by 2,5% dispase II in 2mM calcium and 1.3mM magnesium for 180 min at 37 °C. Cells were filtered through 100, 40 and 20 μ m cell filters. Epithelial cells were centrifuged for 25min at 1500rpm and 20°C and separated by ficoll density centrifugation for 15 min at 2500rpm at RT. The interphase was collected, washed and resuspended in hAEC medium for subsequent depletion of leukocytes by anti-human CD45 magnetic beads. Beads were added according to manufacturer's protocol and incubated for 15min at 4°C, followed by magnetic separation. The purity of remaining alveolar epithelial cells was assessed by flow cytometry (usually 90-98% epithelial cells). Viability was determined by trypan blue exclusion and was always >95%. Human AEC were plated at a density of 300-450,000 cells/cm² and grown for 5 days until confluence prior to further treatment. For measurement of vectorial water transport, hAEC were seeded at 250,000 cells/cm² in transwell permeable support inserts and cultured for 10 days. Medium was exchanged every second day and cells were exposed to air at the apical side from day 5.

3.6. Primary Alveolar and Bone Marrow-Derived Macrophages

Primary alveolar macrophages (AM) were isolated from bronchoalveolar lavage fluid (BALF), whereas bone marrow-derived macrophages (BMM) were isolated from femur and tibia. Mice were sacrificed by cervical dislocation. For BALF, a small incision was made into the previously exposed trachea to insert a shortened 21-gauge cannula. Mice were lavaged with 10x 500 μ l PBS/ 2mM EDTA. BALF was stored on ice until further treatment. AM were pelleted by centrifugation at 1600rpm for 8min at 4°C and resuspended in AM medium (RPMI, 2%FCS, 1% Penicillin/Streptomycin, 1% L-Glutamine). AM were seeded at a density of 75-100,000 cells/cm² and left to adhere for 2h before further treatment. For isolation of BMM, femur and tibia were removed, cleaned from surrounding tissue and washed in prewarmed BMM medium (DMEM, 10%FCS, 1% Penicillin/Streptomycin, 1% L-Glutamine). Next, the epiphyses were cut, a 18mm-gauge cannula was inserted to flush out the bone marrow with BMM medium. Bone marrow cells were washed with PBS, centrifuged at 1600rpm for 8min at 4°C and filtered through a 40 μ m cell filter. Cells were split into three T75 cell culture flasks, allowed to adhere for 1h to select for BMM and

washed with BMM medium. BMM were then cultured in BMM media containing 25ng/ml GM-CSF, polarizing them towards an M1-like, inflammatory macrophage phenotype. Cells were cultured for 9 days and plated into cell culture plates 24h prior to further treatment at a density of 100-125,000 cells/cm².

3.7. Virus Strains

A/Puerto Rico/8/1934 H1N1	seasonal, mouse adapted Influenza virus originated from Stephan Pleschka, Virology, Gießen (GER) and propagated on MDCK II cells
A/Udorn/1972 (H3N2)	seasonal Influenza virus, egg-grown, kindly supplied by Scott GR Budinger, Chicago (USA)
Ad-Null, Adenovirus	replication deficient adenovirus carrying no construct, purchased from Viraquest, North Liberty (USA)
Ad-DN-AMPK, Adenovirus	replication deficient adenovirus carrying a dominant negative form of the kinase AMPK, purchased from Viraquest, North Liberty (USA)

3.8. Influenza A Virus Propagation And Titration

The virus A/Puerto Rico/8/34 (H1N1) (PR8) was propagated on canine epithelial MDCK II cells. Cells were passaged in a T75-cell culture flask at a ratio of 1:3 a day prior to infection to achieve a 85-90% confluence of the cells at the time point of infection. Cells were washed with PBS and infected with a multiplicity of infection (MOI) of 0.001. The virus dilution was prepared in MDCK II infection media (MDCK medium as described above but supplemented with 0.2% BSA instead of FCS). Cells were inoculated with 5ml virus dilution for 1h at 37°C and 5% CO₂, were then washed and further incubated with 10ml infection medium. Cell culture supernatants containing virus particles released from the infected cells were harvested after 72h and centrifuged at 3000rpm at 4°C for 30min. Supernatants were stored as aliquots at -80°C.

To determine the amount of virus particles capable of multicycle replication (plaque forming units, pfu), MDCK II cells were seeded in 6-well plates a day prior to infection to achieve a confluence of 85-90% at the timepoint of infection. Cells were washed with PBS and infected with 333µl of subsequent 1:10 dilutions of the virus stock in PBS/0.2%BSA, covering a range of dilutions from 1:10³ to 1:10⁹. Virus dilutions were inoculated at 37°C 5% CO₂ for 1h, cells were then washed and covered with 1.5ml Avicel medium (2xMEM,

1% Penicillin/Streptomycin, 0.1% NaHCO₃, 0.2% BSA, 2µg/ml Trypsin-TPCK, 1.25% Avicel). Due to its high viscosity, Avicel prevents viral spread through the cell culture by diffusion of viral particles in the surrounding media and only allows virus spread from cell to cell. Cells were incubated for further 48h at 37°C 5% CO₂ to allow formation of plaques caused by local cell death of infected MDCK II cells. After this incubation, cells were fixed with 4 %PFA for 20min at 4°C followed by permeabilization by 0.3% Triton-X-100 for 15min at RT. Blocking of unspecific antigenic epitopes was performed using Normal Horse Serum (NHS) diluted 1:100 in PBS/0.2%BSA. Plaques were visualized by immunohistochemical staining with anti-Influenza NP antibody diluted 1:100 in PBS/10% NHS/0,05% Tween 80 for 1h at RT followed by a Horse raddish peroxidase (HRP)-marked secondary anti-mouse antibody diluted 1:200 for 1h at RT. Addition of TrueBlue, an HRP-substrate yielding a blue colour after enzymatic progressing, allowed counting of plaques per well.

The titer of the virus stock was calculated by:

$$\text{number of plaques per well} * \text{dilution}^{-1} * 1\text{ml} / 333\mu\text{l} = \text{pfu/ml}$$

3.9. In Vivo Experiments And Preparation Of Animal Materials

3.9.1. Intratracheal Intubation

For *in vivo* IAV infection, mice were premedicated with Atropin (application 0.05mg/kg; diluted in 0.9% sterile NaCl to 0.05mg/ml and applied subcutaneously at 0.02ml per 20g body weight) and anesthetized with Xylazine hydrochloride (application 16mg/kg; diluted in 0.09% sterile NaCl to 3.33mg/ml) and Ketamine hydrochloride (application 100mg/kg; diluted in 0.09% sterile NaCl plus 3.33mg/ml Xylazine hydrochloride to a concentration of 25mg/ml) applied intraperitonally at 0.2ml per 20g body weight.

Mice were kept on a heating pad to minimize loss of body temperature. Achieved anesthesia was verified by pinching of the tip of the tail. Mice were then fixed at the upper teeth and hindlegs in supine position on an intubation stand, and an endotracheal tube was inserted orally, passing the vocal chords into the trachea. Using a Hamilton syringe, mice were inoculated with 500pfu (plaque forming units) of PR8 or 10⁵pfu A/Udorn/307/1972 (H3N2) (Udorn) diluted in 70µl sterile PBS^{-/-}. Endotracheal delivery of adenoviruses was performed at 1x10⁹ pfu in 70µl of 50% sterile PBS and 50% surfactant vehicle (Chiesi, Hamburg (GER)) to ensure equal distribution of the replication-deficient virus in the distal lung (217).

Control groups were inoculated with 70 μ l of sterile PBS without additives. Treated mice were monitored 1-3 times per day.

3.9.1. Adoptive Transfer

For adoptive transfer of exudate macrophages, wt mice were infected with 500pfu of PR8 and lavaged to obtain BALF (as described in 3.6) on d7 pi. The BALF was then centrifuged at 1400rpm for 10min at 4°C and the pelleted cells were incubated with a mixture of antibodies (CD45, Ly6G, CD11b, SiglecF, CD11c) in 250 μ l MACS-buffer (PBS, 7.4% EDTA, 0.5% FCS pH 7,2) for 20min at 4°C. The cells were washed to remove unbound antibodies and were resuspended in 3ml of MACS-buffer. Exudate macrophages ($CD45^{pos}$ $Ly6G^{hi}$ $CD11b^{hi}$ $SiglecF^{low}$ $CD11c^{low}$) were then flow-sorted using a BD FACSAria™ III Cell Sorter. The purity of sorted exudate macrophages was $\geq 93\%$. Sorted exudate macrophages were resuspended in sterile PBS^{-/-} and 30.000 cells per 50 μ l were transferred (i.t.) to PR8-infected *ccr2*-deficient mice on d3 pi, and the effects of transfer with respect to Na,K-ATPase-mediated fluid clearance were analyzed on d7 pi.

3.9.2. Alveolar Fluid Clearance

The rate of fluid removal from the alveolar airspace was assessed by measurements of changes in Evans Blue tagged albumin in an isoosmolar alveolar instillate over 30 minutes as described previously (106). Mice were anesthetized as described in 3.9.1 and maintained supine. Body temperature was monitored using an anal probe and maintained with a heating pad and lamp. The trachea was cannulated with a 20-gauge angiocath. Mice were paralyzed with 2.0mg/kg pancuronium bromide applied intraperitoneally and directly connected to a mouse ventilator (Harvard Apparatus) using a tidal volume of 10 ml/kg at a frequency of 160 breaths per minute and 100% of oxygen. After instillation of 300 μ l isoosmolar (324mOsm) NaCl solution containing 5% Evan's blue tagged (0.15 mg/ml) bovine serum albumin followed by 200 μ l of air, mice were ventilated over 30 minutes. Then fluid was reaspirated from the endotracheal catheter and Evans Blue concentrations were analysed using a microplate reader (Bio-Rad, 620nm filter) and AFC calculated as follows:

$$AFC = 1 - (C_0/C_{30}),$$

where C_0 is the protein concentration before instillation, and C_{30} is the protein concentration of the sample reaspirated after 30 minutes of ventilation.

3.9.3. Blood Gas Analysis

Arterial blood was gained from punctuation of the left ventricle of mice anesthetized as described in 3.9.1 and collected in a capillary. Blood was sampled by the Radiometer ABL 5 containing three electrodes measuring pO₂, pCO₂ and pH.

3.9.4. Preparation Of Lung Homogenate For Flow Cytometry

For analysis of protein expression on lung distal cells by flow cytometry, mice were sacrificed by exsanguination. Lungs were perfused via the right ventricle with sterile PBS. The lung was removed, heart, trachea and the larger airways were dissected and the remaining lobes washed with cold PBS. Lungs were kept in PBS on ice until further processing. Lobes were sheared with forceps and scissors and single cell suspensions made by dissociation of the remaining tissue in 5ml PBS. Cells were pelleted by centrifugation at 800rpm for 8min at 4°C, resuspended in 1ml PBS, counted and adjusted to 10⁷cells/ml.

3.10. In Vitro Experiments

3.10.1. Influenza A Infection Of Cultured Cells

To infect epithelial cell lines or primary cells with PR8, the virus stock was diluted in PBS⁺⁺, 0.2% BSA to the indicated MOI. The final concentration of the inoculum was calculated as follows:

$$\text{Number of cells/well} * \text{MOI} * 1\text{ml/inoculation volume } \mu\text{l} = \text{pfu/ml}$$

The cells were washed with PBS and inoculated with the final virus dilution for 1h 37°C 5% CO₂. After this incubation the virus dilution was removed and replaced by infection medium containing 0.2% BSA instead of FCS. For co-culture experiments, bottom seeded alveolar or BMM were combined with AEC seeded on transwells after PR8 inoculation. Chemicals were added together with the infection medium at the indicated concentrations. Infected cells were kept at 37°C 5% CO₂.

3.10.2. Adenoviral Transduction Of A549 Cells

For adenoviral transduction of epithelial A549, 85-95% confluent cells were starved over night by replacement of A549 medium for HAM F12 containing Penicillin/Streptomycin and L-Glutamine but no FCS. Cells were washed after 12-16h and 5ml of adenoviruses Ad-Null or Ad-DN-AMPK diluted in infection medium to a MOI of 10 were added to the cells. After 6-8h of incubation at 37°C 5% CO₂, cells were washed and the virus inoculum was

replaced by A549 medium. Cells were incubated at 37°C 5% CO₂ for 48h prior to IAV infection for additional 24h.

3.10.3. Transfection Of A549 Cells

A549 were transfected with plasmids for microscopy or with small interfering (si)RNA for knockdown of the Calcium-/Calmodulin kinase kinase β (CaMKKβ) using Lipofectamine 2000. Prior to transfection, cells grown in 6cm cell culture dishes to a confluence of 50-60% were starved over night by replacement of A549 medium for HAM F12 containing Penicillin/Streptomycin and L-Glutamine without FCS. The next morning, 400pmol siRNA and 20μl Lipofectamine were mixed in a volume of 3ml OptiMEM, handshaked for 1min and incubated at RT for 30min to allow formation of siRNA containing micelles. After this incubation, cells were washed with PBS and supplemented with 3ml of micelle-containing OptiMEM. Cells were incubated at 37°C 5% CO₂ and swirled every 30min. The supernatant was exchanged for A549 medium 8h post transfection to minimize Lipofectamine-induced cytotoxic effects. siRNA-transfected cells were incubated at 37°C 5% CO₂ prior to IAV infection for additional 24h prior to further analysis. The following plasmids were used in this study:

pCAGGS plasmids carrying polymerase II driven viral proteins PA, PB1, PB2 and NP or pPol I plasmids coding for HA, NA and M proteins were a kind gift of Thorsten Wolff, RKI Berlin. pCAGGS constructs encoding for polymerase II driven M2 tagged with mCherry fluorescent protein on C- or N-terminus were a kind gift from Alexandra Dudek, Peter Reuther and Martin Schwemmle, Institute of Virology, Freiburg. GFP-Na,K-ATPase α1 (GFP-NKAα1) plasmid was provided by Emilia Lecuona and Iasha Sznajder, Department of Pulmonary and Critical Care Medicine, Chicago. For knockdown experiments, the following siRNAs were used:

siRNA CaMKKβ 5'-UUUCGAAUCAUGGUCUUACCAGGA-3'

siRNA scrambled 5'- ACGUUGUUAUCUAAUCGUCUCGAGA-3'

3.10.4. Vectorial Water Transport

Vectorial transport of water over an electrochemical resistant cell layer of human AEC was determined by changes of FITC-dextran (70kDa) concentrations in apical and basal cell culture media. hAEC were seeded as described in 3.5 in 0,4μm pore size transwell cell culture dishes and cultured until achieving electrochemical resistances of ≥800Ω /cm² as measured by Millicell-ERS2 device. Cells were infected with PR8 at MOI 0.1 or PBS

treated for 1h at 37°C and then supplied with 3mg/ml 70kDa FITC-dextran (Sigma Aldrich) labeled cell culture media including selected inhibitors at indicated concentrations. After 6h of incubation at 37°C, apical and basal media were analysed for FITC-dextran concentration by (FL_x 800, Bio-Tek Instruments). Cells were analyzed microscopically for bound FITC-dextran without apparent differences in the treatment groups. Vectorial water transport (VWT) was calculated by changes in FITC-dextran concentration between apical (C_a) and basal (C_b) media in comparison to starting conditions (C_0):

$$C_0 = [1 - (C_0/C_a)] - [1 - (C/C_b)]$$

3.11. Analysis Of Gene Expression

3.11.1. RNA Isolation

For RNA isolation, cells were washed with PBS and then lysed with 350µl RLT buffer provided by the RNeasy Kit (Qiagen), leading to cell lysis, protein denaturation and thus RNase deactivation. Samples were processed according to the manufacturer's instructions. By adding 350µl ethanol, RNA was precipitated and then bound to a silica membrane, washed and finally eluted in small volumes. RNA amounts were measured using the spectrophotometer Nanovue Plus (GE Healthcare).

3.11.2. cDNA Synthesis

For cDNA synthesis 250ng of isolated RNA plus dH₂O in a total volume of 13.5µl were heated up to 70°C for 5min to break up secondary RNA structures and linearize the RNA. Samples were then put on ice for 3-5min. Next, 11.5µl of PCR Master Mix were added including a reverse transcriptase needed for transcription of RNA into cDNA according to the manufacturer's instructions. Samples were kept at 37°C for 1h and then heated up to 95°C for 5min to inactivate the reverse transcriptase. All incubation steps were performed in a PeqSTAR thermocycler (Peqlab, Erlangern (GER)).

3.11.3. Quantitative Real-Time Polymerase Chain Reaction (qRT-PCR)

qRT-PCR was performed with SYBR green in the AB Step one plus Detection System (Applied Bioscience) using the reaction setup provided by the manufacturer's instructions.

β-Actin expression served as normalization control. Data are presented as ΔCt ($Ct_{\text{target gene}} - Ct_{\text{reference gene}}$). The following primers were used:

β-Actin FP, 5'-ACCCTAAGGCCAACCGTGA-3'

	RP, 5'-CAGAGGCATACAGGGACAGCA-3'
Atp1a1	FP, 5'-CGGAACAGATTGAGCCGAGG-3'
	RP, 5'-ATTCGGGAGTAGTGGGAGGG-3'
Atp1a2	FP, 5'-TGCTTCTTAGCCTACGGTATCC-3'
	RP, 5'-CCGGTGACGATAACTACAGCC-3'
Atp1a3	FP, 5'-AGAATGCCTACCTGGAGCTG-3'
	RP, 5'-ATGAGACCCACAAAGCAAAGG-3'
Atp1b1	FP, 5'-GCTGCTAACCATCAGTGAAC-3'
	RP, 5'-GGGGTCATTAGGACCGGAAGGA-3'
Fxyd	FP, 5'-GAGAATCCCTCGAGTACGACT-3'
	RP, 5'-CAGCGAACCTTTGCTGAGA-3'
Trail	FP, 5'-GAAGACCTCAGAAAGTGGC-3'
	RP, 5'- GACCAGCTCTCCATTCTTA -3'

Primer specificity was validated by analyzing the melt curve of the qRT-PCR product.

3.12. Analysis Of Protein Expression

3.12.1. SDS-PAGE And Western Blotting

To analyze quantitative changes in total protein abundance of infected versus control conditions, cells were treated with NP40-lysis buffer (20mM Tris (pH 7.5), 150mM NaCl, 1mM EDTA (pH 8.0), 1mM EGTA (pH 8.0), 0.5% NP40, 2mM Sodium Orthovanadat (pH 10.0), protease inhibitor, at 20 μ l/cm² confluent cell layer). Cell lysates were transferred to ice for 10min and centrifuged at 10,000rpm for 10min at 4°C to remove cellular debris. The protein concentration in the remaining supernatant was determined using the Dc Protein Assay Kit (Bio-Rad) according to the manufacturer's instructions. The Bradford Assay uses the changes of absorption and emission spectra of triphenylmethane upon binding to protein residues in acidic solution for colorimetric quantification of protein concentration. Colorimetric quantification was performed using a 96-well microplate reader (Bio-rad) at a wavelength of 640nm. For primary cells, 40-50 μ g protein/sample were processed for SDS-PAGE, for cell lines 20-25 μ g of protein were used. To determine Na,K-ATPase levels, samples were diluted in Laemmli buffer (8% SDS, 40% glycerol, 240mM Tris pH 6.8, 0.04% bromphenol blue) and heated up to 37°C for 30min to prevent agglutination of the highly hydrophobic Na,K-ATPase α 1 subunit. For all other analyses samples were heated up to 95°C for 4min. Protein samples were briefly cooled down on ice and centrifuged and then

loaded on 7,5-10% protein TGX mini gels. PAGE (polyacrylamide gel electrophoresis) was performed under denaturing and reducing conditions for 1,5h at 90-120V and 40mA. Proteins were transferred on PVDF membranes at 100V 265mA for 70min. Unspecific epitopes were blocked by incubating the membranes in PBS containing 0.05% Tween 20 and 5% milk powder (blocking buffer) for 1h. The membrane was then incubated with the first antibody diluted in blocking buffer over night at 4°C, then washed three times for 10min in PBS/0.05% Tween 20 and incubated for 1h with an HRP-linked secondary antibody also diluted in blocking buffer. Protein bands were visualized using the chemiluminescent reaction of HRP with luminol, enhanced with ECL plus kit (Bio-Rad), detected with the MicroChemi system (DNR Bio-Imaging Systems Ltd.). Bands were quantified in relation to internal controls (β -Actin, Glut1, AMPK) using ImageJ software.

3.12.2. Surface Biotinylation

To analyze plasma membrane expressed proteins at a given time point, cells were incubated with non-cell permeable EZ-link Sulfo-NHS-SS-Biotin binding unspecifically to all surface located and therefore exposed amine-residues. To prevent internalisation and degradation processes during labeling, all steps were performed with pre-cooled reagents on ice. Cells were washed thrice with PBS and then incubated with PBS⁺⁺ containing 1mg/ml biotin for 20min shaking regularly. To remove unbound biotin, cells were then washed thrice for 10min with 10mM glycine in PBS. Remaining wash solutions were completely aspirated prior to lysis of cells with NP-40 lysis buffer. Cell lysates were kept on ice for 30min, intensively vortexed and then centrifuged at 10,000rpm for 10min at 4°C to pellet cellular debris. The supernatant was subjected to Bradford quantification as described in 3.12.1 . 300 μ g of protein in a total volume of 300 μ l lysis buffer were supplemented with 60 μ l streptavidin-coupled beads and incubated at a rotation speed of 40rpm over night at 4°C, allowing a specific binding of biotin-labeled proteins to the beads. To remove unspecifically bound residues, beads were then washed once with Solution A, twice with Solution B and thrice with Solution C (see 3.5), each time using a volume of 300 μ l and centrifuging the beads at 10.000rpm for 3min at 4°C. To remove bound protein, beads were resuspended in 20 μ l Laemmli buffer and heated up to 37°C for 30min. Beads were centrifuged and the remaining supernatant loaded onto an SDS-PAGE.

Wash Buffers for biotinylation:

- Solution A 150mM NaCl , 50mM Tris pH 7.4, 5mM EDTA pH 8.0

- Solution B 500mM NaCl , 50mM Tris pH 7.4, 5mM EDTA pH 8.0
- Solution C 500mM NaCl , 20mM Tris pH 7.4, 0.2% BSA

3.12.3. Co-Immunoprecipitation

To test for interaction between viral proteins and the Na,K-ATPase, A549 cells grown to confluence in a T75cm² cell culture flask were infected with an MOI of 0.1 for 16h. Cells were then transferred to ice and washed with pre-cooled PBS. Cells were lysed by addition of 1ml IP lysis buffer (20mM HEPES pH 7.4, 150mM NaCl, 0.5% NP-40, 2mM EDTA, 2mM EGTA, 5% glycerol) containing freshly added protease inhibitor and phosphatase inhibitor for 15min on ice. Cells were scraped, vortexed and incubated for additional 10min on ice. Cell lysate was centrifuged at 10,000rpm 5min at 4°C, and supernatants subjected to protein quantification by Bradford Assay. 40µg were incubated with 3µg anti-Na,K-ATPase α1 antibody, anti-Influenza M1, anti-Influenza M2, anti-Influenza NS1, anti-Influenza PB1 or respective IgG controls for 5h at 4°C gently rotating at 20rpm. 30µl protein A/G Plus-agarose beads were blocked for unspecific protein binding with 300µl 3% BSA in PBS for 5h at 4°C. Beads were then centrifuged at 2,000rpm for 3min at 4°C. Cell lysate/antibody suspensions were added to the beads and incubated for additional 4h rotating gently at 4°C. Beads were then washed 5 times with 300µl IP wash buffer (20mM HEPES pH 7.4, 150mM NaCl, 0.1% NP-40, 2mM EDTA, 2mM EGTA, 5% glycerol) containing freshly added protease and phosphatase inhibitor and finally resuspended in 30µl Laemmli buffer. Samples for detection of Na,K-ATPase were warmed up at 37°C for 30min, all other were heated to 62°C for 20min and then subjected to SDS-PAGE and Western Blotting.

3.12.4. Enzyme Linked Immunosorbent Assay (ELISA)

Commercially available ELISA kits were used according to the manufacturer's instructions to determine concentrations of IFN-α, IFN-β, TGF-β, TNF-α and TRAIL released from cells into the cell culture supernatants. Samples stored at -80°C were thawed on ice, and used undiluted or in a 1:2 dilution for ELISA. Samples and standards were transferred to an antibody-coated 96well plate and incubated for specific antibody-epitope reaction. Next, wells were washed, incubated and stained with a soluble, cytokine-specific primary and secondary antibody and cytokine abundance was then quantified by addition of a luminescent substrate and colorimetric detection at the given wavelength in a microplate reader (Bio-rad). Cytokine concentrations were calculated on basis of samples of known concentrations in a standard curve.

3.12.5. Cytometric Bead Array (CBA)

Besides applying ELISA for cytokine quantification, commercially available CBA kits (BD Bioscience) were used for analyzing murine MCP-1, KC, IL-1 α and RANTES in cell culture supernatants. CBAs allow the parallel detection of multiple cytokines in a single sample, as single cytokines are captured by beads having different fluorescent characteristics. These fluorescent variations are detected by flow cytometry (3.12.6), allowing a separate evaluation of multiple bead populations equaling the individual cytokines. The quantification is performed using a detector antibody of different fluorescent characteristics than the capture beads, whose intensity is compared to intensities measured for samples of known concentrations in a standard curve.

3.12.6. Flow Cytometry

Multicolor flow cytometry was performed with an LSR Fortessa using DIVA software (BD Bioscience). 1-5 x 10⁵ cells resuspended in FACS buffer (PBS, 7.4% EDTA, 0.5% FCS pH 7.2, 0.01% NaAz) were stained directly after production of single cell suspensions from lung tissue or cell cultures in 96-well plates. Cells were pelleted by centrifugation at 1200rpm for 3min at 4°C, then resuspended and blocked with 10 μ l Sandoglobulin®. Cells were incubated with fluorochrome-labeled or unlabeled antibodies for 15min at 4°C. Cells were washed between staining steps with 100 μ l FACS buffer and routinely stained before analysis with 7-AAD for dead cell exclusion.

Staining protocol for analysis of Na,K-ATPase α 1 subunit expression:

Staining step	Antibody	Dilution
1	goat anti-Influenza A Virus	1:75
2	donkey anti-goat APC	1:400
	rat anti-CD74	1:100
3	goat anti-rat PE	1:800
4	rat anti-mouse CD326 APC/Cy7	1:50
	rat anti-mouse Podoplanin PE/Cy7	1:40
	mouse anti-human/mouse/rat Na,K-ATPase α 1	1:20
	AlexaFluor 488 or respective mouse IgG AlexaFluor 488	
5	7-AAD	3.5 μ l/sample

For evaluation of cell purity, murine and human AEC were first permeabilized with 0.2% Saponin in PBS for 20min at 4°C and then stained with rabbit anti-human pro-S-PC

followed by goat anti-rabbit APC (1:400) and rat anti-mouse CD326 APC/Cy7 or anti-human CD326 FITC (1:100), respectively. Corresponding isotype antibodies were used as negative controls. Data are presented as median fluorescent intensity (MFI) and were normalized to control groups set to 1 for *ex vivo* experiments. NKA $\alpha 1^+$ AEC from *in vivo* experiments are given as percentage of the epithelial (EpCAM $^+$) cell population.

3.13. Microscopy

3.13.1. Fixation And Preparation Of Lung Tissue For Histology

For histological staining of mouse lung tissue, lungs were clipped at the trachea before opening of the chest cavity, then perfused, removed and fixed for 24h in 4% PFA. Lungs were embedded in Parrafin (Leica ASP200S), cut into 3-5 μ m thick sections and stained with hematoxylin and eosin in the following procedure:

Xylene 5min (twice), 100% ethanol 30sec (twice), 96% ethanol 30sec, 96% ethanol 30sec, 70% ethanol 30sec, 70% ethanol 30sec, hematoxylin 3min, 0.1% HCl 2sec, H₂O 5min, Eosin G solution 3min, H₂O 30sec, 70% ethanol 30sec, 90% ethanol 30sec, 100% ethanol 30sec (twice), xylene 5min (twice).

Analysis was performed with a Leica DM 200 microscope.

3.13.2. Fixation Of Cell Cultures For Immunofluorescence Microscopy

For immunofluorescence microscopy, cells were washed with PBS and then air-dried for 1min at RT. Cells were fixed and permeabilized by a pre-cooled (-20°C) 1:1 aceton/methanol suspension that was left on the cells for 3min at RT. Cells were then washed thrice with PBS/0.3% BSA and blocked with 3% BSA in PBS over night at 4°C.

3.13.3. Fixation Of Lung Tissue For Immunofluorescence Microscopy

Murine lungs were perfused with PBS and then filled with 1.5ml of a 1:1 TissueTek:PBS mixture via an intratracheal 21-gauge cannula. Lungs were then clipped at the trachea, removed and washed in PBS. Lung were then embedded in TissueTek:PBS, frozen in liquid nitrogen and stored at -80°C. Cryoslices of 4-5 μ m thickness were prepared using a Leica CM 1850 UV cryotome. Cryoslices were air-dried and fixed for 20min with 4% PFA at RT. Cryoslices were washed with PBS/0.2% BSA and permeabilized with 0.3% Triton-X-100 for 10min at RT. Cryosliced lungs were blocked using 10% Normal Horse Serum in PBS for 1h at RT.

3.13.4. Antibody Staining and Fluorescent Laser-Scanning Microscopy

For fluorescent microscopy, fixed and blocked samples were incubated with fluorescent-labeled or unlabeled primary antibodies diluted in PBS/0.2% BSA over night at 4°C. If visualization with a secondary, fluorescent-labeled antibody was necessary, samples were washed 5 times for 5 min RT with PBS/0.2% BSA. The secondary antibody was diluted in PBS/0.2% BSA and incubated for 1h RT in the dark. Samples were intensely washed once more before mounting under cover glasses with Vectashield Hard Set mounting medium containing DAPI for nuclear staining. Antibodies were used at the following dilutions: mouse anti-human/mouse/rat Na,K-ATPase α 1 subunit AlexaFluor 555 1:20, mouse anti-Influenza A NP FITC 1:20, mouse anti-Influenza A M1/M2 1:250/1:50, rabbit anti-mouse Occludin 1:20, rabbit anti-mouse ZO-1 1:40, donkey anti-rabbit APC 1:400, chicken anti-goat AlexaFluor 488 1:400. Fluorescent laser-scanning microscopy was performed using a Leica TCS SP5 confocal microscope with 63x ocular and pinhole of 60 μ m. Z-Stacks were acquired using a 0.4 μ m distance between stacks. Acquired pictures were analyzed using LAS AF software.

3.13.5. Live Cell Imaging

Live cell imaging was performed with A549 cells 24h post transfection with plasmids encoding for Na,K-ATPase α 1 subunit coupled with GFP (green fluorescent protein) (GFP-NKA α 1) and viral matrix protein 2 coupled to mCherry (mCherry-M2). Data were acquired in cooperation with Vladimir Gelfand and Joshua Rappoport, Northwestern University of Chicago, at a Nikon eclipse Ti inverted microscope with a 63x ocular, with approximately 8-10 frames per laser/filter per minute in xy axis. Colocalization and -transport were analyzed using FIJI/ImageJ software.

3.14. Statistics

All data are given as mean \pm SEM. Statistical significance of two groups was analyzed by unpaired Student's *t* test. Statistical difference of three or more groups were analyzed by one-way ANOVA and post-hoc Tukey (GraphPad Prism 5). A *p* value less than 0.05 was considered significant, **p*<0.05; ***p*<0.01; ****p*<0.005

4. Results

4.1. Impaired alveolar fluid clearance after IAV infection is associated with decreased expression of Na₊K₊-ATPase α1 subunit on alveolar epithelial cells

To address the extent of acute lung injury in mice infected with IAV, alveolar fluid clearance capacities, oxygenation and alveolar edema formation was monitored in animals infected with 500PFU of PR8 (H1N1). A substantial impairment of alveolar fluid clearance (AFC) was present already at day 2 (d2) and was even more pronounced at d7 post infection (pi) (Figure 4-1 A). Reduced AFC capacities d7 pi were paralleled by severe hypoxemia (Figure 4-1 B) as well as alveolar edema formation (Figure 4-1 C).

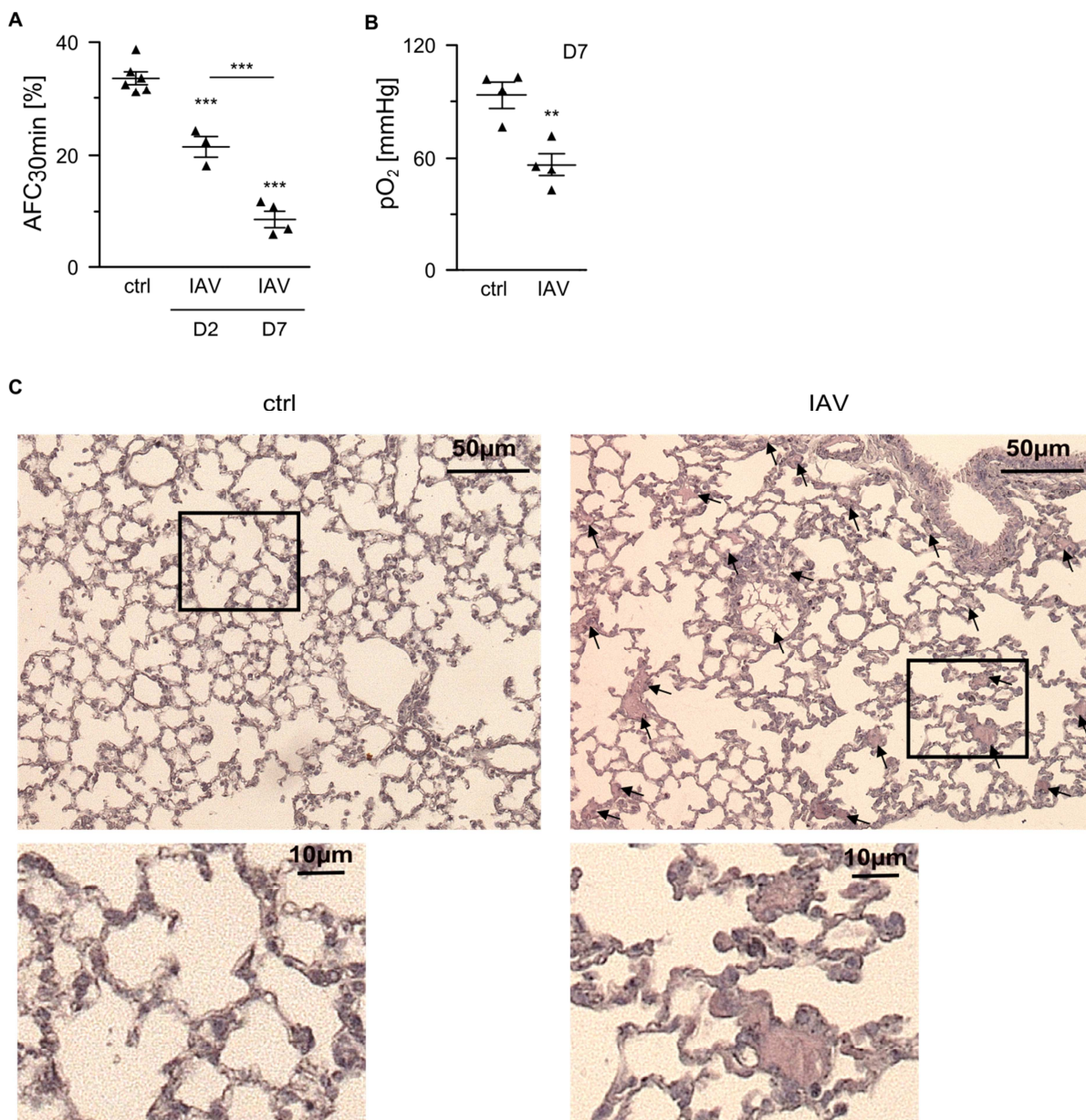


Figure 4-1 Murine PR8 infection promotes formation of alveolar edema. (A) *In vivo* alveolar fluid clearance (AFC) capacities 2 or 7 days after inoculation of mice with PBS (ctrl) or 500PFU PR8 (IAV) in n = 3-6 mice. (B) Arterial partial pressure of oxygen (pO₂) measurements 7 days after inoculation of mice with PBS (ctrl) or 500PFU PR8 (IAV) in n = 3 mice. (C) Representative sections of n=3 murine lungs 7 days after PBS (ctrl) or 500PFU PR8 inoculation *in vivo*, stained

with hematoxylin and eosin. Arrows mark edematous regions in overview, boxes represent regions magnified in the lower panel.

To determine whether IAV infection would impact on expression levels of Na,K-ATPase as the main driving force of AFC, the expression of Na,K-ATPase α 1 subunit (NKA α 1) which mediates the channel function of the ion pump complex was analyzed in primary isolated alveolar epithelial cells (AEC) after *ex vivo* PR8 infection. In murine AEC, mRNA of Na,K-ATPase subunit isoforms α 1, α 2, α 3, β 1 and FXYD protein was detectable (Figure 4-2). Yet, gene expression levels of NKA α 1 were not significantly altered at 6h and 24h post IAV infection in cultured AEC.

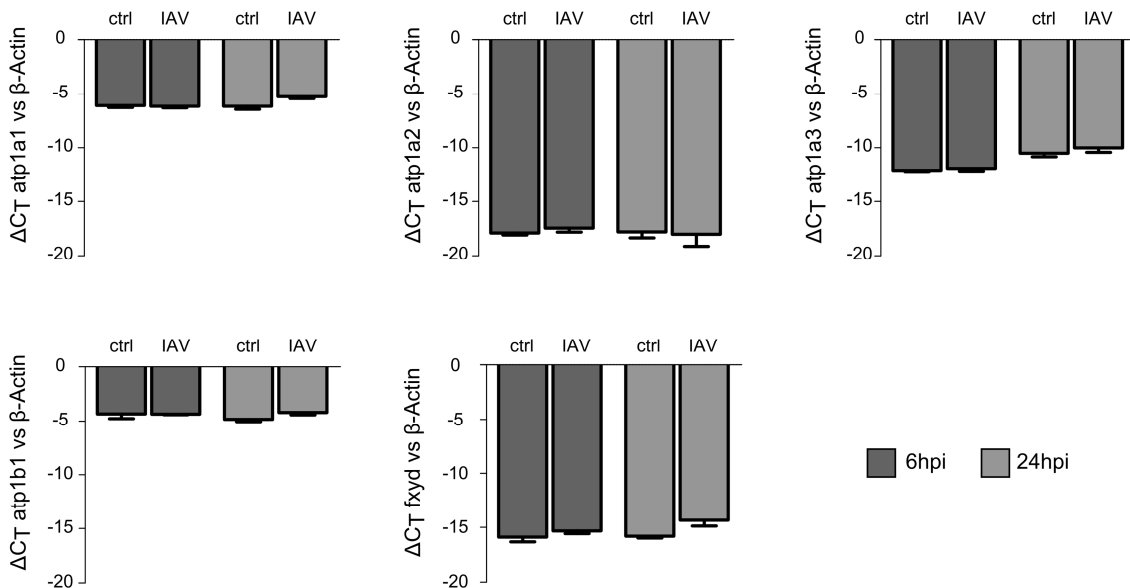


Figure 4-2 Na,K-ATPase subunit mRNA expression in murine (m-) AEC 6 hours and 24 hours post infection (hpi).

Murine AEC were treated with PBS (ctrl) or infected with PR8 at MOI 0.1 (IAV) and processed for quantitative real-time PCR 6h and 24hpi. Bar graphs represent means \pm SEM of 3 independent experiments.

However, when looking at protein abundance of NKA α 1 by Western blot, levels of total protein were significantly decreased at 16 and 24hpi in murine (m)AEC (Figure 4-3 A) and at 16hpi in human (h)AEC (Figure 4-3 B), demonstrating that IAV infection impacts on NKA α 1 protein expression in AEC.

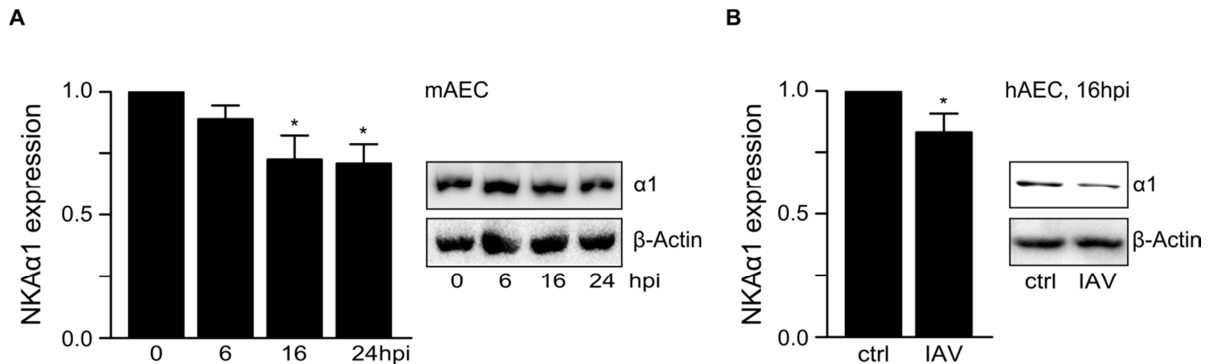


Figure 4-3 Total abundance of NKA α 1 protein is decreased in AEC after PR8 infection. (A,B) Densitometric quantification of western blot analyses of Na,K-ATPase α 1 subunit (110kDa) expression in relation to β -Actin (42kDa) in total cell lysates of (A) murine AEC inoculated *ex vivo* with PR8 at MOI 0.1 for the indicated time points or (B) human AEC inoculated with PBS (ctrl) or PR8 at MOI 0.1 for 16h. Representative Western blots and bar graphs show means \pm SEM of 7-9 independent experiments.

Na,K-ATPase is stored in large quantities in internal reservoirs but is only actively contributing to ion transport and fluid clearance when expressed on the basolateral cell membrane (98, 99). Therefore, we investigated NKA α 1 surface expression by cell membrane biotinylation and subsequent pulldown or by flow cytometry in *ex vivo* infected AEC (gating strategy shown in Figure 4-4 A).

Indeed, surface abundance of NKA α 1 was reduced on mAEC in the time course of infection (Figure 4-4 B, C) and profoundly decreased on hAEC at 16hpi (Figure 4-4 D, E). FACS analyses revealed that NKA α 1 was expressed on both type I and type II AEC, identified by staining with Podoplanin/T1 α or CD74 (218, 219), respectively (gating Figure 4-4 F), and equally decreased following infection (Figure 4-4 G, H).

Of note, plasma membrane expressed NKA α 1 was also significantly reduced on distal lung epithelial cells isolated from *in vivo* infected mice 2d pi. This decrease was even more pronounced at 7d pi (Figure 4-4 I). The kinetics of the decrease in membrane bound NKA α 1 correlated closely with the reduction of alveolar fluid clearance and the increase in formation of edema in the murine lung (Figure 4-1 A, C).

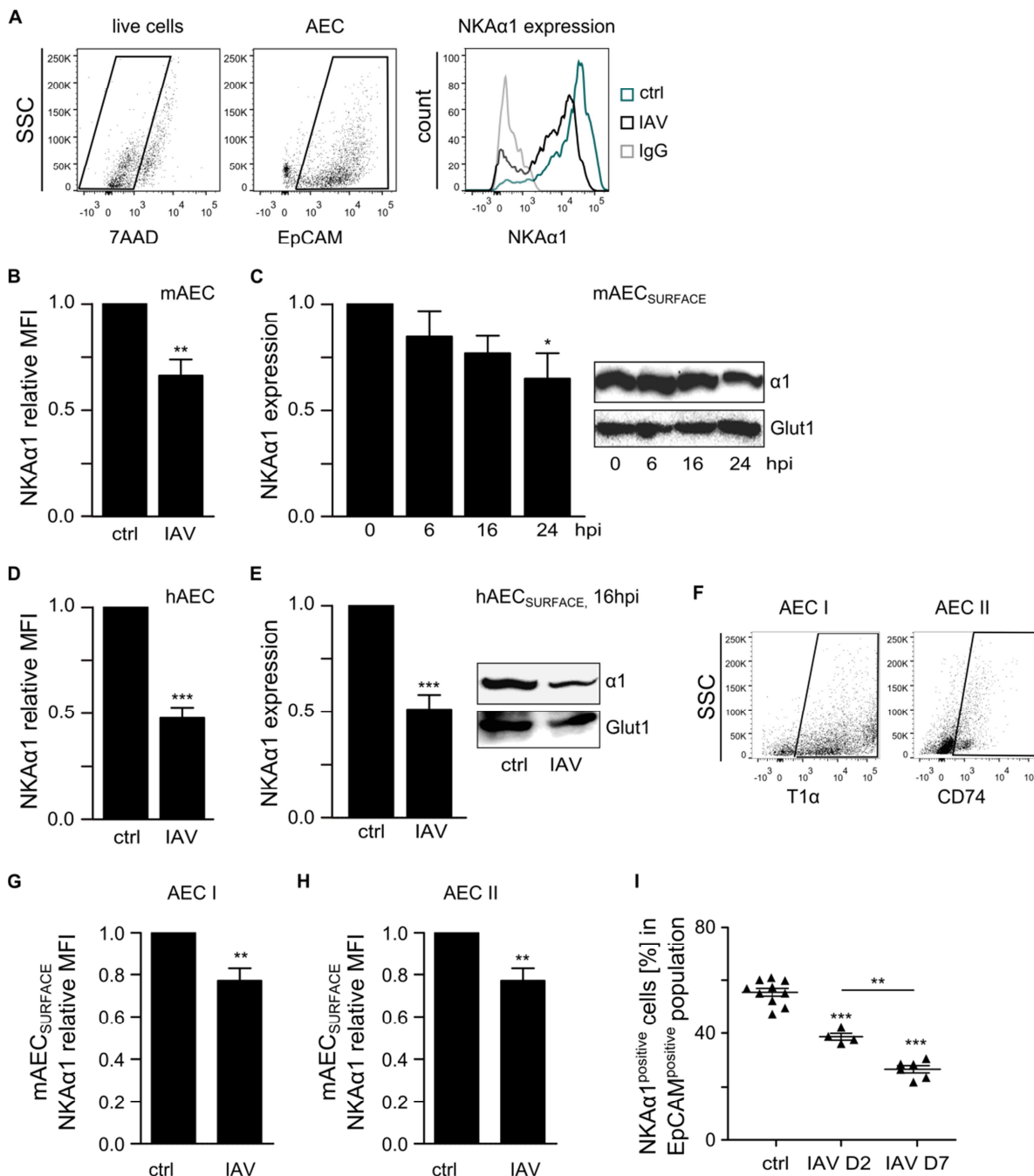


Figure 4-4 Plasma membrane expressed NK α 1 is decreased upon IAV infection *ex vivo* and *in vivo*. (A) Gating strategy showing representative dot plots for live cells (7AAD^{-}), epithelial cells (EpCAM^{+}) and a representative histogram of $\text{NK}\alpha 1^{+}$ staining or the respective IgG controls from AEC cultures. (B, D) Relative median fluorescent intensities intensity (MFI) of $\text{Na},\text{K}-\text{ATPase } \alpha 1$ detected by FACS on live (B) mAEC or (D) hAEC treated *ex vivo* with PBS or PR8 at MOI 0.1 for 24h or 16h, respectively. (C, E) Densitometric analysis of $\text{Na},\text{K}-\text{ATPase } \alpha 1$ subunit expression in comparison to the housekeeping protein Glucose transporter 1 (Glut1, 55kDa) within the cell surface fraction of PR8-infected (C) mAEC at the indicated time points or (E) hAEC 16hpi. (F) Gating strategy showing representative dot plots for AEC I ($\text{T1}\alpha^{+}$) or AEC II (CD74^{+}). (G, H) Relative median fluorescent intensities intensity (MFI) of $\text{NK}\alpha 1$ detected by FACS on live (G) AEC I or (H) AEC II treated *ex vivo* with PBS or PR8 at MOI 0.1 for 24h. (I) Flow cytometric analysis of $\text{NK}\alpha 1$ expression on EpCAM^{+} epithelial cells from distal lung homogenate of PBS (ctrl) or 500 PFU PR8 (IAV) inoculated wt mice 2d or 7d pi. Values of PBS-treated control conditions were normalized to 1. Bar graphs represent means \pm SEM of 5-6 independent experiments for (B, D, E, G, H) and 8 independent experiments for (C).

4.2. A paracrine epithelial-macrophage crosstalk via epithelial type I IFN and IFN-dependent macrophage TRAIL reduces NKA α 1 surface expression on AEC

Interestingly, the analysis of plasma membrane expressed NKA α 1 in correlation to the expression of viral hemagglutinin (HA) in infected AEC (gating Figure 4-5 A) yielded that surface expressed NKA α 1 on mAEC as well as on hAEC was predominantly reduced within the non-infected, HA negative fraction of AEC (Figure 4-5 B, C). This finding was confirmed *in vivo*, where distal lung epithelial cells similarly displayed a decrease of NKA α 1 primarily in non-infected cells (Figure 4-5 D), suggesting that NKA α 1 was not decreased directly by a viral factor within the infected cell, but that a paracrine cross-talk within the alveolar epithelium might be involved.

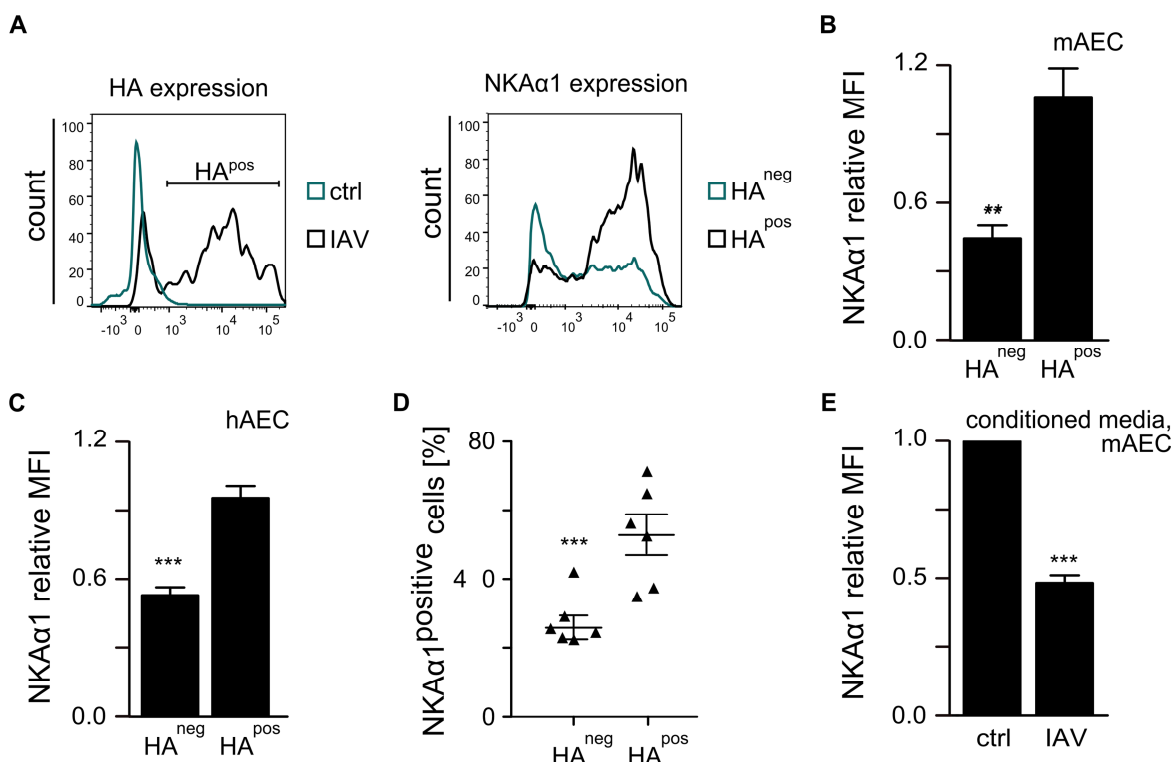


Figure 4-5 Plasma membrane expressed NKA α 1 is decreased by paracrine cross-talk elicited by infected epithelial cells. (A) Gating strategy showing representative histograms for IAV infected mAEC positive for viral hemagglutinin (HA^{pos}) and NKA α 1 expression on HA^{neg} or HA^{pos} AEC. (B, C) depict NKA α 1 MFI of the HA^{pos} versus HA^{neg} cell population in mAEC (B) or hAEC (C) cultures infected *ex vivo* with PR8 at MOI 0.1 for 24h and 16h, respectively. (D) Flow cytometric analysis of NKA α 1 expression on HA^{neg/pos} epithelial cells from distal lung homogenate of wt mice infected with 500PFU at 7d pi. (E) Analysis of NKA α 1 MFI of mAEC treated for 2h with conditioned media from 16h infected (IAV) or PBS-treated (ctrl) cells. For (B-F), values of PBS-treated control conditions were normalized to 1. Bar graphs show means \pm SEM of n = 3 experiments for (B, C), n = 6 for (D) and n = 4 for (E).

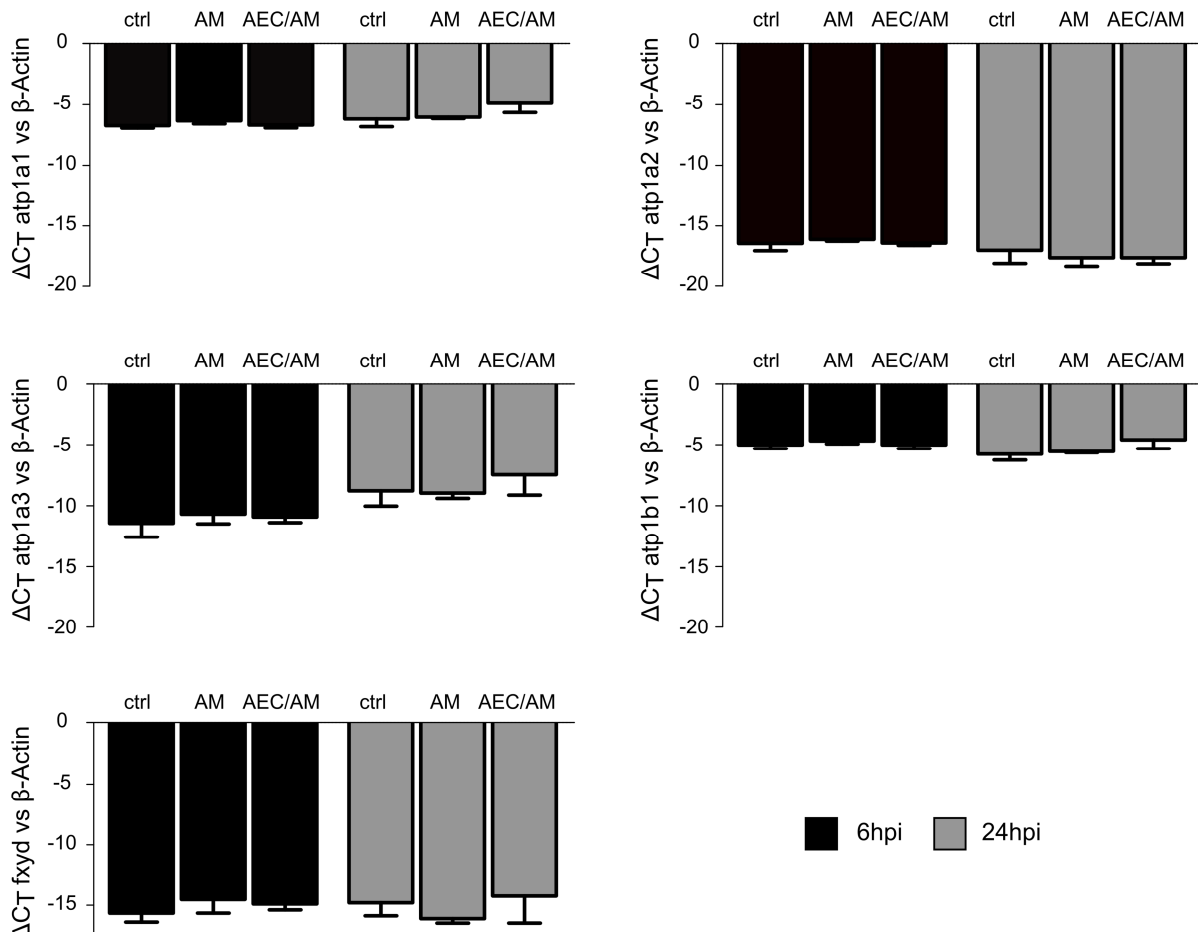


Figure 4-6 Na,K-ATPase subunit mRNA expression in murine (m-) AEC co-cultured with AM 6 hours and 24 hours post infection (hpi). Murine AEC were co-cultured with AM without infection (control), infection of only AM (AM), or both cell types (AEC/AM) at MOI 0.1. AEC were processed for quantitative real-time PCR 6h and 24hpi. Bar graphs represent means \pm SEM of 3 independent experiments.

Indeed, treatment of mAEC with conditioned media of infected, but not of PBS-treated mAEC was sufficient to decrease NKA α 1 surface expression (Figure 4-5 E). Given previous findings that both resident alveolar (AM) and bone marrow-derived (BMM) lung macrophages substantially contribute to AEC damage (175, 182), a co-culture model of AEC and macrophages was applied to address whether presence of AM or BMM would further decrease Na,K-ATPase expression. In line with our results from the AEC monoculture model, NKA α 1 gene expression levels were not changed in co-culture with alveolar macrophages (AM), independently of infection of either cell type (none of the cell types infected (ctrl), only AM infected (AM), or both cell types infected (AEC/AM)) (Figure 4-6). However, we observed that in the co-culture model, presence of infected AM or BMM alone significantly reduced AEC total (Figure 4-7 A, B) and surface expressed (Figure 4-7 C, D) NKA α 1 protein, respectively. Infection of both cell types (AEC/AM or AEC/BMM)

added to the effects observed in cultures of infected mAEC (Figure 4-7). As epithelial cells and macrophages were in no physical contact to each other, these results implied an additional involvement of a macrophage-released mediator in the observed downregulation of plasma membrane NKA α 1.

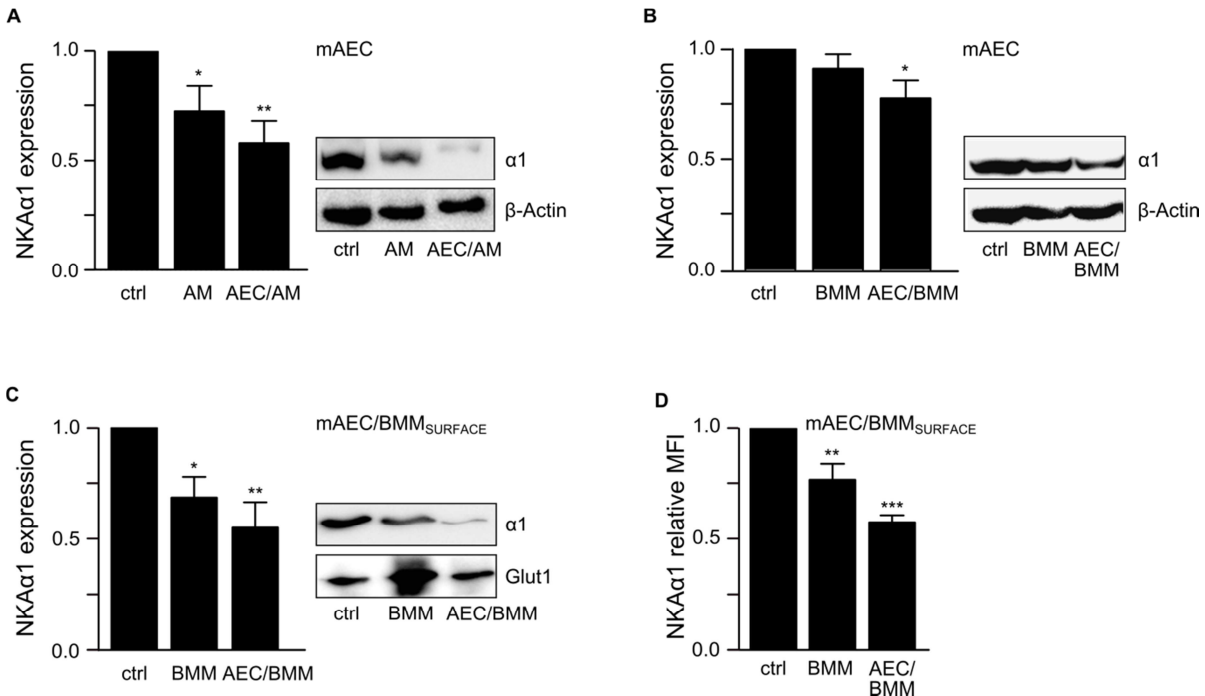


Figure 4-7 Total and plasma membrane expressed NKA α 1 is decreased in presence of infected macrophages. (A-C) Densitometric analysis of total (A, B) or surface expressed (C) NKA α 1 in mAEC co-cultured with AM (A) or BMM (B, C) without infection (ctrl), infection of only macrophages (AM; BMM) or of both cell types (AEC/AM; AEC/BMM) for 24h with PR8 at MOI 0.1. (D) Relative median fluorescent intensities intensity (MFI) of NKA α 1 detected by FACS on live mAEC co-cultured with BMM without infection (ctrl), infection of only macrophages (BMM) or of both cell types (AEC/BMM) for 24h with PR8 at MOI 0.1. Bar graphs represent means \pm SEM of n = 7-9 experiments for (A-C) and n = 6 for (D).

To identify soluble factors within the AEC-macrophage cross-talk network that mediated the observed effect on NKA α 1 abundance, we analyzed co-culture supernatants for pro-inflammatory cytokines by ELISA and Cytometric Bead Array (Figure 4-8). Interferon- α (IFN α) and - β (IFN β) were found to be highly released from infected AEC (Figure 4-8 A, B), whereas TRAIL (TNF-related apoptosis-inducing ligand), TNF- α (tumor necrosis factor alpha), TGF- β (transforming growth factor beta), KC (keratinocyte chemoattractant), RANTES (regulated on activation, normal T cell expressed and secreted), MCP-1/CCL2 (monocyte chemoattractant protein 1) and IL-1 α (Interleukin-1 alpha) were primarily detected in presence of BMM (Figure 4-8 C-I).

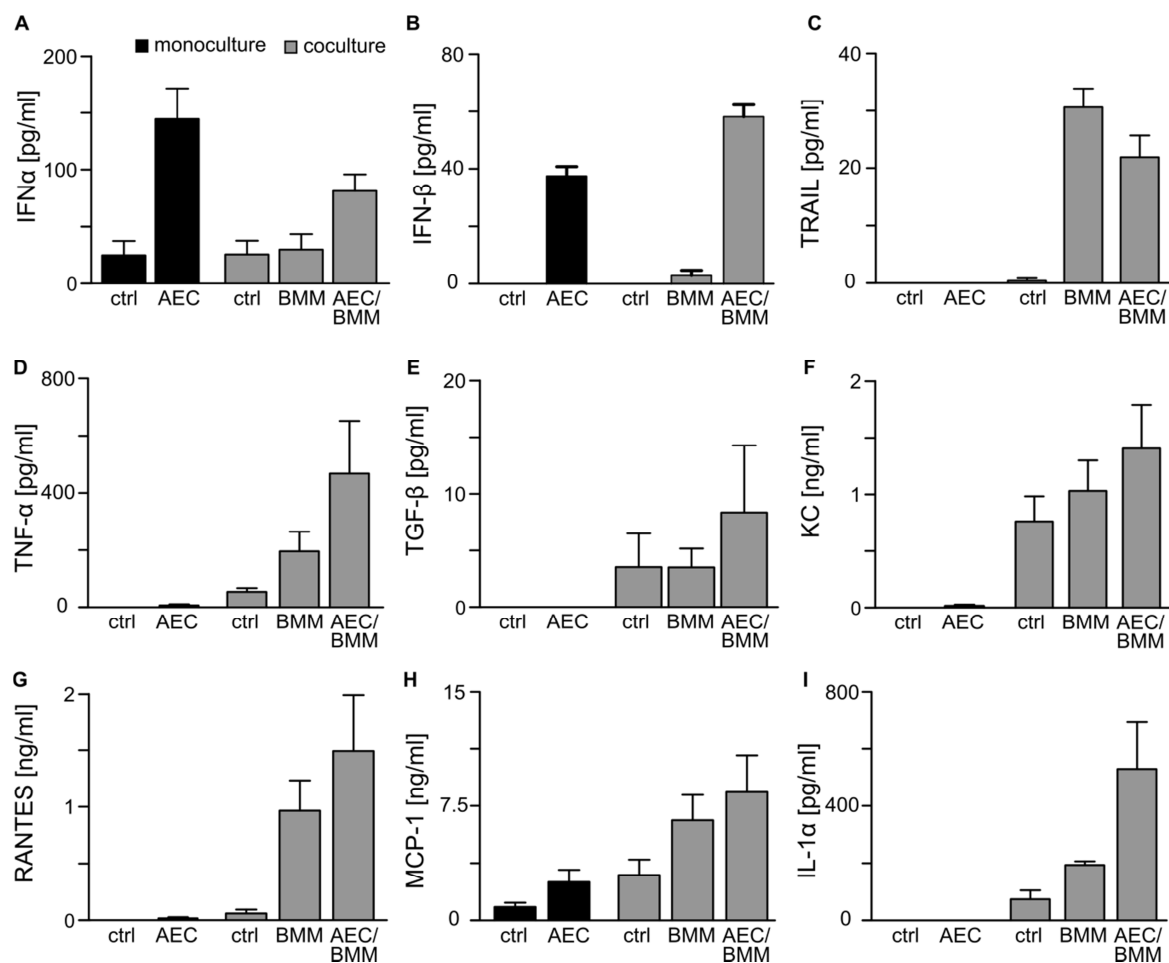


Figure 4-8 Cytokine expression in cell culture supernatants 24h after IAV infection. Cell culture supernatant was collected from AEC monocultured (black bars) and treated with PBS (ctrl) or infected with PR8 at MOI of 0.1 for 24h (IAV) or from AEC co-cultured with BMM (grey bars) without infection (ctrl), infection of only BMM (BMM) or infection of both cell types (AEC/BMM) with PR8 at MOI 0.1 for 24h. Analysis of IFN α (A), IFN β (B), TRAIL (C), TNF- α (D) and TGF- β (E) were performed by ELISA, whereas KC (F), RANTES (G), MCP-1/CCL2 (H) and IL-1 α (I) were analyzed by cytometric bead array. Bar graphs represent means \pm SEM of n = 3-5 experiments.

It was recently demonstrated that type I IFN-dependent release of TRAIL by IAV-infected AM is a major contributor to IAV-induced pathogenesis, leading to alveolar epithelial apoptosis and hence disrupting the structural integrity of the alveolar epithelial barrier (45, 201). Therefore, type I IFN and TRAIL were considered as top candidates to impact on NKA α 1-dependent fluid clearance in the non-infected AEC fraction after IAV infection.

As shown before for AM (201), the release of TRAIL by BMM was type I IFN-dependent, demonstrated by use of BMM isolated from type I IFN receptor-deficient mice (*ifnar*^{-/-}) (Figure 4-9 A). Treatment of uninfected AEC with either IFN α or TRAIL diminished plasma membrane expressed NKA α 1, and combined treatment with both IFN α and TRAIL reduced NKA α 1 to similar levels as co-infection of AEC and BMM (Figure 4-9 B).

Recombinant IFN β did not influence NKA α 1 levels directly. When using *ifnar*^{-/-} AEC to block paracrine IFN α signaling between PR8 infected and non-infected AEC in monocyte, NKA α 1 abundance was rescued at 24hpi, whereas *trail*^{-/-} AEC still displayed a strong decrease in NKA α 1 expression (Figure 4-9 C), suggesting that in absence of macrophages, NKA α 1 surface downregulation was solely dependent on signaling through type I interferon.

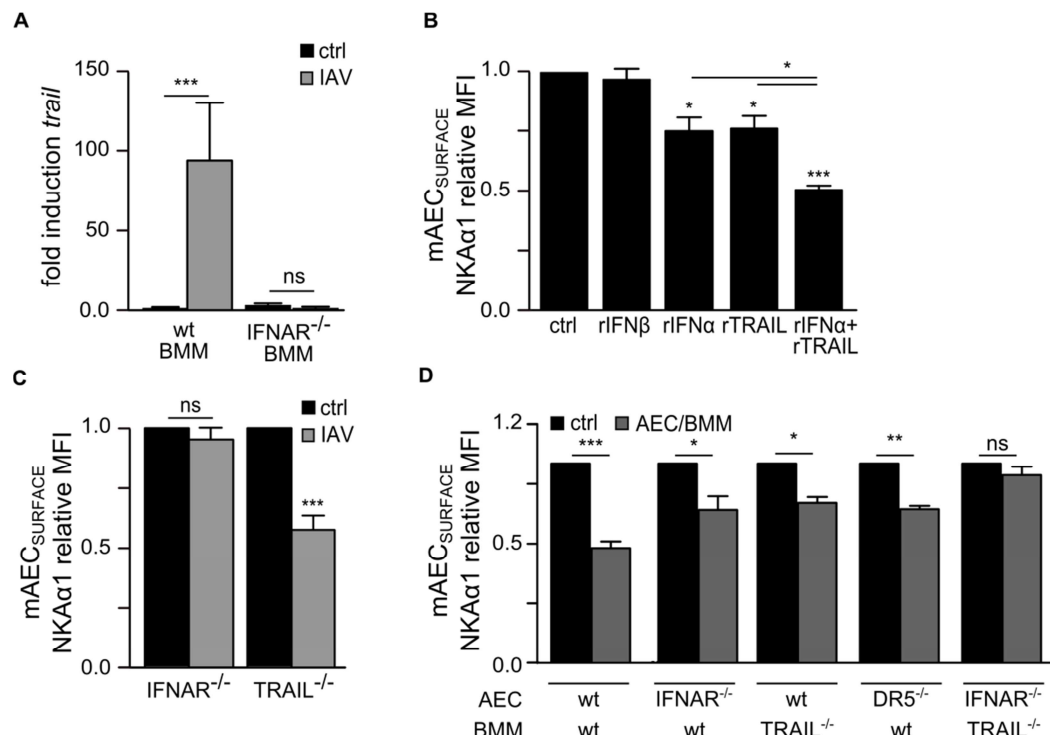


Figure 4-9 PR8-induced loss of Na,K-ATPase surface expression is dependent on an IFN-TRAIL signaling loop involving epithelial IFN α and type I IFN-induced macrophage TRAIL. (A) TRAIL mRNA expression quantified by qRT-PCR in non-infected (ctrl) or PR8 infected (IAV; MOI 1, 16hpi) BMM isolated from wt or interferon- α / β receptor (IFNAR) deficient mice. (B-D) NKA α 1 relative MFI on (B) mAEC treated with 10ng recombinant IFN β (rIFN β), 25U/ml mouse recombinant IFN α (rIFN α) or/and 100pg/ml mouse recombinant TRAIL (rTRAIL) for 16h; (C) mAEC derived from IFNAR or TRAIL deficient mice inoculated with PBS (ctrl) or PR8 at MOI 0.1 (IAV) and incubated for 24h. (D) mAEC derived from wt, IFNAR $^{-/-}$ or death receptor (DR5) deficient mice co-cultured with BMM from wt or TRAIL $^{-/-}$ mice and infection of none (ctrl) or both cell types (AEC/BMM) with PR8 at MOI 0.1 for 24h *ex vivo*. Values of PBS-treated control conditions were normalized to 1. Bar graphs represent means \pm SEM of 3 independent experiments for (A), 6-8 independent experiments for (B) and 4-6 independent experiments for (C, D).

Next, co-culture infections were performed using AEC and BMM from wildtype (wt), *ifnar*^{-/-}, *trail*^{-/-}, or *dr5*^{-/-} (death receptor 5; TRAIL receptor) mice to define the role of the type I IFN/TRAIL/DR5 signaling network in basolateral NKA α 1 plasma membrane abundance after IAV infection. These studies revealed that lack of IFNAR signaling in AEC together

with lack of TRAIL in BMM completely prevented NKA α 1 surface downregulation on AEC. Partial blockade of the IFN-TRAIL signaling loop by combination of *ifnar*^{-/-} AEC with wt BMM (allowing BMM TRAIL action), or of either wt AEC with *trail*^{-/-} BMM or *dr5*^{-/-} AEC with wt BMM (allowing AEC type I IFN signaling) correspondingly resulted in partial decrease of plasma membrane NKA α 1 (Figure 4-9 D). Together, these data indicate that IAV-induced downregulation of epithelial surface NKA α 1 depends on a signaling network between AEC and macrophages, involving epithelial type I IFN and IFN-dependent macrophage TRAIL interacting with its receptor DR5.

4.3. IAV-induced reduction of NKA α 1 in AEC is mediated by the kinases CaMKK β and AMPK

Na,K-ATPase internalization was found to be mediated by activation of AMP-activated protein kinase (AMPK) during lung injury-associated epithelial dysfunction (108, 120). It was therefore tested if AMPK was involved in regulation of NKA α 1 abundance after IAV infection. As shown in Figure 4-10 A&B, AMPK was activated after PR8 infection in AEC mono-cultures and AEC/BMM co-cultures, demonstrated by phosphorylation of the AMPK downstream substrate acetyl-CoA carboxylase (pACC) (220).

Incubation of AEC with conditioned media of IAV-infected AEC and treatment with rTRAIL or rIFN α were sufficient to induce AMPK activation (Figure 4-10 C, D). Treatment of AEC with the AMPK activator AICA-Riboside (AICAR) served as positive control (Figure 4-10 D) (221, 222). AICAR treatment led to decreased abundance of basolateral NKA α 1 in non-infected AEC but did not further decrease it in IAV-infected AEC. Importantly, chemical inhibition of AMPK by Compound C restored NKA α 1 levels in AEC after IAV infection (Figure 4-10 E) (223). Compound C treatment increased basolateral NKA α 1 levels beyond those found in uninfected controls in AEC/BMM co-cultures after IAV infection of either BMM alone or both AEC and BMM (Figure 4-10 F). In addition, adenoviral overexpression of a dominant-negative AMPK (DN-AMPK) in A549 cells rescued NKA α 1 expression after IAV infection (Figure 4-10 E).

Both transforming growth factor beta-activated kinase 1 (TAK1) and Calcium/Calmodulin-dependent protein kinase kinase β (CaMKK β) are possible upstream kinases of AMPK (224). It could be demonstrated that chemical inhibition of CaMKK β by STO-609 resulted in complete inhibition of AMPK activity and restored surface NKA α 1 on mAEC after IAV infection, whereas inhibition of TAK1 by (5Z)-7-Oxozeanol (Oxozeanol) (225) caused

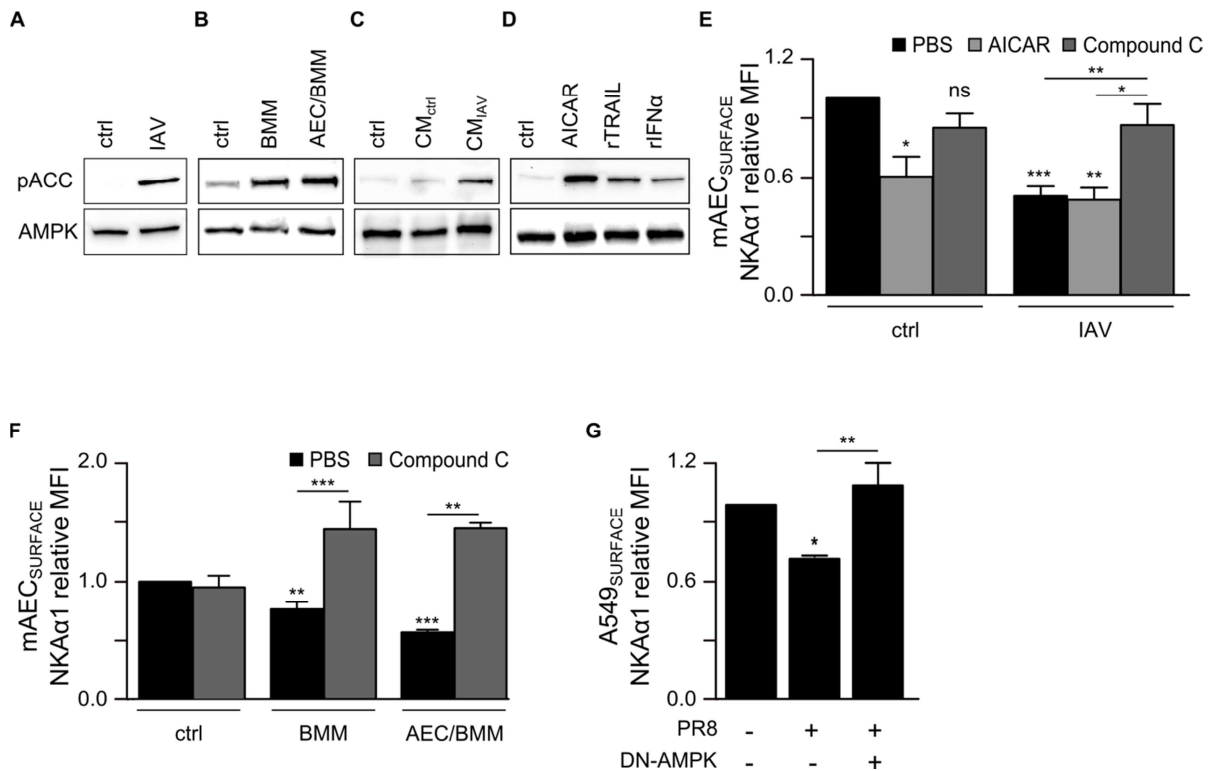


Figure 4-10 IAV-induced loss of Na,K-ATPase α1 subunit surface expression is mediated by activation of AMPK.

(A-D) Representative Western blots of $n = 3-4$ independent experiments of the AMPK substrate phospho-acetyl-CoA carboxylase (pACC, 280kDa) and AMP-activated protein kinase (AMPK, 62kDa). (A) mAEC were infected with PBS (ctrl) or PR8 (IAV) and incubated for 24h. (B) Co-cultures of murine AEC and BMM were left un-infected (ctrl), only macrophages were infected (BMM) or both cell types were infected (AEC/BMM). (C) mAEC were treated with conditioned media (CM) of 16h PR8-infected (IAV) or PBS-treated (ctrl) mAEC for 2h. (D) mAEC treated with the AMPK activator AICAR (1mM), rTRAIL (100pg/ml) or rIFN α (25U/ml) for 16h. (E) Relative MFI of NKA α 1 on mAEC inoculated with PBS (ctrl) or PR8 (IAV) and incubated for 24h without additional treatment or in presence of 1mM AICAR or 20 μ M of the AMPK inhibitor Compound C. (F) Relative MFI of NKA α 1 on mAEC co-cultured with BMM without infection (ctrl), infection of only macrophages (BMM), or both cell types (AEC/BMM) *ex vivo* with PR8 and treated with 20 μ M Compound C for 24h. Values of PBS-treated control conditions were normalized to 1. (G) Relative MFI of NKA α 1 on A549 cells transduced with DN-AMPK for 24h prior to treatment with PBS (ctrl) or PR8 for additional 24h. All bar graphs represent means \pm SEM of 4-6 independent experiments.

partial inhibition of AMPK activity without affecting NKA α 1 expression (Figure 4-11 A, B). SiRNA knockdown of CaMKK β fully restored NKA α 1 expression on A549 cells after IAV infection and prevented AMPK activation (Figure 4-11 C, D). In addition, chelation of intracellular calcium needed for CaMKK β activation by BAPTA-AM increased NKA α 1 expression on mAEC after IAV infection (Figure 4-11 B). To determine whether restored surface NKA α 1 levels after IAV-infection would result in improved vectorial water transport, FITC-dextran containing media was added to transwell-grown, highly confluent hAEC and analyzed increase in FITC-dextran concentrations in the apical versus basal

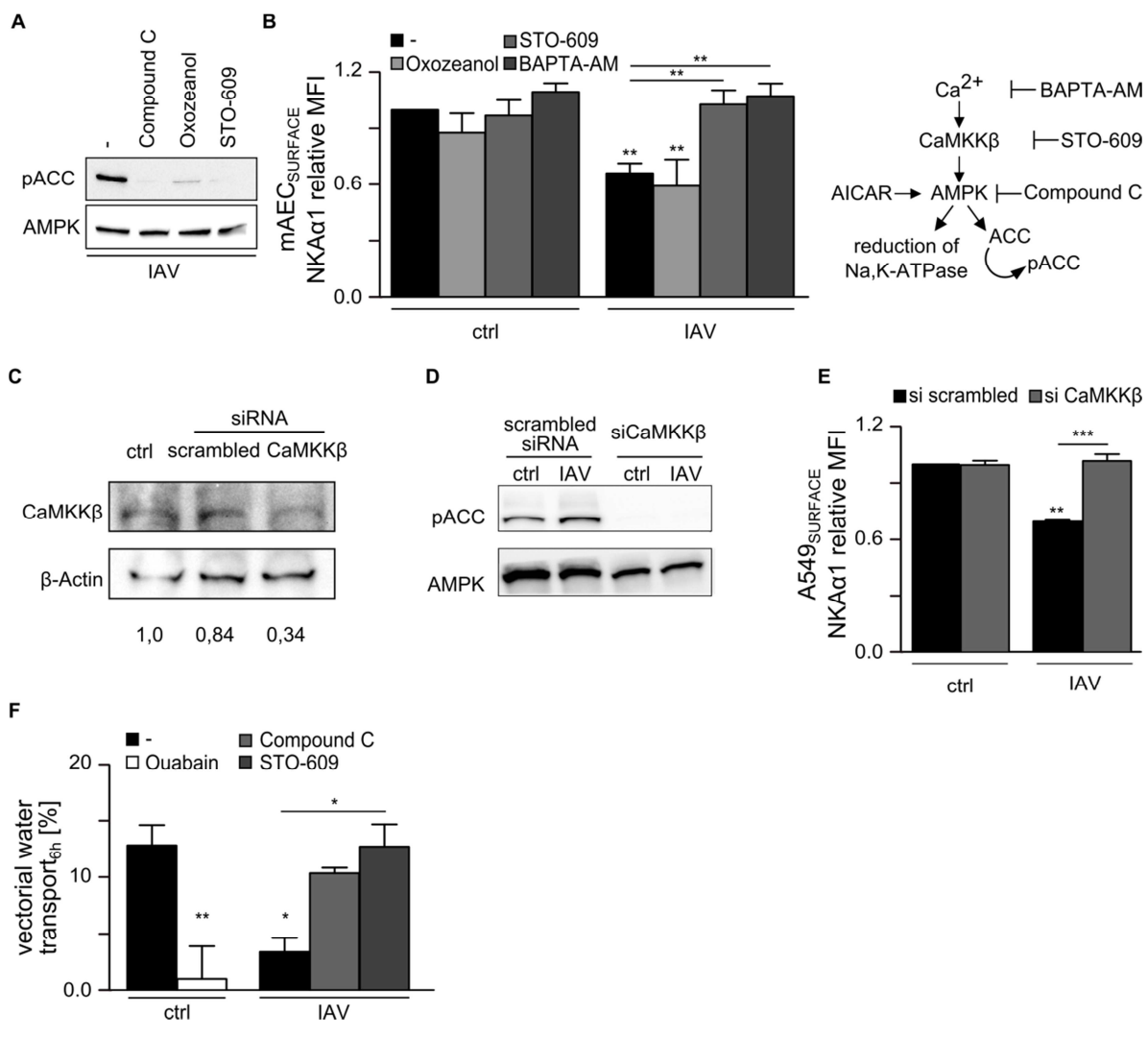


Figure 4-11 Calcium-dependent activation of CaMKK β is upstream of IAV-induced AMPK activation and subsequent loss of Na,K-ATPase a1 subunit surface expression. (A) Representative Western blot of n = 3-4 independent experiments of AMPK and its downstream substrate pACC from 24h PR8-infected mAEC without additional treatment or in presence of 20 μ M Compound C, 0,1 μ M TAK1 inhibitor (5Z)-7-Oxozeanol or the 0,5 μ M CaMKK β inhibitor STO-609. (B) Relative MFI of NKA α 1 on mAEC inoculated with PBS (ctrl) or PR8 (IAV) and incubated for 24h without additional treatment or in presence of 20 μ M Compound C, 0,1 μ M (5Z)-7-Oxozeanol, 0,5 μ M STO-609 or 10 μ M of the Ca²⁺ chelator BAPTA-AM and schematic depiction of the used inhibitors. Bar graphs represent means \pm SEM of 4-6 independent experiments. (C) Representative Western blot of 3 independent experiments of A549 cell lysates for CaMKK β (68kDa) and β -Actin 72h after transfection with scrambled or CaMKK β -specific siRNA. (D) Representative Western blot (3 independent experiments) for AMPK or its substrate pACC in A549 cell lysates 72h after transfection with scrambled or CaMKK β -specific siRNA and 24h after PR8 infection. (E) Relative MFI of NKA α 1 on A549 cells treated with CaMKK β -specific siRNA for 48h prior to treatment with PBS (ctrl) or infection with PR8 for additional 24h. Bar graphs represent means \pm SEM of 3 independent experiments. (F) Vectorial water transport of confluent hAEC culture at 6h after inoculation with PBS (ctrl) or PR8 (IAV) without additional treatment (-), in presence of 25 μ M Ouabain, 10 μ M Compound C or 0,5 μ M STO-609. Bar graphs represent means \pm SEM of 4-6 independent experiments.

medium in presence of the different inhibitors. Indeed, inhibition of Na,K-ATPase function by ouabain or IAV infection decreased, whereas blockade of AMPK or CaMKK β significantly improved vectorial water transport after IAV infection (Figure 4-11 E). Collectively, these data demonstrate that IAV-induced IFN α and TRAIL-dependent loss of epithelial surface NKA α 1 and fluid reabsorption is mediated by Calcium-dependent CaMKK β and AMPK signaling.

4.4. IAV-induced paracrine reduction of plasma membrane NKA α 1 protein and AFC capacity require the presence of IFNAR and TRAIL and macrophage recruitment *in vivo*.

To address whether Na,K-ATPase levels were also decreased after IAV infection *in vivo*, NKA α 1 surface expression on distal lung epithelial cells was analyzed by flow cytometry. NKA α 1 was significantly downregulated on the cell surface at d2 pi and further decreased at d7 pi (Figure 4-12 A). Of note, *ifnar* $^{-/-}$ mice were completely protected from IAV-induced surface loss of NKA α 1 at d7 pi. Consistent with our *in vitro* findings demonstrating a role for TRAIL from monocyte-derived macrophages in the reduction of basolateral Na,K-ATPase protein abundance during IAV, both mice lacking C-C chemokine receptor type 2 (*CCR2* $^{-/-}$), which are unable to recruit macrophages to the lung after IAV-infection (30), and TRAIL-deficient (*trail* $^{-/-}$) mice showed increased expression of surface NKA α 1 on distal lung epithelial cells in response to IAV infection. Corresponding to the IFN/TRAIL-mediated loss of NKA α 1 expression, AFC was significantly reduced after IAV infection in wt mice, and this reduction in AFC was attenuated in *ifnar* $^{-/-}$, *trail* $^{-/-}$ and *CCR2* $^{-/-}$ mice. (Figure 4-12 B). Moreover, reduced AFC upon IAV infection could be mimicked in *CCR2* $^{-/-}$ mice after adoptive transfer of wt but not *trail* $^{-/-}$ exudate macrophages (Figure 4-12 C). Furthermore, inhibition of AMPK activity by intratracheal application of adenoviral-expressed DN-AMPK prior to infection prevented the IAV-induced reduction in NKA α 1 surface expression and restored AFC to baseline levels (Figure 4-12 D, E). These data highlight a crucial role for cross-talk involving IFN, TRAIL and AMPK signaling for loss of Na,K-ATPase-driven alveolar edema clearance capacity after IV infection *in vivo*.

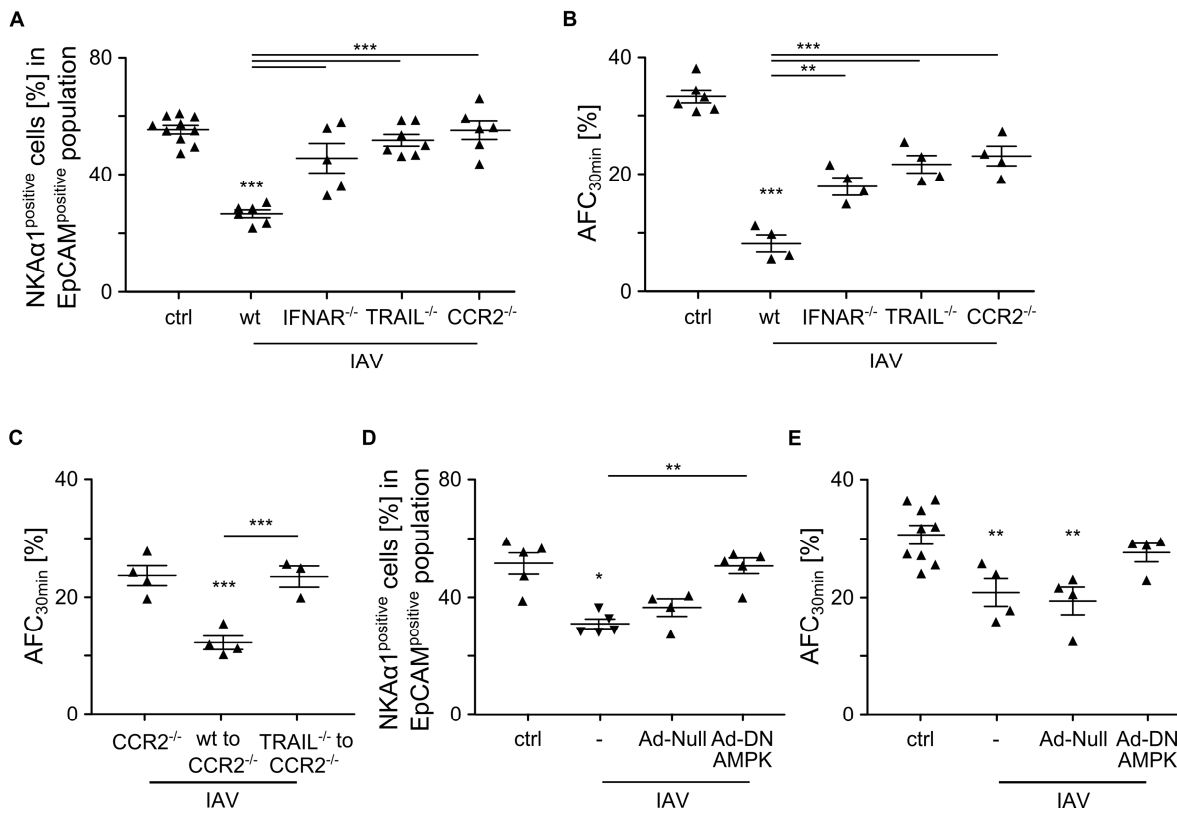
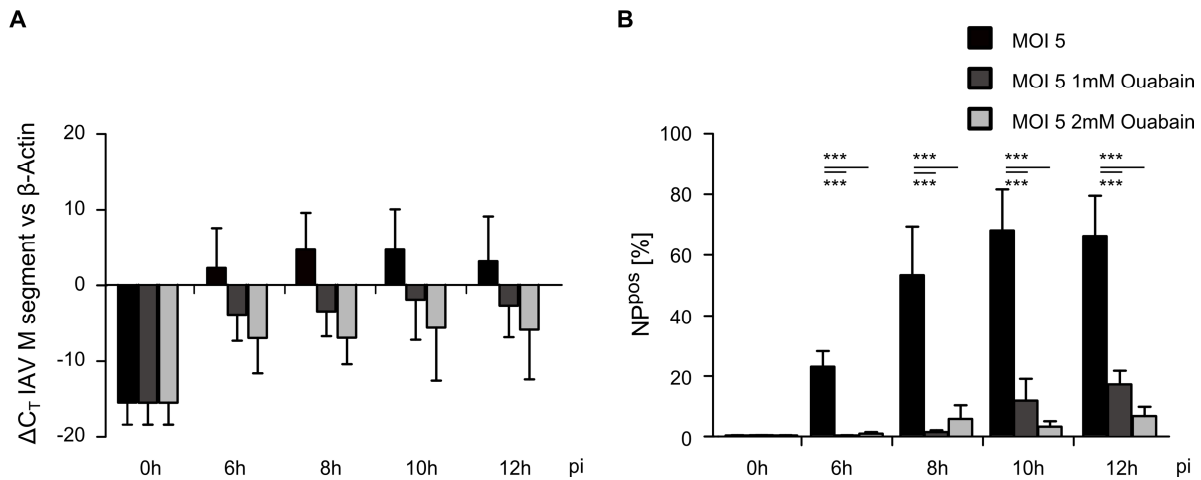


Figure 4-12 IAV-induced reduction of epithelial NK α 1 surface expression and AFC capacity require the presence of IFNAR and TRAIL as well as macrophage recruitment and are mediated by AMPK *in vivo*. (A) Flow cytometric analysis of NK α 1 subunit expression on EpCAM^{positive} epithelial cells from distal lung homogenate. Wt mice were inoculated with PBS (ctrl) or wt, *ifnar*^{-/-}, *trail*^{-/-} or *CCR2*^{-/-} mice were inoculated with PR8 (IAV) and sacrificed 7 days post infection. (B, C) *In vivo* measurements of alveolar fluid clearance (AFC) rates over a time interval of 30 minutes. (B) Wt, *ifnar*^{-/-}, *trail*^{-/-} or *CCR2*^{-/-} mice were inoculated with PBS (ctrl) or PR8 (IAV) 7 days prior to analysis. (C) *CCR2*^{-/-} mice were inoculated with 500pfu of PR8 and AFC was analyzed 7d pi without further treatment (*CCR2*^{-/-}) or after adoptive transfer of exudate macrophages from 7d infected wt (wt to *CCR2*^{-/-}) or *trail*^{-/-} (*trail*^{-/-} to *CCR2*^{-/-}) mice at day 3 pi. In (D) and (E), wt animals were inoculated with PBS (ctrl), or with adenovirus delivery of either no construct (Ad-Null) or a dominant-negative form of AMPK (Ad-DN AMPK) for 7 days prior to infection with PBS or Udorn (IAV) 2 days prior to AFC analysis. (D) Flow cytometric analysis of NK α 1 subunit expression on EpCAM^{positive} epithelial cells from distal lungs of wt mice inoculated with PBS (ctrl), Ad-Null or Ad-DN AMPK for 7 days prior to infection with PBS or Udorn (IAV) at 2 days post infection. (E) *In vivo* measurements of AFC rates over a time interval of 30 minutes.

4.5. Na,K-ATPase activity is necessary for efficient IAV replication

As the flow cytometric analysis revealed that the paracrine IFN/TRAIL/DR5 network was acting on non-infected cells, whereas infected cells maintained their baseline expression of Na,K-ATPase (Figure 4-5), it became of interest to test whether the preservation of Na,K-ATPase expression levels in infected cells was directly influenced by IAV infection or even manipulated by the virus to provide efficient IAV replication. Therefore, viral replication was monitored in presence of ouabain, a specific inhibitor of Na,K-ATPase ion pumping

activity. Viral RNA levels, quantified by qRT-PCR of IAV M segment, tended to be decreased after ouabain treatment in MLE-12 cells, a mouse cell line displaying AEC type II-like characteristics (Figure 4-13 A). Importantly, IAV replication measured by flow cytometric analysis of NP^{pos} (nucleoprotein^{positive}) epithelial cells, was significantly impaired by ouabain (Figure 4-13 B), suggesting a crucial role for Na,K-ATPase activity for IAV replication cycle in lung epithelial cells.



4-13 IAV replication is impaired in presence of ouabain. MLE-12 cells were infected with PR8 MOI 5 and then supplemented with infection media containing no, 1mM or 2mM ouabain. Cells were harvested at 6h, 8h, 10h and 12h pi. Viral replication was monitored by (A) quantification of vRNA by qRT-PCR for IAV M segment or (B) quantification of viral protein by flow cytometry for NP^{positive} epithelial cells. Bar graphs represent means \pm SEM of 3 independent experiments.

4.6. Na,K-ATPase is relocalized to the apical cell membrane in IAV-infected epithelial cells

Na, K-ATPase can only establish a sodium ion gradient from the alveolar lumen to the interstitial space and thus contribute to effective edema clearance when correctly inserted into the basolateral membrane of the alveolar epithelial cells. Consequently, it was assessed by confocal imaging if Na,K-ATPase was found to preserve its typical distribution after IAV infection, especially in the infected AEC that still displayed normal levels of total plasma membrane expressed NKA α 1 (Figure 4-5). In IAV infected AEC, viral replication could be monitored by staining for the viral NP that could be detected from 6h pi in the nuclear compartment, indicating synthesis of viral proteins and formation of progeny RNP (ribonucleoproteins) in the nucleus (Figure 4-14, B). At later time points, NP was found at the apical cell compartment, demonstrating accumulation of viral protein for budding and virion formation (Figure 4-14, C, D). In non-infected alveolar epithelial cells, NKA α 1 showed a predominantly basolateral localization pattern as a prerequisite for vectorial

sodium ion transport. However, the basolateral localization of NKA α 1 was lost in NP^{pos} AEC in the time course of IAV infection, and was subsequently found to be relocalized to the apical cell surface (Figure 4-14 C, D), probably adding to decreased edema clearance in IAV infection *in vivo* by impairing directed transport of sodium ions, or even by driving reverse fluid accumulation in the alveoli.

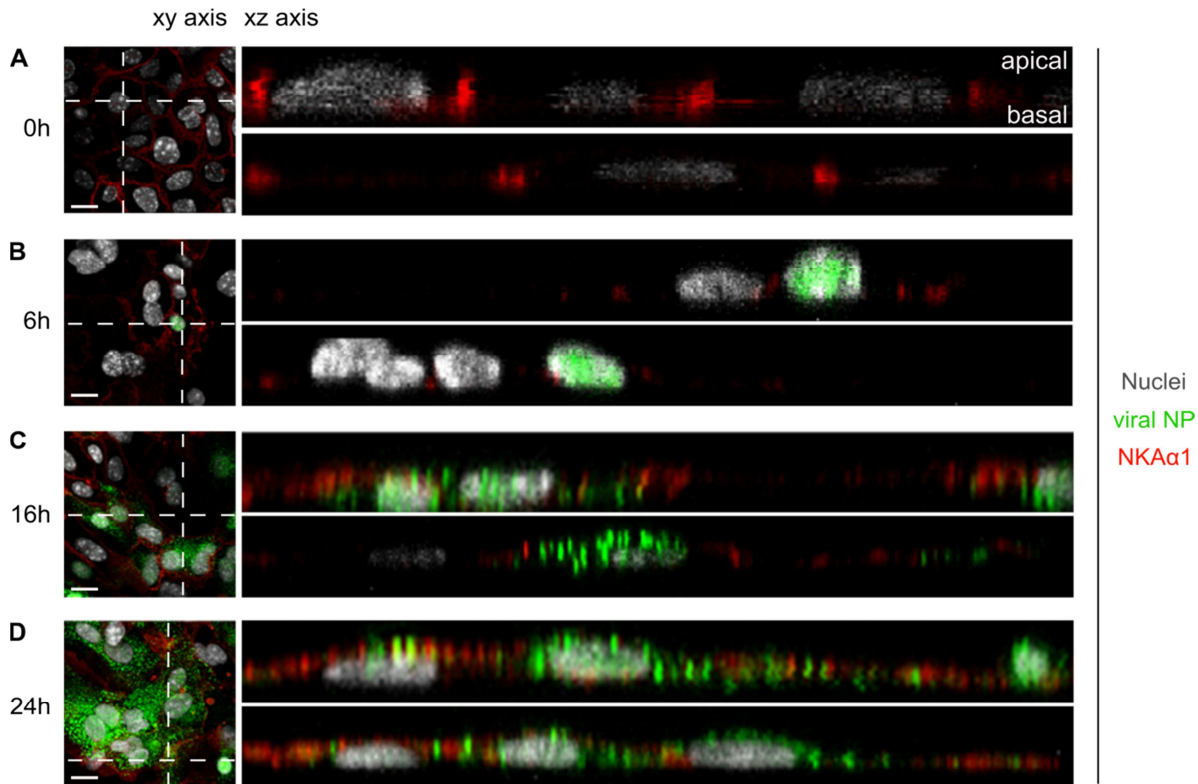


Figure 4-14 NKA α 1 is relocalized to the apical cell membrane after IAV infection. Murine AEC were infected with PR8 at MOI 0.1 and fixed at (A) 0hpi, (B) 6hpi, (C) 16hpi and (D) 24hpi. Expression and localization of viral NP and NKA α 1 were addressed by immunostaining and confocal microscopy and are depicted as xy top view (left panel). Crosshairs represent intersections chosen for xz visualization (right panel). Scale bars represent 15 μ m length.

To test whether apical localization of Na,K-ATPase was an unspecific, infection-related event caused by loss of cell polarity, the localization pattern of the tight junction proteins occludin and zona occludens-1 (ZO-1) was analyzed in mAEC after IAV infection. Both proteins remained to be localized to the lateral membrane of the cells up to 24h after IAV infection (Figure 4-15), indicative of polarity maintenance in infected mAEC.

To investigate if Na,K-ATPase was also relocalized *in vivo*, immunostaining of cryoslices from d3 or d5 IAV-infected mice were used to analyze the localization of NKA α 1 and occludin after IAV infection within the alveolar compartment. PBS-treated wt mice displayed a basolateral distribution of NKA α 1 and occludin. Analysis of cryoslices from d3 or d5 IAV-infected animals revealed that after IAV infection, viral protein accumulated at

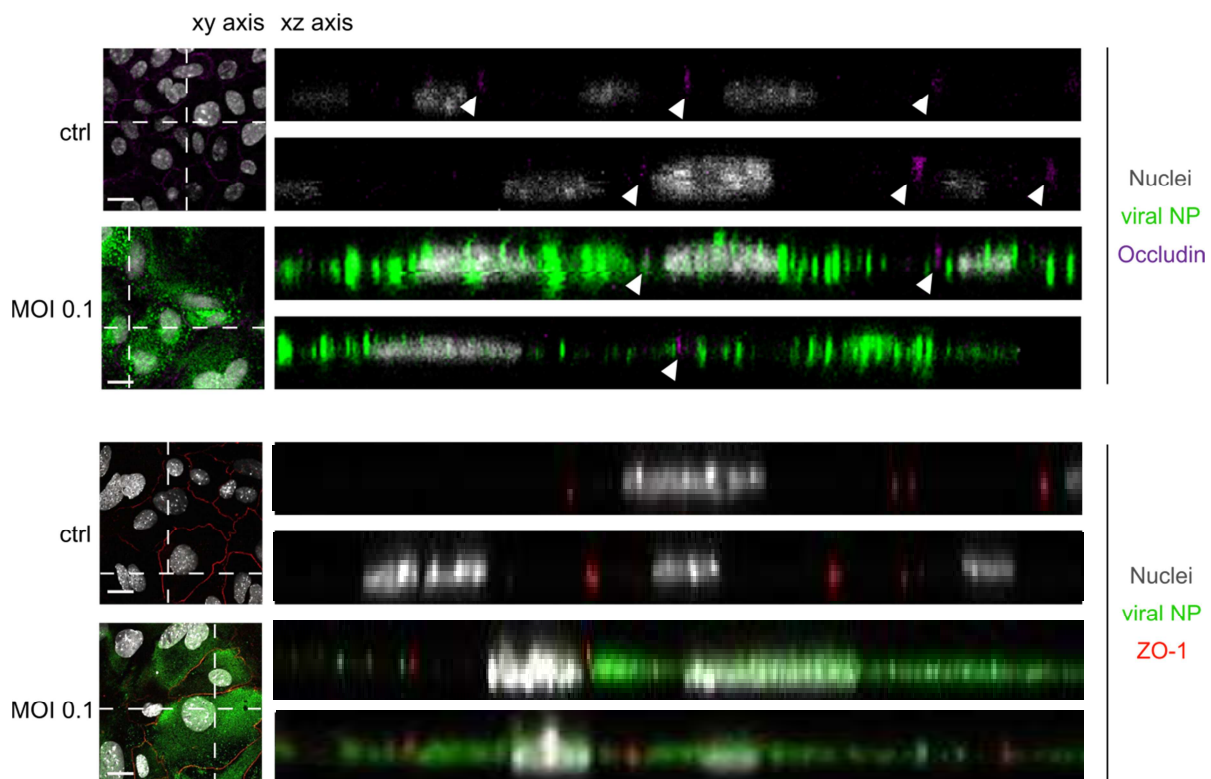


Figure 4-15 Localization of the junctional proteins occludin and ZO-1 is not altered after IAV infection. Murine AEC were treated with PBS (ctrl) or infected with PR8 at MOI 0.1 and fixed 24h pi. Expression and localization of viral NP, occludin (upper panel) and ZO-1 (lower panel) were visualized by immunostaining and confocal microscopy and are depicted as xy top view and xz intersection and represent n = 3-5 independent experiments. Scale bars represent 15 μ m length.

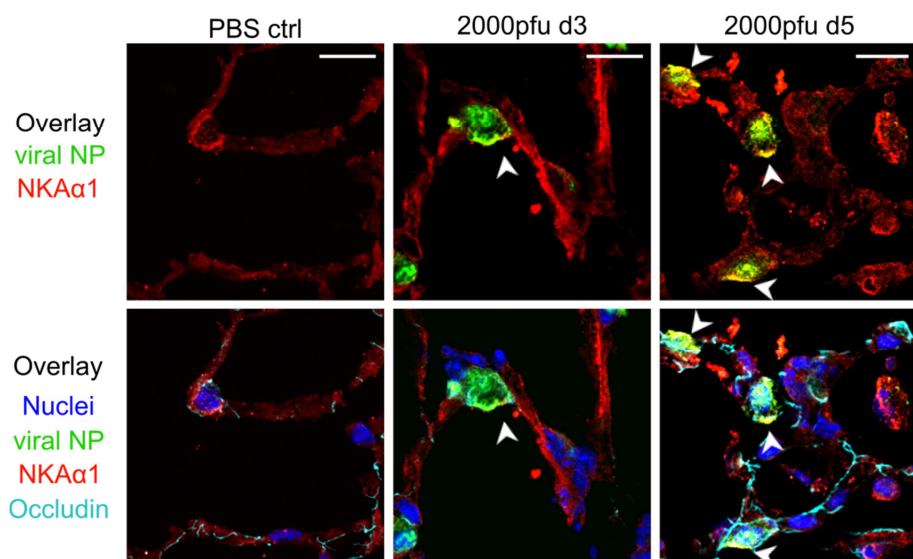


Figure 4-16 NKA α 1 is relocalized to the apical cell membrane after IAV infection *in vivo*. Wt mice were treated with PBS (ctrl) or infected with 2000pfu PR8 and sacrificed at d3 or d5 pi. Expression and localization of viral NP (green), NKA α 1 (red) and occludin (cyan) were visualized by immunostaining and confocal microscopy of cryosliced lung preparations. Scale bars represent 15 μ m length. Arrowheads mark viral budding site. Yellow color indicates co-localisation of NP and NKA α 1 at the apical regions of AEC.

the apical, luminal-oriented cell compartment as observed during apical viral budding. Accordingly, NKA α 1 was expressed at the apical cell surface, whereas occludin remained, with rare exceptions, localized to the basolateral cell membrane (Figure 4-16).

4.7. Na,K-ATPase apical relocalization is caused by interaction with IAV matrix protein 2

Previous results suggested that Na,K-ATPase is involved in viral replication (Figure 4-13). To study whether *vice versa*, viral replication is necessary for NKA α 1 relocalization during IAV-infection, a heat-inactivated PR8 virus was used for inoculation. The heat-inactivated PR8 can bind to host cells and is internalized, but is replication-deficient. In comparison to PR8 infected cells (ctrl), heat-inactivated virus did not induce apical NKA α 1 relocalization (Figure 4-17).

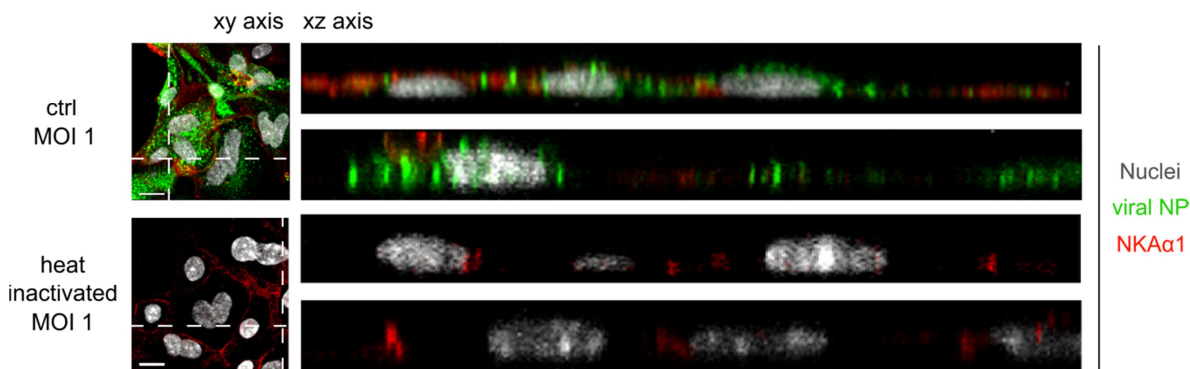


Figure 4-17 Heat-inactivated IAV does not induce relocalization of NKA α 1. Murine AEC were infected with PR8 (upper panel) or heat-inactivated PR8 (lower panel) at MOI 1 and fixed 24h pi. Expression and localization of viral NP and NKA α 1 were visualized by immunostaining and confocal microscopy and are depicted as xy top view and xz intersection and represent n = 3-5 independent experiments. Scale bars represent 15 μ m length.

Reports by Shufo et al. (226) implied that NKA β 1 is able to directly interact with viral M2 proton channel protein using a yeast-two-hybrid approach. To determine if in mammalian cells NKA α 1 redistribution was depending on a viral protein, IAV segments that share endoplasmatic- and Golgi-dependent translation and maturation with the Na,K-ATPase (HA, NA and M, the last encoding for both the viral proteins M1 and M2), were overexpressed using a plasmid-based system. Human lung epithelial A549 cells were transfected with pPol-I constructs that allow the synthesis of negative-oriented viral RNA (vRNA), for viral HA, NA or M segment. In addition, pCAGGS-based expression vectors were co-transfected, encoding for Pol-II constructs of viral NP, PA, PB1 and PB2. This allowed formation of the viral polymerase complex and consequently transcription of mRNA encoding for HA, NA or M segment protein from the vRNA generated by the pPol-I constructs. Analysis of these

cells 24h after transfection suggested that only presence of the viral M segment, but not HA or NA, could induce a redistribution of Na,K-ATPase to the apical cell membrane (Figure 4-18).

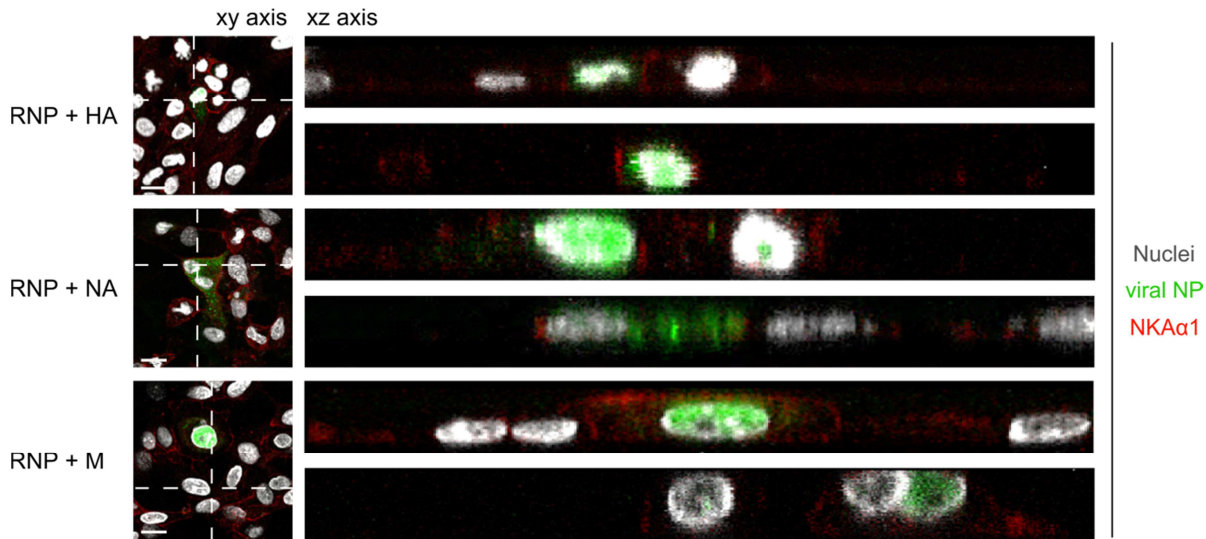


Figure 4-18 Expression of the viral M segment is sufficient to induce relocalization of NKA α 1. A549 were transfected with pCAGGS-based vectors encoding for Pol-II constructs of viral NP, PA, PB1 and PB2, allowing formation of the viral polymerase complex, plus pPol-I constructs for viral HA (top panel), NA (middle panel) or M segment (bottom panel). Cells were fixed 24h after transfection. Expression and localization of viral NP and NKA α 1 were visualized by immunostaining and confocal microscopy and are depicted as xy top view and xz intersections and represent n = 3 independent experiments. Scale bars represent 15 μ m length.

As the viral M segments encodes for both viral proteins M1 and M2, co-immunoprecipitation experiments were used to analyze whether NKA α 1 was able to interact with M2 or M1 protein after IAV infection. Indeed, using NKA α 1 as bait, M2, and to a minor extent also M1, could be identified as interaction partners for NKA α 1 (Figure 4-19 A). The reciprocal experiment demonstrated that only M2, but not M1 or the viral PB1 or NS1, can pull-down the NKA α 1 (Figure 4-19 B).

Furthermore, live-cell imaging of a plasmid-based overexpression of GFP-tagged NKA α 1 and mCherry-tagged M2 in A549 demonstrated that both proteins colocalize in intracellular, motile and vesicular structures (Figure 4-20), suggesting a co-transport of both proteins targeting a common cellular compartment. Taken together, co-immunoprecipitation and live-cell imaging identified the M2-NKA α 1 interaction as possible mechanism for basolateral-to-apical plasma membrane relocalization of Na,K-ATPase upon IAV infection that might further decrease AFC capacities in the infected epithelium and add to edema formation.

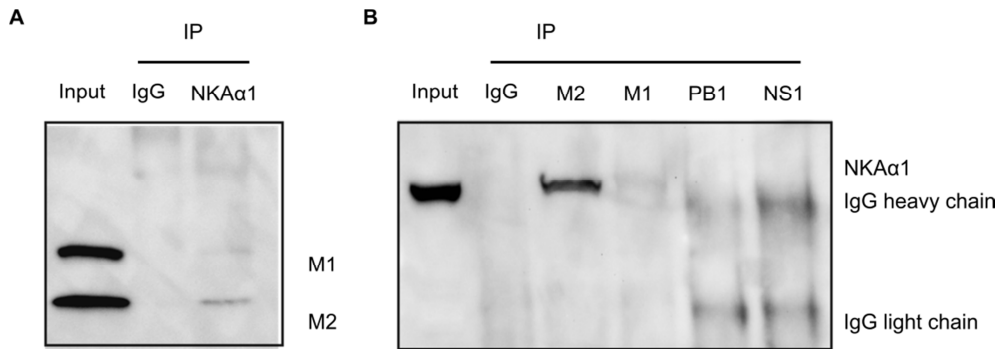


Figure 4-19 NKA α 1 and M2 do co-immunoprecipitate. A549 were infected for 8h with MOI 1, then lysed and subjected to co-immunoprecipitation. In (A), NKA α 1 or the respective IgG were used as bait and immunoblot was done for viral M1 (25kDa) and M2 (9kDa). In (B), viral proteins M2, M1 and respective IgG or PB1 and NS1 were used as bait and immunoblot was done for NKA α 1 (110kDa). Representative Western blots of n = 3 independent experiments are shown.

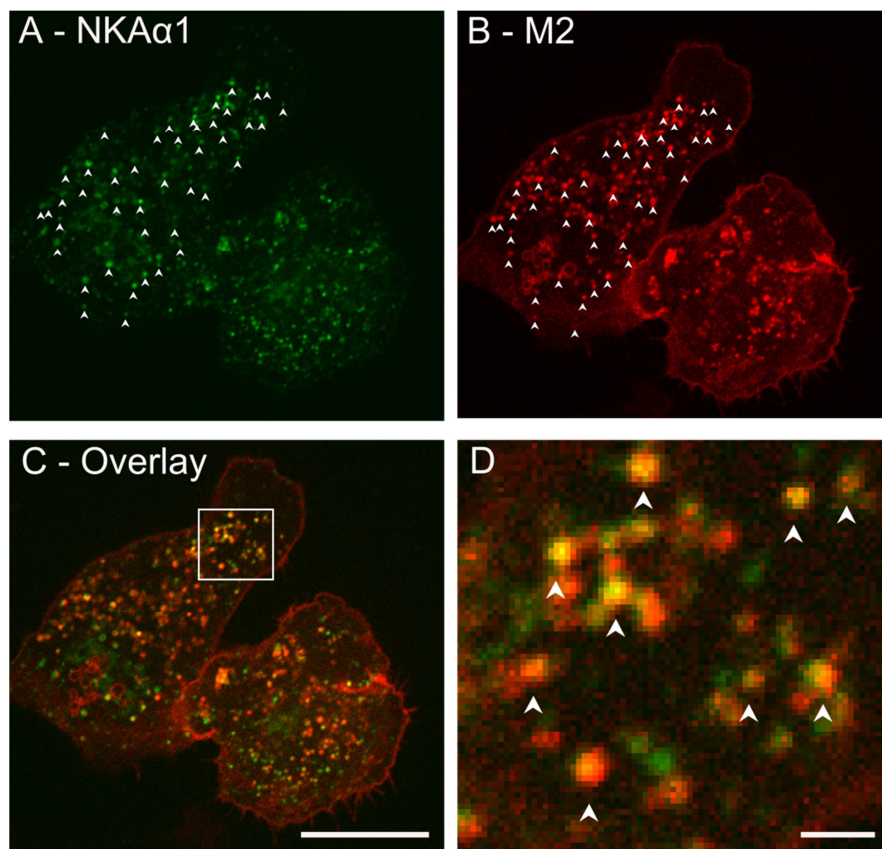


Figure 4-20 NKA α 1 and M2 colocalize upon coexpression in A549 cells. A549 cells were transfected for 24h with plasmids encoding for (A) a GFP-tagged NKA α 1 (green) and (B) mCherry-tagged M2 protein (red) and then visualized using live cell microscopy. (C) Overlay image showing partial colocalization of NKA α 1 (green) and M2 (red). Scale bar in (C) represent 10 μ m length. Boxed region in (C) is enlarged in (D). Arrowheads point at motile vesicular structures stained positive for both proteins. Scale bar in (D) represents 1 μ m length.

5. Discussion

IAV pneumonia is characterized by infection of alveolar epithelial cells and can rapidly progress to ARDS with poor outcome. A functional and structural impairment of the alveolar epithelial barrier after IAV infection leads to pulmonary edema, and decreased fluid reabsorption is closely correlated to mortality in ARDS patients (6, 7).

In this work putative effects of IAV infection on regulation and function of alveolar epithelial Na,K-ATPase were investigated as a number of studies revealed its importance in alveolar fluid transport in lung injury (100, 103, 105, 217). The data demonstrate that the total protein and the plasma membrane expression of the NKA α 1 subunit of the ion pump is reduced after IAV infection, indicating that the fraction of Na,K-ATPase relevant for active sodium extrusion out of the cell is affected (100, 103, 105, 217). Vectorial sodium and fluid transport is a coordinated process that requires the electrochemical gradient provided by basolaterally located Na,K-ATPase, thereby constituting the driving force of alveolar water reabsorption. Partially, sodium and water transport can also be modified by regulation of the apically located epithelial sodium channels (ENaC) and chloride channels such as the cystic fibrosis transmembrane receptor (CFTR). In contrast to ENaC and CFTR, that are directly degraded by action of the viral protein M2 expressed in IAV infected cells (184, 185, 227), Na,K-ATPase plasma membrane abundance was disproportionately reduced in neighboring, non-infected epithelial cells. This suggests that NKA α 1 reduction is not mediated by direct interaction with a viral component but essentially relies on paracrine signals released from the infected epithelial cells and macrophages. Using a co-culture system, the importance of epithelial IFN α and IFN-induced macrophage TRAIL in this process could be demonstrated. Both mediators were able to reduce plasma membrane NKA α 1 even in absence of viral components.

The role of type I IFNs in IAV infection is controversial. They are key cytokines in innate antiviral immune responses and are rapidly produced by infected alveolar epithelial cells after viral challenge (228, 229). IFNs activate antiviral transcriptional programs in both epithelial and immune cells in the lung that are important for viral clearance and may play a role in limiting the severity of the immune response via the induction of production of IL-10 (228–230). Accordingly, IFNs have been suggested as a therapeutic option to promote anti-IAV host defenses (231, 232). An important source of IFN but also of other pro-inflammatory cytokines in IAV-induced innate immune responses are alveolar and CCR2-recruited bone marrow-derived macrophages (196, 197, 233). Resident alveolar

macrophages are one of the first cell types sensing viral infection and thus promote initial innate but also later adaptive immune responses to IAV infection (152). In concert with further macrophage populations recruited upon infection, they establish a pro-inflammatory environment by production and release of mediators such as IFN, leading to enhanced viral clearance and better disease outcomes (196, 234). However, it is well recognized that excessive production of cytokines during IAV infection contributes to lung injury and is also closely correlated to severity and outcome of disease (199, 235), as shown for infection with the highly pathogenic avian influenza H5N1 or the pandemic 2009 H1N1 virus (198, 236). Particularly, alveolar and recruited macrophages have been shown to play an important role in amplifying lung injury after IAV-infection and were attributed a central role in enhanced immunopathology by raising an exuberant inflammatory response to IAV infection (45, 197, 198, 201, 233). Especially, mediators expressed early in the anti-viral response and associated to innate immune responses, largely consisting of IFN and IFN-dependent signaling mediators, worsen IAV-induced lung inflammation, lung injury severity and mortality and also hamper resolution of inflammation (152, 199).

TRAIL has been widely associated with induction of extrinsic apoptosis in a variety of cells, including leukocyte subsets and cancer cells, via its receptor DR5 (DR; death receptor) (237, 238). In the current study a novel role of a macrophage TRAIL/epithelial DR5 interaction could be elucidated, resulting in down-regulation of Na,K-ATPase from the surface of AEC by activating the energy sensor AMPK. AMPK regulates cellular energy metabolism, by up-regulating ATP-generating and down-regulating ATP-consuming mechanisms, thus generally promoting cellular survival (116, 239, 240). AMPK activation has been demonstrated to occur in response to stimuli that threaten metabolic homeostasis including alveolar hypercapnia and hypoxia and resulted, in line with this work, in Na,K-ATPase endocytosis and degradation (108, 120).

The DR5-mediated AMPK activation precedes apoptotic events in AEC such as caspase-3 cleavage, occurring at 48hpi (201), suggesting induction of two independent signaling pathways. Indeed, the TRAIL/AMPK pathway was previously associated with non-apoptotic autophagy in epithelial cells, highlighting the complexity of the IFN/TRAIL network in cellular injury and protection in response to cellular stress (241).

We demonstrate activation of AMPK signaling by paracrine mediators in response to IAV infection, which results in reduced vectorial sodium transport. Inhibition of AMPK *in vivo* largely restored Na,K-ATPase activity and AFC rates in IAV-infected mice, highlighting

AMPK as central regulator of AFC in various conditions of pulmonary injury *in vivo* and supporting it as a therapeutic target for the treatment of IAV (242).

The presented *ex vivo* studies provide complementary lines of evidence demonstrating an additive role for epithelial produced IFN α and IFN-dependent macrophage- induced TRAIL in the downregulation of basolateral Na,K-ATPase plasma membrane abundance during IAV infection. Accordingly, *ifnar*^{-/-} mice lacking the receptor for IFN α but also for IFN β , a crucial inducer of TRAIL in AM, displayed similar Na,K-ATPase levels as uninfected animals, highlighting the crucial role of type I IFN in Na,K-ATPase regulation after IAV infection. Similarly, *trail*^{-/-} mice and mice lacking bone marrow-derived macrophage recruitment (*ccr2*^{-/-}) were protected from IAV-induced epithelial loss of surface NKA α 1. Consequently, restored levels of AEC surface Na,K-ATPase resulted in significantly improved AFC in IAV-infected *ifnar*^{-/-}, *trail*^{-/-} and *ccr2*^{-/-} mice, whereas adoptive transfer of wt macrophages but not *trail*^{-/-} macrophages in *ccr2*^{-/-} mice diminished AFC after IAV infection. Notably, AFC was significantly but not completely restored in *ifnar*^{-/-} mice, which can be attributed to the severely compromised viral clearance in these mice, likely associated with increased or persistent epithelial injury which may further affect clearance capacity (230, 243–245). However, it cannot be excluded completely that other IFN-independent macrophage-released mediators additionally affect NKA α 1 expression *in vivo*. Moreover, the presented data suggest that signaling of IFN and TRAIL through their respective epithelial cytokine receptors IFNAR and DR5 activates AMPK via a pathway that requires CaMKK β but not TAK1 kinase activity. CaMKK β itself is in turn activated by increases in intracellular calcium (242). Chelation of intracellular calcium was shown to prevent activation of AMPK and degradation of Na,K-ATPase. Previous studies demonstrated that in hypoxic conditions, influx of extracellular calcium through stromal interaction molecule 1 (STIM1)-activated calcium release-activated calcium (CRAC) channels can lead to CaMKK β - and AMPK-mediated endocytosis of Na,K-ATPase (108). Wang et al. (2008) demonstrated that the calcium-dependent tyrosine kinase Pyk2 interacts with the IFNAR-associated tyrosine kinases Jak1/Tyk2, providing a possible link to CaMKK β activation. However, the cell-specific signals involved in the context of IAV infection remain to be elucidated.

Alterations of sodium currents within the IAV-infected cell inhibit viral replication as suggested by the here presented data as well as previous reports, in which ouabain, the specific inhibitor of Na,K-ATPase activity, significantly reduced viral infection levels (247).

A recent report by Burkard et al. demonstrated that, in contrast to coronaviruses, Na,K-ATPase is not involved in viral entry of IAV (248), suggesting, in concert with the presented data, that viral replication is affected after nuclear import of vRNA and, most likely, occurs at post-transcriptional level. Confocal microscopy studies revealed that NKA α 1 is mistargeted to the apical cell membrane in IAV infected AEC. This process most probably adds significantly to a reduced AFC capacity of the alveolar epithelium, as the net amount of basolateral Na,K-ATPase adding to vectorial sodium and water transport is further decreased. Assuming that Na,K-ATPase located to the apical membrane might retain its ion pumping activity, sodium ion transport direction might even be reversed, yielding in elevated sodium and thus water contents in the alveolar lumen. Further immunoprecipitation and live cell imaging studies revealed that it is most likely the interaction with the viral M2 protein that drives the apical relocalization of NKA α 1 protein. Interestingly, Na,K-ATPase has been found to be incorporated into IAV virus-like particles (249), indicating that host NKA α 1 might have an important function within the viral membrane and is therefore targeted to the budding site by binding to the M2 protein. The above mentioned data strongly suggest that Na,K-ATPase activity and localization are closely interconnected to efficient virus replication. Therefore, it seems probable that the decrease of Na,K-ATPase in adjacent cells depending on IFN-dependent signaling might in first place be a host strategy to build up an antiviral state in non-infected cells. In this regard, Moseley et al. demonstrated that treatment of mice with the AMPK activator AICAR, that was here identified to decrease Na,K-ATPase levels in non-infected AEC (Figure 4-10 E), prior to infection can reduce IAV-induced mortality (242). Thus, a limited decrease in Na,K-ATPase levels in non-infected cells in IAV infection might limit viral spread but still enable sodium ion conductance levels that ensure sufficient fluid reabsorption rates. However, a further decrease in Na,K-ATPase expression later in IAV infection, potentially by recruitment of additional macrophages to the alveolar space and the following overshooting inflammatory response including signaling by macrophage-released TRAIL, might then contribute to reduced AFC rates, edema formation, prolonged hypoxemia and increased mortality.

In conclusion, the presented data provide evidence that IAV infection causes reduction in the surface expression of Na,K-ATPase in non-infected AEC and an M2-mediated apical mistargeting of NKA α 1 in infected AEC resulting in significantly impaired AFC (Figure 7). The interaction between Na,K-ATPase and the viral M2 protein in infected AEC induces a relocalization of NKA α 1 from the basolateral to the apical cell membrane most probably

decreasing or even reverting sodium ion transport and fluid clearance towards the interstitial space. Importantly, a prominent decrease of NKA α 1 plasma membrane expression in non-infected alveolar epithelial cells is induced via CaMKK β and AMPK by a paracrine signaling elicited by infected epithelial cells and macrophages. This decrease is mediated by alveolar epithelial cell-released IFN α directly and is amplified through IFN-induced release of TRAIL from recruited macrophages resulting in significant inhibition of lung edema clearance. As the AMPK-mediated loss of Na,K-ATPase and AFC capacities were found to be amenable to manipulation *in vivo*, a timely and well-balanced modulation of Na,K-ATPase abundance and activity might represent a novel strategy to improve fluid reabsorption and hypoxia and thus outcomes in IAV-induced lung injury and ARDS.

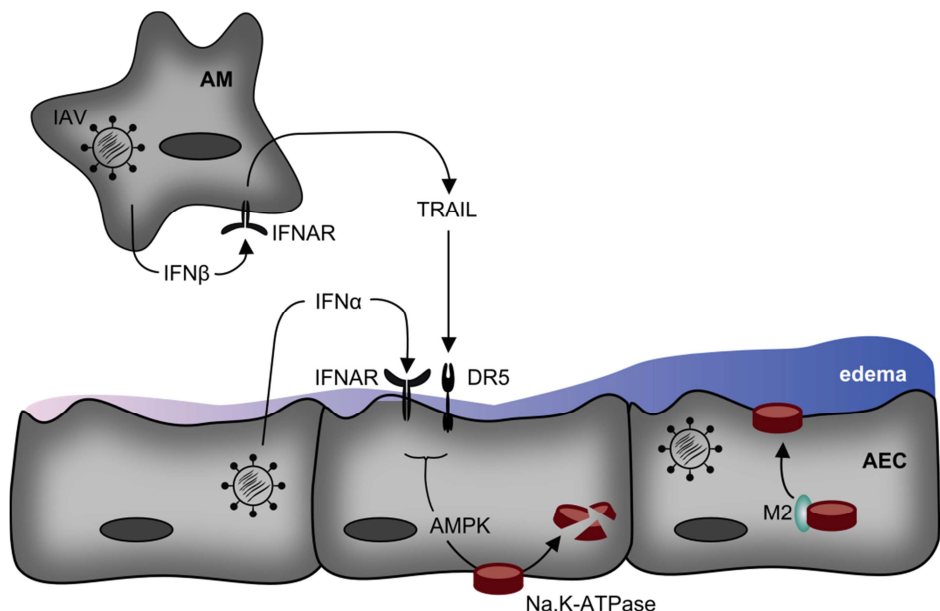


Figure 6-1 Model of type I IFN-mediated loss of Na,K-ATPase-mediated edema clearance in IAV infection and M2-dependent mistargeting of NKA α 1 to the apical compartment of IAV infected AEC. IAV infection results in alveolar epithelial cell (AEC) release of IFN α and induction of IFN β -dependent release of TRAIL in alveolar macrophages (AM). Ligation to their receptors, IFNAR and DR5, results activation of the stress kinase AMP-activated kinase (AMPK). Activation of AMPK initiates endocytosis and degradation of Na,K-ATPase from the cell plasma membrane and impacts on fluid reabsorption. In parallel, expression of the viral proton channel M2 in IAV infected AEC leads to a mistargeting of Na,K-ATPase from the basolateral to the apical cell membrane. Both effects, reduced NKA α 1 expression in non-infected AEC as well as NKA α 1 mislocalization in infected AEC, are most likely to increase the persistence of lung edema after IAV infection

6. Summary

Influenza A viruses (IAV) cause primary viral pneumonia resulting in acute respiratory distress syndrome (ARDS) associated with severe alveolar edema formation. As impairment of edema resolution in ARDS patients is correlated with high mortality, this study investigated metabolism and function of Na,K-ATPase, a major regulator of fluid homeostasis, to define mechanisms affecting alveolar fluid clearance (AFC) in IAV-infection.

In vivo IAV infection of wildtype (wt) mice resulted in reduced AFC, edema formation and hypoxia that occurred in parallel with a decrease in total and plasma membrane expressed Na,K-ATPase α 1 subunit (NKA α 1). NKA α 1 was primarily decreased in non-infected cells in a monoculture of alveolar epithelial cells (AEC) and in presence of co-cultured, infected macrophages. We found paracrine signaling of type I interferons (IFN) and the macrophage released, IFN-dependent cytokine TRAIL (TNF-related apoptosis inducing ligand) to be sufficient to decrease NKA α 1 in a CaMKK β - and AMPK-dependent way. Blockade of this pathway using specific chemical inhibitors, adenoviral overexpression or siRNA approaches restored NKA α 1 levels as well as vectorial water transport in *ex vivo* infected AEC. Additionally, *trail* $^{-/-}$ or *ifnar* $^{-/-}$ mice, mice transduced with a dominant-negative form of AMPK or *ccr2* $^{-/-}$ mice lacking pulmonary macrophage recruitment showed improved NKA α 1 levels and AFC after IAV infection. In parallel, inhibition of Na,K-ATPase channel activity by ouabain reduced the amount of IAV infected cells, implying a role for Na,K-ATPase in the IAV replication cycle. IAV infection or transfection of the viral M segment led to a mistargeting of NKA α 1 from the basolateral to the apical cell surface in infected AEC, associated with a close interaction between the viral M2 protein and the NKA α 1, likely resulting in impaired or even reverted fluid clearance in the infected fraction of AEC. Together, this work demonstrates that AFC is inhibited after IAV infection both in infected cells by M2-mediated mistargeting and in non-infected neighboring cells by paracrine IFN/TRAIL/DR5 signaling resulting in AMPK-mediated decrease of plasma membrane NKA α 1. Targeting these pathways may be a novel therapeutic strategy to improve AFC, oxygenation and finally outcome in patients with IAV-induced ARDS.

7. Zusammenfassung

Influenza A Virus (IAV) Infektionen des distalen Respirationstraktes führen zu einer viralen Pneumonie und zum akuten Lungenversagen (ARDS) des Erwachsenen. Ein Hauptmerkmal des ARDS ist die Ausbildung eines alveolären Ödems, und die Überlebenschancen des Patienten korrelieren eng mit dessen Fähigkeit, diese überschüssige Flüssigkeit aus dem Alveolarraum zu resorbieren (alveolar fluid clearance, AFC). Da die Na,K-ATPase durch die Etablierung eines Natrium-Gradienten hin zum Interstitium maßgeblich zur alveolären Flüssigkeitsresorption beiträgt, wurden deren Regulation und Lokalisation nach der IAV Infektion näher charakterisiert.

Es konnte gezeigt werden, dass die *in vivo* IAV Infektion von Wildtyp (wt) Mäusen zu deutlich reduzierten AFC Raten, Hypoxie und einer Ödemausbildung führte. Gleichzeitig konnten signifikant verringerte Mengen Totalprotein wie auch Zellmembran-ständigen Oberflächenprotein der Na,K-ATPase $\alpha 1$ Untereinheit (NKA $\alpha 1$) detektiert werden. Diese NKA $\alpha 1$ Reduktion wurde nicht in IAV infizierten, sondern ausschließlich in nicht-infizierten, benachbarten alveolären Epithelzellen (AEC) beobachtet. Darüber hinaus konnte eine NKA $\alpha 1$ Reduktion in primär isolierten, nicht-infizierten AEC durch Kokultivierung mit infizierten Makrophagen oder durch Transfer von Zellkulturüberständen infizierter Zellen induziert werden. Im weiteren Verlauf der Arbeit wurden epithelial produziertes Interferon (IFN)- α und das IFN- β abhängige, von Makrophagen sezernierte TRAIL (TNF-related apoptosis-inducing ligand) als Mediatoren identifiziert, die die Expression der NKA $\alpha 1$ über die Aktivierung der Kinasen CaMKK β und AMPK signifikant reduzieren.

Die Inhibition beider Kinasen über adenovirale Überexpression dominant negativer Varianten oder mittels siRNA konnte in IAV-infizierten AEC die NKA $\alpha 1$ Expression wie auch die Kapazität zum vektorialen Flüssigkeitstransport *in vitro* wiederherstellen. Des Weiteren zeigte die Infektion von TRAIL-, IFNAR (IFN-Rezeptor)-, und CCR2-defizienten Mäusen und von Mäusen mit Inhibition der AMPK Funktion, dass eine Blockade des IFN/TRAIL/DR5/AMPK Signalweges *in vivo* zu einer erhöhten NKA $\alpha 1$ Expression und einer wiederhergestellten AFC Raten führt.

Gleichzeitig konnte in IAV-infizierten AEC eine Interaktion zwischen NKA $\alpha 1$ und dem viralen Protein M2 gezeigt werden, die eine Mislokalisierung der NKA $\alpha 1$ von der basalen zur apikalen Zellmembran induzierte, was – zusätzlich zur verringerten Expression der Na,K-ATPase in nicht-infizierten Zellen – ebenfalls die vektoriale Flüssigkeitsresorption des alveolären Epithels behindert.

Zusammengefasst zeigt diese Studie, dass die Freisetzung von IFN α durch AEC und von TRAIL durch Makrophagen in der IAV Infektion zur verminderten Expression der NKA $\alpha 1$ in nicht-infizierten AEC führt, während in infizierten AEC eine M2-abhängige Mislokalisierung der NKA $\alpha 1$ hin zur apikalen Zellmembran stattfindet, wodurch die Kapazität des alveolären vektorialen Flüssigkeitstransportes nach der IAV Infektion signifikant verringert ist. Die Modulation der zugrunde liegenden Signalwege stellt eine neue Möglichkeit dar, AFC, Oxygenierung und letztlich auch die Überlebenschancen von IAV-infizierten ARDS-Patienten deutlich zu verbessern.

8. References

1. Brun-Buisson C, Minelli C, Bertolini G, Brazzi L, Pimentel J, Lewandowski K, Bion J, Romand J-A, Villar J, Thorsteinsson A, Damas P, Armaganidis A, Lemaire F. Epidemiology and outcome of acute lung injury in European intensive care units. Results from the ALIVE study. *Intensive Care Med* 2004;30:51–61.
2. Matthay MA, Zemans RL. The acute respiratory distress syndrome: pathogenesis and treatment. *Annu Rev Pathol* 2011;6:147–63.
3. Ranieri VM, Rubenfeld GD, Thompson BT, Ferguson ND, Caldwell E, Fan E, Camporota L, Slutsky AS. Acute respiratory distress syndrome: the Berlin Definition. *JAMA* 2012;307:2526–33.
4. Matthay MA, Ware LB, Zimmerman GA. The acute respiratory distress syndrome. *J Clin Invest* 2012;122:2731–40.
5. Matthay MA, Robriquet L, Fang X. Alveolar Epithelium Role in Lung Fluid Balance and Acute Lung Injury. *Proc Am Thorac Soc* 2005;2:206–213.
6. Matthay MA. Alveolar Fluid Clearance in Patients With ARDS *. *CHEST J* 2002;122:340S.
7. Sznajder JI. Alveolar edema must be cleared for the acute respiratory distress syndrome patient to survive. *Am J Respir Crit Care Med* 2001;163:1293–4.
8. Sznajder J, Factor P, Ingbar D. Lung Edema Clearance: 20 Years of Progress: Invited Review: Lung edema clearance: role of Na+-K+-ATPase. *J Appl* 2002;93:1860–1866.
9. Brune K, Frank JA, Schwingshackl A, Finigan JH, Sidhaye VK. Pulmonary epithelial barrier function- some new players and mechanisms. *Am J Physiol Lung Cell Mol Physiol* 2015;ajplung.00309.2014.doi:10.1152/ajplung.00309.2014.
10. Martin TR, Frevert CW. Innate immunity in the lungs. *Proc Am Thorac Soc* 2005;2:403–11.
11. Haslett C. Granulocyte apoptosis and its role in the resolution and control of lung inflammation. *Am J Respir Crit Care Med* 1999;160:S5–11.
12. Holt PG, Strickland DH, Wikström ME, JahnSEN FL. Regulation of immunological homeostasis in the respiratory tract. *Nat Rev Immunol* 2008;8:142–52.
13. Herold S, Mayer K, Lohmeyer J. Acute lung injury: how macrophages orchestrate resolution of inflammation and tissue repair. *Front Immunol* 2011;2:65.
14. Guilliams M, De Kleer I, Henri S, Post S, Vanhoutte L, De Prijck S, Deswarte K, Malissen B, Hammad H, Lambrecht BN. Alveolar macrophages develop from fetal

- monocytes that differentiate into long-lived cells in the first week of life via GM-CSF. *J Exp Med* 2013;210:1977–92.
15. Kumaravelu P, Hook L, Morrison AM, Ure J, Zhao S, Zuyev S, Ansell J, Medvinsky A. Quantitative developmental anatomy of definitive haematopoietic stem cells/long-term repopulating units (HSC/RUs): role of the aorta-gonad-mesonephros (AGM) region and the yolk sac in colonisation of the mouse embryonic liver. *Development* 2002;129:4891–4899.
 16. Tavian M, Péault B. Embryonic development of the human hematopoietic system. *Int J Dev Biol* 2005;49:243–50.
 17. Fogg DK, Sibon C, Miled C, Jung S, Aucouturier P, Littman DR, Cumano A, Geissmann F. A clonogenic bone marrow progenitor specific for macrophages and dendritic cells. *Science* 2006;311:83–7.
 18. Hettinger J, Richards DM, Hansson J, Barra MM, Joschko A-C, Krijgsveld J, Feuerer M. Origin of monocytes and macrophages in a committed progenitor. *Nat Immunol* 2013;14:821–30.
 19. Hussell T, Bell TJ. Alveolar macrophages: plasticity in a tissue-specific context. *Nat Rev Immunol* 2014;14:81–93.
 20. Davies LC, Jenkins SJ, Allen JE, Taylor PR. Tissue-resident macrophages. *Nat Immunol* 2013;14:986–95.
 21. Yona S, Kim K-W, Wolf Y, Mildner A, Varol D, Breker M, Strauss-Ayali D, Viukov S, Guilliams M, Misharin A, Hume DA, Perlman H, Malissen B, Zelzer E, Jung S. Fate mapping reveals origins and dynamics of monocytes and tissue macrophages under homeostasis. *Immunity* 2013;38:79–91.
 22. Schlitzer A, McGovern N, Teo P, Zelante T, Atarashi K, Low D, Ho AWS, See P, Shin A, Wasan PS, Hoeffel G, Malleret B, Heiseke A, Chew S, Jardine L, Purvis HA, Hilkens CMU, Tam J, Poidinger M, Stanley ER, Krug AB, Renia L, Sivasankar B, Ng LG, Collin M, Ricciardi-Castagnoli P, Honda K, Haniffa M, Ginhoux F. IRF4 transcription factor-dependent CD11b⁺ dendritic cells in human and mouse control mucosal IL-17 cytokine responses. *Immunity* 2013;38:970–83.
 23. Lambrecht BN. Alveolar macrophage in the driver's seat. *Immunity* 2006;24:366–8.
 24. Westphalen K, Gusarov GA, Islam MN, Subramanian M, Cohen TS, Prince AS, Bhattacharya J. Sessile alveolar macrophages communicate with alveolar epithelium to modulate immunity. *Nature* 2014;506:503–6.
 25. Watford WT, Wright JR, Hester CG, Jiang H, Frank MM. Surfactant protein A regulates complement activation. *J Immunol* 2001;167:6593–600.
 26. Haczku A. Protective role of the lung collectins surfactant protein A and surfactant protein D in airway inflammation. *J Allergy Clin Immunol* 2008;122:861–79; 880–1.

27. Morris DG, Huang X, Kaminski N, Wang Y, Shapiro SD, Dolganov G, Glick A, Sheppard D. Loss of integrin alpha(v)beta6-mediated TGF-beta activation causes Mmp12-dependent emphysema. *Nature* 2003;422:169–73.
28. Murray PJ. The primary mechanism of the IL-10-regulated antiinflammatory response is to selectively inhibit transcription. *Proc Natl Acad Sci U S A* 2005;102:8686–91.
29. Snelgrove RJ, Goulding J, Didierlaurent AM, Lyonga D, Vekaria S, Edwards L, Gwyer E, Sedgwick JD, Barclay AN, Hussell T. A critical function for CD200 in lung immune homeostasis and the severity of influenza infection. *Nat Immunol* 2008;9:1074–83.
30. Shultz LD, Rajan T V, Greiner DL. Severe defects in immunity and hematopoiesis caused by SHP-1 protein-tyrosine-phosphatase deficiency. *Trends Biotechnol* 1997;15:302–7.
31. Taylor PR, Martinez-Pomares L, Stacey M, Lin H-H, Brown GD, Gordon S. Macrophage receptors and immune recognition. *Annu Rev Immunol* 2005;23:901–44.
32. Maris NA, Dessing MC, de Vos AF, Bresser P, van der Zee JS, Jansen HM, Spek CA, van der Poll T. Toll-like receptor mRNA levels in alveolar macrophages after inhalation of endotoxin. *Eur Respir J* 2006;28:622–6.
33. Beutler BA. TLRs and innate immunity. *Blood* 2009;113:1399–407.
34. Opitz B, Püschel A, Schmeck B, Hocke AC, Rousseau S, Hammerschmidt S, Schumann RR, Suttorp N, Hippenstiel S. Nucleotide-binding oligomerization domain proteins are innate immune receptors for internalized *Streptococcus pneumoniae*. *J Biol Chem* 2004;279:36426–32.
35. Byrne BG, Dubuisson J-F, Joshi AD, Persson JJ, Swanson MS. Inflammasome components coordinate autophagy and pyroptosis as macrophage responses to infection. *MBio* 2013;4:e00620–12.
36. Opitz B, Rejaibi A, Dauber B, Eckhard J, Vinzing M, Schmeck B, Hippenstiel S, Suttorp N, Wolff T. IFNbeta induction by influenza A virus is mediated by RIG-I which is regulated by the viral NS1 protein. *Cell Microbiol* 2007;9:930–8.
37. Yoneyama M, Kikuchi M, Natsukawa T, Shinobu N, Imaizumi T, Miyagishi M, Taira K, Akira S, Fujita T. The RNA helicase RIG-I has an essential function in double-stranded RNA-induced innate antiviral responses. *Nat Immunol* 2004;5:730–7.
38. Cabanski M, Steinmüller M, Marsh LM, Surdziel E, Seeger W, Lohmeyer J. PKR regulates TLR2/TLR4-dependent signaling in murine alveolar macrophages. *Am J Respir Cell Mol Biol* 2008;38:26–31.

39. García MA, Gil J, Ventoso I, Guerra S, Domingo E, Rivas C, Esteban M. Impact of protein kinase PKR in cell biology: from antiviral to antiproliferative action. *Microbiol Mol Biol Rev* 2006;70:1032–60.
40. Strieter RM, Belperio JA, Keane MP. Host innate defenses in the lung: the role of cytokines. *Curr Opin Infect Dis* 2003;16:193–8.
41. Maus U a, Wellmann S, Hampl C, Kuziel W a, Srivastava M, Mack M, Everhart MB, Blackwell TS, Christman JW, Schlöndorff D, Bohle RM, Seeger W, Lohmeyer J. CCR2-positive monocytes recruited to inflamed lungs downregulate local CCL2 chemokine levels. *Am J Physiol Lung Cell Mol Physiol* 2005;288:L350–8.
42. Martinez FO. Macrophage activation and polarization. *Front Biosci* 2008;13:453.
43. Sica A, Mantovani A. Macrophage plasticity and polarization: in vivo veritas. *J Clin Invest* 2012;122:787–95.
44. MacMicking J, Xie QW, Nathan C. Nitric oxide and macrophage function. *Annu Rev Immunol* 1997;15:323–50.
45. Herold S, Steinmueller M, von Wulffen W, Cakarova L, Pinto R, Pleschka S, Mack M, Kuziel W a, Corazza N, Brunner T, Seeger W, Lohmeyer J. Lung epithelial apoptosis in influenza virus pneumonia: the role of macrophage-expressed TNF-related apoptosis-inducing ligand. *J Exp Med* 2008;205:3065–77.
46. Gordon S. Alternative activation of macrophages. *Nat Rev Immunol* 2003;3:23–35.
47. Gordon S, Taylor PR. Monocyte and macrophage heterogeneity. *Nat Rev Immunol* 2005;5:953–64.
48. Martinez FO, Gordon S. The M1 and M2 paradigm of macrophage activation: time for reassessment. *F1000Prime Rep* 2014;6:13.
49. Maus UA, Janzen S, Wall G, Srivastava M, Blackwell TS, Christman JW, Seeger W, Welte T, Lohmeyer J. Resident Alveolar Macrophages Are Replaced by Recruited Monocytes in Response to Endotoxin-Induced Lung Inflammation. *Am J Respir Cell Mol Biol* 2012;
50. Hashimoto D, Chow A, Noizat C, Teo P, Beasley MB, Leboeuf M, Becker CD, See P, Price J, Lucas D, Greter M, Mortha A, Boyer SW, Forsberg EC, Tanaka M, van Rooijen N, García-Sastre A, Stanley ER, Ginhoux F, Frenette PS, Merad M. Tissue-resident macrophages self-maintain locally throughout adult life with minimal contribution from circulating monocytes. *Immunity* 2013;38:792–804.
51. Zigmond E, Varol C, Farache J, Elmaliyah E, Satpathy AT, Friedlander G, Mack M, Shpigel N, Boneca IG, Murphy KM, Shakhar G, Halpern Z, Jung S. Ly6C hi monocytes in the inflamed colon give rise to proinflammatory effector cells and migratory antigen-presenting cells. *Immunity* 2012;37:1076–90.

52. Guth AM, Janssen WJ, Bosio CM, Crouch EC, Henson PM, Dow SW. Lung environment determines unique phenotype of alveolar macrophages. *Am J Physiol Lung Cell Mol Physiol* 2009;296:L936–46.
53. Ito S, Tanaka Y, Nishio N, Thanasegaran S, Isobe K-I. Establishment of self-renewable GM-CSF-dependent immature macrophages in vitro from murine bone marrow. *PLoS One* 2013;8:e76943.
54. Tsou C-L, Peters W, Si Y, Slaymaker S, Aslanian AM, Weisberg SP, Mack M, Charo IF. Critical roles for CCR2 and MCP-3 in monocyte mobilization from bone marrow and recruitment to inflammatory sites. *J Clin Invest* 2007;117:902–9.
55. Herold S, Wulffen W Von, Steinmueller M, Pleschka S, Kuziel WA, Mack M, Srivastava M, Seeger W, Maus UA, Lohmeyer J. Alveolar epithelial cells direct monocyte transepithelial migration upon influenza virus infection: impact of chemokines and adhesion molecules. *J Immunol* 2006;177:1817–1824.
56. Weibel ER. Gas exchange: large surface and thin barrier determine pulmonary diffusing capacity. *Minerva Anestesiol* 1999;65:377–82.
57. Mason RJ. Biology of alveolar type II cells. *Respirology* 2006;11 Suppl:S12–5.
58. Castranova V, Rabovsky J, Tucker JH, Miles PR. The alveolar type II epithelial cell: A multifunctional pneumocyte. *Toxicol Appl Pharmacol* 1988;93:472–483.
59. Meng W, Takeichi M. Adherens junction: molecular architecture and regulation. *Cold Spring Harb Perspect Biol* 2009;1:a002899.
60. Danjo Y, Gipson I. Actin “purse string” filaments are anchored by E-cadherin-mediated adherens junctions at the leading edge of the epithelial wound, providing coordinated cell movement. *J Cell Sci* 1998;111:3323–3332.
61. Knust E, Bossinger O. Composition and formation of intercellular junctions in epithelial cells. *Science* 2002;298:1955–9.
62. Felder E, Siebenbrunner M, Busch T, Fois G, Miklavc P, Walther P, Dietl P. Mechanical strain of alveolar type II cells in culture: changes in the transcellular cytoskeleton network and adaptations. *Am J Physiol Lung Cell Mol Physiol* 2008;295:L849–57.
63. Herold S, Gabrielli NM, Vadász I. Novel concepts of acute lung injury and alveolar-capillary barrier dysfunction. *Am J Physiol Lung Cell Mol Physiol* 2013;305:L665–81.
64. Matalon S. Mechanisms and regulation of ion transport in adult mammalian alveolar type II pneumocytes. *Am J Physiol* 1991;261:C727–38.
65. Folkesson HG, Matthay MA. Alveolar epithelial ion and fluid transport: recent progress. *Am J Respir Cell Mol Biol* 2006;35:10–9.

66. Cozens AL, Yezzi MJ, Kunzelmann K, Ohrui T, Chin L, Eng K, Finkbeiner WE, Widdicombe JH, Gruenert DC. CFTR expression and chloride secretion in polarized immortal human bronchial epithelial cells. *Am J Respir Cell Mol Biol* 1994;10:38–47.
67. Horisberger JD, Lemas V, Kraehenbühl JP, Rossier BC. Structure-function relationship of Na,K-ATPase. *Annu Rev Physiol* 1991;53:565–84.
68. Kaplan JH. Biochemistry of Na,K-ATPase. *Annu Rev Biochem* 2002;71:511–35.
69. Leak L V. Lymphatic removal of fluids and particles in the mammalian lung. *Environ Health Perspect* 1980;35:55–75.
70. Aukland K, Nicolaysen G. Interstitial fluid volume: local regulatory mechanisms. *Physiol Rev* 1981;61:556–643.
71. Matthay M a, Folkesson HG, Clerici C. Lung epithelial fluid transport and the resolution of pulmonary edema. *Physiol Rev* 2002;82:569–600.
72. Matthay MA, Wiener-Kronish JP. Intact Epithelial Barrier Function Is Critical for the Resolution of Alveolar Edema in Humans. *Am Rev Respir Dis* 2012;
73. Rajasekaran SA, Palmer LG, Moon SY, Peralta Soler A, Apodaca GL, Harper JF, Zheng Y, Rajasekaran AK. Na,K-ATPase Activity Is Required for Formation of Tight Junctions, Desmosomes, and Induction of Polarity in Epithelial Cells. *Mol Biol Cell* 2001;12:3717–3732.
74. Wiener-Kronish JP, Albertine KH, Matthay MA. Differential responses of the endothelial and epithelial barriers of the lung in sheep to Escherichia coli endotoxin. *J Clin Invest* 1991;88:864–75.
75. Ware LB. Pathophysiology of acute lung injury and the acute respiratory distress syndrome. *Semin Respir Crit Care Med* 2006;27:337–49.
76. Kühlbrandt W. Biology, structure and mechanism of P-type ATPases. *Nat Rev Mol Cell Biol* 2004;5:282–95.
77. Geering K. Functional roles of Na,K-ATPase subunits. *Curr Opin Nephrol Hypertens* 2008;17:526–32.
78. Reinhard L, Tidow H, Clausen MJ, Nissen P. Na(+),K (+)-ATPase as a docking station: protein-protein complexes of the Na(+),K (+)-ATPase. *Cell Mol Life Sci* 2013;70:205–22.
79. Sznajder JI, Factor P, Ingbar DH. Invited review: lung edema clearance: role of Na(+)-K(+)-ATPase. *J Appl Physiol* 2002;93:1860–6.
80. Geering K. The functional role of beta subunits in oligomeric P-type ATPases. *J Bioenerg Biomembr* 2001;33:425–38.

81. Geering K. Oligomerization and maturation of Na,K-ATPase: functional interaction of the cytoplasmic NH₂ terminus of the beta subunit with the alpha subunit. *J Cell Biol* 1996;133:1193–1204.
82. Lindzen M, Gottschalk K-E, Füzesi M, Garty H, Karlish SJD. Structural interactions between FXYD proteins and Na⁺,K⁺-ATPase: alpha/beta/FXYD subunit stoichiometry and cross-linking. *J Biol Chem* 2006;281:5947–55.
83. Morth JP, Pedersen BP, Toustrup-Jensen MS, Sørensen TL-M, Petersen J, Andersen JP, Vilse B, Nissen P. Crystal structure of the sodium-potassium pump. *Nature* 2007;450:1043–9.
84. Vadász I, Raviv S, Sznajder JI. Alveolar epithelium and Na,K-ATPase in acute lung injury. *Intensive Care Med* 2007;33:1243–51.
85. Matthay MA, Wiener-Kronish JP. Intact Epithelial Barrier Function Is Critical for the Resolution of Alveolar Edema in Humans. 2012;
86. Rajasekaran SA, Palmer LG, Quan K, Harper JF, Ball WJ, Bander NH, Peralta Soler A, Rajasekaran AK. Na,K-ATPase beta-subunit is required for epithelial polarization, suppression of invasion, and cell motility. *Mol Biol Cell* 2001;12:279–95.
87. Shoshani L, Contreras G, Moreno J, Balda S, Matter K, Cereijido M. The Polarized Expression of Na⁺, K⁺-ATPase in Epithelia Depends on the Association between α_L - Subunits Located in Neighboring Cells † a L . Rolda. *Mol Biol Cell* 2005;16:1071–1081.
88. Padilla-Benavides T, Roldán ML, Larre I, Flores-Benitez D, Villegas-Sepúlveda N, Contreras RG, Cereijido M, Shoshani L. The polarized distribution of Na⁺,K⁺-ATPase: role of the interaction between {beta} subunits. *Mol Biol Cell* 2010;21:2217–25.
89. Tian J, Cai T, Yuan Z, Wang H, Liu L, Haas M, Maksimova E, Huang X-Y, Xie Z-J. Binding of Src to Na⁺/K⁺-ATPase forms a functional signaling complex. *Mol Biol Cell* 2006;17:317–26.
90. Li Z, Cai T, Tian J, Xie JX, Zhao X, Liu L, Shapiro JI, Xie Z. NaKtide, a Na/K-ATPase-derived peptide Src inhibitor, antagonizes ouabain-activated signal transduction in cultured cells. *J Biol Chem* 2009;284:21066–76.
91. Ye Q, Li Z, Tian J, Xie JX, Liu L, Xie Z. Identification of a potential receptor that couples ion transport to protein kinase activity. *J Biol Chem* 2011;286:6225–32.
92. Haas M, Askari A, Xie Z. Involvement of Src and Epidermal Growth Factor Receptor in the Signal-transducing Function of Na⁺/K⁺-ATPase. *J Biol Chem* 2000;275:27832–27837.
93. Aydemir-Koksoy A, Abramowitz J, Allen JC. Ouabain-induced signaling and vascular smooth muscle cell proliferation. *J Biol Chem* 2001;276:46605–11.

94. Yuan Z, Cai T, Tian J, Ivanov A V, Giovannucci DR, Xie Z. Na/K-ATPase tethers phospholipase C and IP₃ receptor into a calcium-regulatory complex. *Mol Biol Cell* 2005;16:4034–45.
95. Schoner W, Scheiner-Bobis G. Endogenous and exogenous cardiac glycosides: their roles in hypertension, salt metabolism, and cell growth. *Am J Physiol Cell Physiol* 2007;293:C509–36.
96. Azarias G, Kruusmägi M, Connor S, Akkuratov EE, Liu X-L, Lyons D, Brismar H, Broberger C, Aperia A. A specific and essential role for Na,K-ATPase α 3 in neurons co-expressing α 1 and α 3. *J Biol Chem* 2013;288:2734–43.
97. Weigand KM, Swarts HGP, Fedosova NU, Russel FGM, Koenderink JB. Na,K-ATPase activity modulates Src activation: a role for ATP/ADP ratio. *Biochim Biophys Acta* 2012;1818:1269–73.
98. Bertorello AM, Ridge KM, Chibalin A V., Katz AI, Sznajder JI. Isoproterenol increases Na⁺-K⁺-ATPase activity by membrane insertion of alpha -subunits in lung alveolar cells. *Am J Physiol Lung Cell Mol Physiol* 1999;276:L20–27.
99. Lecuona E, Sun H, Vohwinkel C, Ciechanover A, Sznajder JI. Ubiquitination participates in the lysosomal degradation of Na,K-ATPase in steady-state conditions. *Am J Respir Cell Mol Biol* 2009;41:671–9.
100. Lecuona E, Trejo HE, Sznajder JI. Regulation of Na,K-ATPase during acute lung injury. *J Bioenerg Biomembr* 2007;39:391–5.
101. Wujak LA, Becker S, Arnoldt V, Wygrecka M, Seeger W, Morty RE. Histone deacetylase-dependent control of lung alveolar fluid clearance. *FASEB J* 2013;27:736.4–.
102. Wujak LA, Becker S, Arnoldt V, Morty RE. Epigenetic control of lung fluid clearance. *FASEB J* 2012;26:885.5–.
103. Adir Y, Welch LC, Dumasius V, Factor P, Sznajder JI, Ridge KM. Overexpression of the Na-K-ATPase alpha2-subunit improves lung liquid clearance during ventilation-induced lung injury. *Am J Physiol Lung Cell Mol Physiol* 2008;294:L1233–7.
104. Azzam ZS, Dumasius V, Saldias FJ, Adir Y, Sznajder JI, Factor P. Na,K-ATPase overexpression improves alveolar fluid clearance in a rat model of elevated left atrial pressure. *Circulation* 2002;105:497–501.
105. Machado-Aranda D, Adir Y, Young JL, Briva A, Budinger GRS, Yeldandi A V, Sznajder JI, Dean DA. Gene transfer of the Na⁺,K⁺-ATPase beta1 subunit using electroporation increases lung liquid clearance. *Am J Respir Crit Care Med* 2005;171:204–11.

106. Mutlu M, Machado-aranda D, Norton JE, Bellmeyer A, Urich D. Electroporation-mediated Gene Transfer of the Na⁺, K⁺-ATPase Rescues Endotoxin-induced Lung Injury. doi:10.1164/rccm.200608-1246OC.
107. Althaus M, Pichl A, Clauss WG, Seeger W, Fronius M, Morty RE. Nitric oxide inhibits highly selective sodium channels and the Na⁺/K⁺-ATPase in H441 cells. *Am J Respir Cell Mol Biol* 2011;44:53–65.
108. Gusarova G a, Trejo HE, Dada L a, Briva A, Welch LC, Hamanaka RB, Mutlu GM, Chandel NS, Prakriya M, Sznajder JI. Hypoxia leads to Na,K-ATPase downregulation via Ca(2+) release-activated Ca(2+) channels and AMPK activation. *Mol Cell Biol* 2011;31:3546–56.
109. Dada LA, Chandel NS, Ridge KM, Pedemonte C, Bertorello AM, Sznajder JI. Hypoxia-induced endocytosis of Na,K-ATPase in alveolar epithelial cells is mediated by mitochondrial reactive oxygen species and PKC-zeta. *J Clin Invest* 2003;111:1057–64.
110. Mutlu GM, Snyder C, Bellmeyer A, Wang H, Hawkins K, Soberanes S, Welch LC, Ghio AJ, Chandel NS, Kamp D, Sznajder JI, Budinger GRS. Airborne particulate matter inhibits alveolar fluid reabsorption in mice via oxidant generation. *Am J Respir Cell Mol Biol* 2006;34:670–6.
111. Vadász I, Morty RE, Olschewski A, Königshoff M, Kohstall MG, Ghofrani HA, Grimminger F, Seeger W. Thrombin impairs alveolar fluid clearance by promoting endocytosis of Na⁺,K⁺-ATPase. *Am J Respir Cell Mol Biol* 2005;doi:10.1165/rcmb.2004-0407OC.
112. M O-K, H K. Insulin stimulates the translocation of Na⁺/K⁽⁺⁾-dependent ATPase molecules from intracellular stores to the plasma membrane in frog skeletal muscle. *Biochem J* 1990;272:727–733.
113. Barquin N, Ciccolella DE, Ridge KM, Sznajder JI. Dexamethasone upregulates the Na-K-ATPase in rat alveolar epithelial cells. *Am J Physiol Lung Cell Mol Physiol* 1997;273:L825–830.
114. Shahedi M, Laborde K, Bussières L, Sachs C. Acute and early effects of aldosterone on Na-K-ATPase activity in Madin-Darby canine kidney epithelial cells. *Am J Physiol* 1993;264:F1021–6.
115. Helenius IT, Dada L a, Sznajder JI. Role of ubiquitination in Na,K-ATPase regulation during lung injury. *Proc Am Thorac Soc* 2010;7:65–70.
116. Witczak C a, Sharoff CG, Goodyear LJ. AMP-activated protein kinase in skeletal muscle: from structure and localization to its role as a master regulator of cellular metabolism. *Cell Mol Life Sci* 2008;65:3737–55.
117. Kramer HF, Witczak CA, Fujii N, Jessen N, Taylor EB, Arnolds DE, Sakamoto K, Hirshman MF, Goodyear LJ. Distinct signals regulate AS160 phosphorylation in

- response to insulin, AICAR, and contraction in mouse skeletal muscle. *Diabetes* 2006;55:2067–76.
118. Treebak JT, Glund S, Deshmukh A, Klein DK, Long YC, Jensen TE, Jørgensen SB, Viollet B, Andersson L, Neumann D, Wallimann T, Richter EA, Chibalin A V, Zierath JR, Wojtaszewski JFP. AMPK-mediated AS160 phosphorylation in skeletal muscle is dependent on AMPK catalytic and regulatory subunits. *Diabetes* 2006;55:2051–8.
 119. Jørgensen SB, Nielsen JN, Birk JB, Olsen GS, Viollet B, Andreelli F, Schjerling P, Vaulont S, Hardie DG, Hansen BF, Richter EA, Wojtaszewski JFP. The alpha2-5'AMP-activated protein kinase is a site 2 glycogen synthase kinase in skeletal muscle and is responsive to glucose loading. *Diabetes* 2004;53:3074–81.
 120. Vadász I, Dada LA, Briva A, Trejo HE, Welch LC, Chen J, Tóth PT, Lecuona E, Witters LA, Schumacker PT, Chandel NS, Seeger W, Sznajder JI. AMP-activated protein kinase regulates CO₂-induced alveolar epithelial dysfunction in rats and human cells by promoting Na,K-ATPase endocytosis. *J Clin Invest* 2008;118:752–62.
 121. Matthay M a, Robriquet L, Fang X. Alveolar epithelium: role in lung fluid balance and acute lung injury. *Proc Am Thorac Soc* 2005;2:206–13.
 122. Guerrero C, Lecuona E, Pesce L, Ridge KM, Sznajder JI. Dopamine regulates Na-K-ATPase in alveolar epithelial cells via MAPK-ERK-dependent mechanisms. *Am J Physiol Cell Mol Physiol* 2001;281:L79.
 123. Borok Z, Danto SI, Dimen LL, Zhang XL, Lubman RL. Na(+)–K(+)–ATPase expression in alveolar epithelial cells: upregulation of active ion transport by KGF. *Am J Physiol* 1998;274:L149–58.
 124. Borok Z, Hami A, Danto SI, Lubman RL, Kim KJ, Crandall ED. Effects of EGF on alveolar epithelial junctional permeability and active sodium transport. *Am J Physiol Lung Cell Mol Physiol* 1996;270:L559–565.
 125. Sznajder JI, Ridge KM, Yeates DB, Ilekis J, Olivera W. Epidermal growth factor increases lung liquid clearance in rat lungs. *J Appl Physiol* 1998;85:1004–1010.
 126. De Jong MD, Simmons CP, Thanh TT, Hien VM, Smith GJD, Chau TNB, Hoang DM, Chau NVV, Khanh TH, Dong VC, Qui PT, Cam B Van, Ha DQ, Guan Y, Peiris JSM, Chinh NT, Hien TT, Farrar J. Fatal outcome of human influenza A (H5N1) is associated with high viral load and hypercytokinemia. *Nat Med* 2006;12:1203–7.
 127. Jain S, Kamimoto L, Bramley AM, Schmitz AM, Benoit SR, Louie J, Sugerman DE, Druckenmiller JK, Ritger KA, Chugh R, Jasuja S, Deutscher M, Chen S, Walker JD, Duchin JS, Lett S, Soliva S, Wells E V, Swerdlow D, Uyeki TM, Fiore AE, Olsen SJ, Fry AM, Bridges CB, Finelli L. Hospitalized patients with 2009 H1N1 influenza in the United States, April-June 2009. *N Engl J Med* 2009;361:1935–44.

128. Short KR, Kroeze EJBV, Fouchier R a M, Kuiken T. Pathogenesis of influenza-induced acute respiratory distress syndrome. *Lancet Infect Dis* 2014;14:57–69.
129. Molinari N-AM, Ortega-Sanchez IR, Messonnier ML, Thompson WW, Wortley PM, Weintraub E, Bridges CB. The annual impact of seasonal influenza in the US: measuring disease burden and costs. *Vaccine* 2007;25:5086–96.
130. Simonsen L. The global impact of influenza on morbidity and mortality. *Vaccine* 1999;17:S3–S10.
131. Ballinger MN, Standiford TJ. Postinfluenza bacterial pneumonia: host defenses gone awry. *J Interferon Cytokine Res* 2010;30:643–52.
132. Morens DM, Taubenberger JK, Fauci AS. Predominant role of bacterial pneumonia as a cause of death in pandemic influenza: implications for pandemic influenza preparedness. *J Infect Dis* 2008;198:962–70.
133. Lamb R, Krug R, Knipe D. Orthomyxoviridae: The Viruses and Their Replication. In: Bernard N. Fields, David Mahan Knipe PMH, editor. *Fields Virol* Lippincott Williams & Wilkins; 2001. p. 1487–1531.
134. Fouchier RAM, Munster V, Wallensten A, Bestebroer TM, Herfst S, Smith D, Rimmelzwaan GF, Olsen B, Osterhaus ADME. Characterization of a novel influenza A virus hemagglutinin subtype (H16) obtained from black-headed gulls. *J Virol* 2005;79:2814–2822.
135. Tong S, Li Y, Rivailler P, Conrardy C, Castillo DAA, Chen L-M, Recuenco S, Ellison JA, Davis CT, York IA, Turmelle AS, Moran D, Rogers S, Shi M, Tao Y, Weil MR, Tang K, Rowe LA, Sammons S, Xu X, Frace M, Lindblade KA, Cox NJ, Anderson LJ, Rupprecht CE, Donis RO. A distinct lineage of influenza A virus from bats. *Proc Natl Acad Sci* 2012;
136. Lamb RA, Choppin PW. The gene structure and replication of influenza virus. *Annu Rev Biochem* 1983;52:467–506.
137. Lamb RA, Lai CJ, Choppin PW. Sequences of mRNAs derived from genome RNA segment 7 of influenza virus: colinear and interrupted mRNAs code for overlapping proteins. *Proc Natl Acad Sci U S A* 1981;78:4170–4.
138. Inglis SC, Almond JW. An Influenza Virus Gene Encoding Two Different Proteins. *Philos Trans R Soc B Biol Sci* 1980;288:375–381.
139. Chen W, Calvo PA, Malide D, Gibbs J, Schubert U, Bacik I, Basta S, O'Neill R, Schickli J, Palese P, Henklein P, Bennink JR, Yewdell JW. A novel influenza A virus mitochondrial protein that induces cell death. *Nat Med* 2001;7:1306–12.
140. Subbarao K, Joseph T. Scientific barriers to developing vaccines against avian influenza viruses. *Nat Rev Immunol* 2007;7:267–78.

141. Matrosovich MN, Gambaryan AS, Teneberg S, Piskarev VE, Yamnikova SS, Lvov DK, Robertson JS, Karlsson KA. Avian influenza A viruses differ from human viruses by recognition of sialyloligosaccharides and gangliosides and by a higher conservation of the HA receptor-binding site. *Virology* 1997;233:224–34.
142. Skehel JJ, Bayley PM, Brown EB, Martin SR, Waterfield MD, White JM, Wilson IA, Wiley DC. Changes in the conformation of influenza virus hemagglutinin at the pH optimum of virus-mediated membrane fusion. *Proc Natl Acad Sci* 1982;79:968–972.
143. Pinto LH, Holsinger LJ, Lamb RA. Influenza virus M2 protein has ion channel activity. *Cell* 1992;69:517–28.
144. Helenius A. Unpacking the incoming influenza virus. *Cell* 1992;69:577–8.
145. Gabriel G, Herwig A, Klenk H-D. Interaction of polymerase subunit PB2 and NP with importin alpha1 is a determinant of host range of influenza A virus. *PLoS Pathog* 2008;4:e11.
146. Resa-Infante P, Gabriel G. The nuclear import machinery is a determinant of influenza virus host adaptation. *Bioessays* 2013;35:23–7.
147. Whittaker G, Bui M, Helenius A. Nuclear trafficking of influenza virus ribonucleoproteins in heterokaryons. *J Virol* 1996;70:2743–56.
148. Elton D, Simpson-Holley M, Archer K, Medcalf L, Hallam R, McCauley J, Digard P. Interaction of the influenza virus nucleoprotein with the cellular CRM1-mediated nuclear export pathway. *J Virol* 2001;75:408–19.
149. Nayak DP, Hui EK-W, Barman S. Assembly and budding of influenza virus. *Virus Res* 2004;106:147–65.
150. Bruce EA, Digard P, Stuart AD. The Rab11 pathway is required for influenza A virus budding and filament formation. *J Virol* 2010;84:5848–59.
151. Palese P, Tobita K, Ueda M, Compans RW. Characterization of temperature sensitive influenza virus mutants defective in neuraminidase. *Virology* 1974;61:397–410.
152. Herold S, Becker C, Ridge KM, Budinger GRS. Influenza virus-induced lung injury: pathogenesis and implications for treatment. *Eur Respir J* 2015;doi:10.1183/09031936.00186214.
153. Bedford T, Cobey S, Beerli P, Pascual M. Global migration dynamics underlie evolution and persistence of human influenza A (H3N2). *PLoS Pathog* 2010;6:e1000918.
154. Rambaut A, Pybus O, Nelson M. The genomic and epidemiological dynamics of human influenza A virus. *Nature* 2008;453:615–619.

155. Russell C a, Jones TC, Barr IG, Cox NJ, Garten RJ, Gregory V, Gust ID, Hampson AW, Hay AJ, Hurt AC, de Jong JC, Kelso A, Klimov AI, Kageyama T, Komadina N, Lapedes AS, Lin YP, Mosterin A, Obuchi M, Odagiri T, Osterhaus ADME, Rimmelzwaan GF, Shaw MW, Skepner E, Stohr K, Tashiro M, Fouchier R a M, Smith DJ. The global circulation of seasonal influenza A (H3N2) viruses. *Science* 2008;320:340–6.
156. Steinhauer DA, Holland JJ. Rapid evolution of RNA viruses. *Annu Rev Microbiol* 1987;41:409–33.
157. Ortiz JR, Neuzil KM, Rue TC, Zhou H, Shay DK, Cheng P-Y, Cooke CR, Goss CH. Population-based incidence estimates of influenza-associated respiratory failure hospitalizations, 2003 to 2009. *Am J Respir Crit Care Med* 2013;188:710–5.
158. Taubenberger J. The origin and virulence of the 1918 “Spanish” influenza virus. ... *Am Philos Soc* 2006;150:1–23.
159. Miller M, Viboud C. The signature features of influenza pandemics—implications for policy. *New Engl J* 2009;360:2595–2598.
160. Cox NJ, Subbarao K. G LOBAL E PIDEMIOLOGY OF INFLUENZA : Past and Present *. *Annu Rev Med* 2000;407–421.
161. Libster R, Bugna J, Coviello S, Hijano DR, Dunaiiewsky M, Reynoso N, Cavalieri ML, Guglielmo MC, Areso MS, Gilligan T, Santucho F, Cabral G, Gregorio GL, Moreno R, Lutz MI, Panigasi AL, Saligari L, Caballero MT, Egües Almeida RM, Gutierrez Meyer ME, Neder MD, Davenport MC, Del Valle MP, Santidrian VS, Mosca G, Garcia Domínguez M, Alvarez L, Landa P, Pota A, et al. Pediatric hospitalizations associated with 2009 pandemic influenza A (H1N1) in Argentina. *N Engl J Med* 2010;362:45–55.
162. Estenssoro E, Ríos FG, Apeteguía C, Reina R, Neira J, Ceraso DH, Orlandi C, Valentini R, Tiribelli N, Brizuela M, Balasini C, Mare S, Domeniconi G, Ilutovich S, Gómez A, Giuliani J, Barrios C, Valdez P. Pandemic 2009 influenza A in Argentina: a study of 337 patients on mechanical ventilation. *Am J Respir Crit Care Med* 2010;182:41–48.
163. Worobey M, Han G-Z, Rambaut A. A synchronized global sweep of the internal genes of modern avian influenza virus. *Nature* 2014;508:254–7.
164. Kuiken T, Taubenberger J. Pathology of human influenza revisited. *Vaccine* 2008;26:D59–66.
165. Kawaoka Y, Krauss S, Webster RG. Avian-to-human transmission of the PB1 gene of influenza A viruses in the 1957 and 1968 pandemics. *J Virol* 1989;63:4603–8.
166. Belshe RB. Implications of the emergence of a novel H1 influenza virus. *N Engl J Med* 2009;360:2667–8.

167. Komar N, Olsen B. Avian influenza virus (H5N1) mortality surveillance. *Emerg Infect Dis* 2008;14:1176–1178.
168. Koopmans M, Wilbrink B, Conyn M, Natrop G, van der Nat H, Vennema H, Meijer A, van Steenbergen J, Fouchier R, Osterhaus A, Bosman A. Transmission of H7N7 avian influenza A virus to human beings during a large outbreak in commercial poultry farms in the Netherlands. *Lancet* 2004;363:587–93.
169. Gao R, Cao B, Hu Y, Feng Z, Wang D, Hu W, Chen J, Jie Z, Qiu H, Xu K, Xu X, Lu H, Zhu W, Gao Z, Xiang N, Shen Y, He Z, Gu Y, Zhang Z, Yang Y, Zhao X, Zhou L, Li X, Zou S, Zhang Y, Li X, Yang L, Guo J, Dong J, et al. Human infection with a novel avian-origin influenza A (H7N9) virus. *N Engl J Med* 2013;368:1888–97.
170. Lin YP, Shaw M, Gregory V, Cameron K, Lim W, Klimov a, Subbarao K, Guan Y, Krauss S, Shortridge K, Webster R, Cox N, Hay a. Avian-to-human transmission of H9N2 subtype influenza A viruses: relationship between H9N2 and H5N1 human isolates. *Proc Natl Acad Sci U S A* 2000;97:9654–8.
171. Li Q, Zhou L, Zhou M, Chen Z, Li F, Wu H, Xiang N, Chen E, Tang F, Wang D, Meng L, Hong Z, Tu W, Cao Y, Li L, Ding F, Liu B, Wang M, Xie R, Gao R, Li X, Bai T, Zou S, He J, Hu J, Xu Y, Chai C, Wang S, Gao Y, et al. Epidemiology of human infections with avian influenza A(H7N9) virus in China. *N Engl J Med* 2014;370:520–32.
172. Matrosovich M, Tuzikov A, Bovin N, Gambaryan A, Klimov A, Maria R, Donatelli I, Kawaoka Y. Early Alterations of the Receptor-Binding Properties of H1 , H2 , and H3 Avian Influenza Virus Hemagglutinins after Their Introduction into Mammals Early Alterations of the Receptor-Binding Properties of H1 , H2 , and H3 Avian Influenza Virus Hemagglutini. *J Virol* 2000;74:8502–8512.
173. Dortmans JCFM, Dekkers J, Wickramasinghe INA, Verheije MH, Rottier PJM, van Kuppeveld FJM, de Vries E, de Haan C a M. Adaptation of novel H7N9 influenza A virus to human receptors. *Sci Rep* 2013;3:3058.
174. Uhlandorff J, Matrosovich T, Klenk H-D, Matrosovich M. Functional significance of the hemadsorption activity of influenza virus neuraminidase and its alteration in pandemic viruses. *Arch Virol* 2009;154:945–57.
175. Mehle A, Dugan VG, Taubenberger JK, Doudna J a. Reassortment and mutation of the avian influenza virus polymerase PA subunit overcome species barriers. *J Virol* 2012;86:1750–7.
176. Mänz B, Schwemmle M, Brunotte L. Adaptation of avian influenza A virus polymerase in mammals to overcome the host species barrier. *J Virol* 2013;87:7200–9.
177. Linster M, van Boheemen S, de Graaf M, Schrauwen EJ a, Lexmond P, Mänz B, Bestebroer TM, Baumann J, van Riel D, Rimmelzwaan GF, Osterhaus ADME, Matrosovich M, Fouchier R a M, Herfst S. Identification, characterization, and

- natural selection of mutations driving airborne transmission of A/H5N1 virus. *Cell* 2014;157:329–39.
178. Jefferson T, Demicheli V, Rivetti D, Jones M, Di Pietrantonj C, Rivetti a. Antivirals for influenza in healthy adults: systematic review. *Lancet* 2006;367:303–13.
 179. Nemeroff ME, Barabino SM, Li Y, Keller W, Krug RM. Influenza virus NS1 protein interacts with the cellular 30 kDa subunit of CPSF and inhibits 3'end formation of cellular pre-mRNAs. *Mol Cell* 1998;1:991–1000.
 180. Twu KY, Noah DL, Rao P, Kuo R-L, Krug RM. The CPSF30 binding site on the NS1A protein of influenza A virus is a potential antiviral target. *J Virol* 2006;80:3957–65.
 181. Golebiewski L, Liu H, Javier RT, Rice AP. The avian influenza virus NS1 ESEV PDZ binding motif associates with Dlg1 and Scribble to disrupt cellular tight junctions. *J Virol* 2011;85:10639–48.
 182. Chen X, Seth S, Yue G, Kamat P, Compans RW, Guidot D, Brown LA, Eaton DC, Jain L. Influenza virus inhibits ENaC and lung fluid clearance. 2010;366–373.doi:10.1152/ajplung.00011.2004.
 183. Kunzelmann K, Beesley a H, King NJ, Karupiah G, Young J a, Cook DI. Influenza virus inhibits amiloride-sensitive Na⁺ channels in respiratory epithelia. *Proc Natl Acad Sci U S A* 2000;97:10282–7.
 184. Lazrak A, Iles KE, Liu G, Noah DL, Noah JW, Matalon S. Influenza virus M2 protein inhibits epithelial sodium channels by increasing reactive oxygen species. *FASEB J* 2009;23:3829–42.
 185. Londino JD, Lazrak A, Jurkuvenaite A, Collawn JF, Noah JW, Matalon S. Influenza matrix protein 2 alters CFTR expression and function through its ion channel activity. *Am J Physiol Lung Cell Mol Physiol* 2013;304:L582–92.
 186. Gack MU, Shin YC, Joo C-H, Urano T, Liang C, Sun L, Takeuchi O, Akira S, Chen Z, Inoue S, Jung JU. TRIM25 RING-finger E3 ubiquitin ligase is essential for RIG-I-mediated antiviral activity. *Nature* 2007;446:916–920.
 187. Clemens MJ, Elia A. The Double-Stranded RNA-Dependent Protein Kinase PKR: Structure and Function. *J Interferon Cytokine Res* 2009;17:503–24.
 188. Kumar A, Haque J, Lacoste J, Hiscott J, Williams BR. Double-stranded RNA-dependent protein kinase activates transcription factor NF-kappa B by phosphorylating I kappa B. *Proc Natl Acad Sci U S A* 1994;91:6288–92.
 189. Gil J, Esteban M. Induction of apoptosis by the dsRNA-dependent protein kinase (PKR): Mechanism of action. *Apoptosis* 5:107–114.

190. Barchet W, Krug A, Cella M, Newby C, Fischer JAA, Dziona A, Pekosz A, Colonna M. Dendritic cells respond to influenza virus through TLR7- and PKR-independent pathways. *Eur J Immunol* 2005;35:236–42.
191. Le Goffic R, Balloy V, Lagranderie M, Alexopoulou L, Escriou N, Flavell R, Chignard M, Si-Tahar M. Detrimental contribution of the Toll-like receptor (TLR)3 to influenza A virus-induced acute pneumonia. *PLoS Pathog* 2006;2:e53.
192. Allen IC, Scull MA, Moore CB, Holl EK, McElvania-TeKippe E, Taxman DJ, Guthrie EH, Pickles RJ, Ting JP-Y. The NLRP3 inflammasome mediates in vivo innate immunity to influenza A virus through recognition of viral RNA. *Immunity* 2009;30:556–65.
193. Thomas PG, Dash P, Aldridge JR, Ellebedy AH, Reynolds C, Funk AJ, Martin WJ, Lamkanfi M, Webby RJ, Boyd KL, Doherty PC, Kanneganti T-D. The intracellular sensor NLRP3 mediates key innate and healing responses to influenza A virus via the regulation of caspase-1. *Immunity* 2009;30:566–75.
194. Ludwig S, Pleschka S, Planz O, Wolff T. Ringing the alarm bells: signalling and apoptosis in influenza virus infected cells. *Cell Microbiol* 2006;8:375–86.
195. Chan M, Cheung C, Chui W, Tsao S, Nicholls J, Chan Y, Chan R, Long H, Poon L, Guan Y, others. Proinflammatory cytokine responses induced by influenza A (H5N1) viruses in primary human alveolar and bronchial epithelial cells. *Respir Res* 2005;6:135.
196. Tumpey TM, García-Sastre A, Taubenberger JK, Palese P, Swayne DE, Pantin-Jackwood MJ, Schultz-Cherry S, Solórzano A, Van Rooijen N, Katz JM, Basler CF. Pathogenicity of influenza viruses with genes from the 1918 pandemic virus: functional roles of alveolar macrophages and neutrophils in limiting virus replication and mortality in mice. *J Virol* 2005;79:14933–44.
197. Lin KL, Suzuki Y, Nakano H, Ramsburg E, Gunn MD. CCR2+ monocyte-derived dendritic cells and exudate macrophages produce influenza-induced pulmonary immune pathology and mortality. *J Immunol* 2008;180:2562–72.
198. Szretter KJ, Gangappa S, Lu X, Smith C, Shieh W-J, Zaki SR, Sambhara S, Tumpey TM, Katz JM. Role of host cytokine responses in the pathogenesis of avian H5N1 influenza viruses in mice. *J Virol* 2007;81:2736–44.
199. Van Reeth K. Cytokines in the pathogenesis of influenza. *Vet Microbiol* 2000;74:109–116.
200. Baskin CR, Bielefeldt-Ohmann H, Tumpey TM, Sabourin PJ, Long JP, García-Sastre A, Tolnay A-E, Albrecht R, Pyles JA, Olson PH, Aicher LD, Rosenzweig ER, Murali-Krishna K, Clark EA, Kotur MS, Fornek JL, Proll S, Palermo RE, Sabourin CL, Katze MG. Early and sustained innate immune response defines pathology and death in nonhuman primates infected by highly pathogenic influenza virus. *Proc Natl Acad Sci U S A* 2009;106:3455–60.

201. Högner K, Wolff T, Pleschka S, Plog S, Gruber AD, Kalinke U, Walmrath H-D, Bodner J, Gattenlöhner S, Lewe-Schlosser P, Matrosovich M, Seeger W, Lohmeyer J, Herold S. Macrophage-expressed IFN- β contributes to apoptotic alveolar epithelial cell injury in severe influenza virus pneumonia. *PLoS Pathog* 2013;9:e1003188.
202. Kallfass C, Lienenklaus S, Weiss S, Staeheli P. Visualizing the beta interferon response in mice during infection with influenza A viruses expressing or lacking nonstructural protein 1. *J Virol* 2013;87:6925–30.
203. Jewell NA, Vaghefi N, Mertz SE, Akter P, Peebles RS, Bakalatz LO, Durbin RK, Flaño E, Durbin JE. Differential type I interferon induction by respiratory syncytial virus and influenza a virus in vivo. *J Virol* 2007;81:9790–800.
204. Malmgaard L. Induction and regulation of IFNs during viral infections. *J Interferon Cytokine Res* 2004;24:439–54.
205. Hoffmann H-H, Schneider WM, Rice CM. Interferons and viruses: an evolutionary arms race of molecular interactions. *Trends Immunol* 2015;36:124–138.
206. Iwasaki A, Pillai PS. Innate immunity to influenza virus infection. *Nat Rev Immunol* 2014;14:315–28.
207. Davidson S, Crotta S, McCabe TM, Wack A. Pathogenic potential of interferon $\alpha\beta$ in acute influenza infection. *Nat Commun* 2014;5:3864.
208. Wiley SR, Schooley K, Smolak PJ, Din WS, Huang C-P, Nicholl JK, Sutherland GR, Smith TD, Rauch C, Smith CA, Goodwin RG. Identification and characterization of a new member of the TNF family that induces apoptosis. *Immunity* 1995;3:673–682.
209. LeBlanc HN, Ashkenazi A. Apo2L/TRAIL and its death and decoy receptors. *Cell Death Differ* 2003;10:66–75.
210. Wu GS, Burns TF, Zhan Y, Alnemri ES, El-Deiry WS. Molecular cloning and functional analysis of the mouse homologue of the KILLER/DR5 tumor necrosis factor-related apoptosis-inducing ligand (TRAIL) death receptor. *Cancer Res* 1999;59:2770–5.
211. Zhivotovsky B. Caspases: the enzymes of death. *Essays Biochem* 2003;39:25–40.
212. Cretney E, Takeda K, Yagita H, Glaccum M, Peschon JJ, Smyth MJ. Increased susceptibility to tumor initiation and metastasis in TNF-related apoptosis-inducing ligand-deficient mice. *J Immunol* 2002;168:1356–61.
213. Müller U, Steinhoff U, Reis LF, Hemmi S, Pavlovic J, Zinkernagel RM, Aguet M. Functional role of type I and type II interferons in antiviral defense. *Science* 1994;264:1918–21.
214. Finnberg N, Gruber JJ, Fei P, Rudolph D, Bric A, Kim S-H, Burns TF, Ajuha H, Page R, Wu GS, Chen Y, McKenna WG, Bernhard E, Lowe S, Mak T, El-Deiry WS. DR5

- knockout mice are compromised in radiation-induced apoptosis. *Mol Cell Biol* 2005;25:2000–13.
215. Kuziel WA, Morgan SJ, Dawson TC, Griffin S, Smithies O, Ley K, Maeda N. Severe reduction in leukocyte adhesion and monocyte extravasation in mice deficient in CC chemokine receptor 2. *Proc Natl Acad Sci U S A* 1997;94:12053–8.
 216. Corti M, Brody AR, Harrison JH. Isolation and primary culture of murine alveolar type II cells. *Am J Respir Cell Mol Biol* 1996;14:309–15.
 217. Mutlu GM, Dumasius V, Burhop J, McShane PJ, Meng FJ, Welch L, Dumasius A, Mohebalmadi N, Thakuria G, Hardiman K, Matalon S, Hollenberg S, Factor P. Upregulation of alveolar epithelial active Na⁺ transport is dependent on beta2-adrenergic receptor signaling. *Circ Res* 2004;94:1091–100.
 218. Marsh LM, Cakarova L, Kwapiszewska G, von Wulffen W, Herold S, Seeger W, Lohmeyer J. Surface expression of CD74 by type II alveolar epithelial cells: a potential mechanism for macrophage migration inhibitory factor-induced epithelial repair. *Am J Physiol Lung Cell Mol Physiol* 2009;296:L442–52.
 219. Williams MC, Cao Y, Hinds A, Rishi AK, Wetterwald A. T1 alpha protein is developmentally regulated and expressed by alveolar type I cells, choroid plexus, and ciliary epithelia of adult rats. *Am J Respir Cell Mol Biol* 1996;14:577–85.
 220. Park SH, Gammon SR, Knippers JD, Paulsen SR, Rubink DS, Winder WW. Phosphorylation-activity relationships of AMPK and acetyl-CoA carboxylase in muscle. *J Appl Physiol* 2002;92:2475–82.
 221. Kaushik VK, Young ME, Dean DJ, Kurowski TG, Saha AK, Ruderman NB. Regulation of fatty acid oxidation and glucose metabolism in rat soleus muscle: effects of AICAR. *Am J Physiol Endocrinol Metab* 2001;281:E335–40.
 222. Sullivan JE, Brocklehurst KJ, Marley AE, Carey F, Carling D, Beri RK. Inhibition of lipolysis and lipogenesis in isolated rat adipocytes with AICAR, a cell-permeable activator of AMP-activated protein kinase. *FEBS Lett* 1994;353:33–36.
 223. Zhou G, Myers R, Li Y, Chen Y, Shen X, Fenyk-Melody J, Wu M, Ventre J, Doepper T, Fujii N, Musi N, Hirshman MF, Goodyear LJ, Moller DE. Role of AMP-activated protein kinase in mechanism of metformin action. *J Clin Invest* 2001;108:1167–74.
 224. Witczak C a, Sharoff CG, Goodyear LJ. AMP-activated protein kinase in skeletal muscle: from structure and localization to its role as a master regulator of cellular metabolism. *Cell Mol Life Sci* 2008;65:3737–55.
 225. Ninomiya-Tsuji J, Kajino T, Ono K, Ohtomo T, Matsumoto M, Shiina M, Mihara M, Tsuchiya M, Matsumoto K. A resorcylic acid lactone, 5Z-7-oxozeanenol, prevents inflammation by inhibiting the catalytic activity of TAK1 MAPK kinase kinase. *J Biol Chem* 2003;278:18485–90.

226. Shuofu MI, Yan LI, Jinghua YAN, Fu GAOG. Na⁺ / K⁺-ATPase β1 subunit interacts with M2 proteins of influenza A and B viruses and affects the virus replication. 2010;53:1098–1105.
227. Londino JD, Lazrak A, Noah JW, Aggarwal S, Bali V, Woodworth BA, Bebok Z, Matalon S. Influenza virus M2 targets cystic fibrosis transmembrane conductance regulator for lysosomal degradation during viral infection. *FASEB J* 2015;doi:10.1096/fj.14-268755.
228. Jewell N a, Vaghefi N, Mertz SE, Akter P, Peebles RS, Bakaletz LO, Durbin RK, Flaño E, Durbin JE. Differential type I interferon induction by respiratory syncytial virus and influenza a virus in vivo. *J Virol* 2007;81:9790–800.
229. Hayden FG, Fritz R, Lobo MC, Alvord W, Strober W, Straus SE. Local and systemic cytokine responses during experimental human influenza A virus infection. Relation to symptom formation and host defense. *J Clin Invest* 1998;101:643–9.
230. Arimori Y, Nakamura R, Yamada H, Shibata K, Maeda N, Kase T, Yoshikai Y. Type I interferon limits influenza virus-induced acute lung injury by regulation of excessive inflammation in mice. *Antiviral Res* 2013;99:230–7.
231. Steel J, Staeheli P, Mubareka S, García-Sastre A, Palese P, Lowen AC. Transmission of pandemic H1N1 influenza virus and impact of prior exposure to seasonal strains or interferon treatment. *J Virol* 2010;84:21–6.
232. Kugel D, Kochs G, Obojes K, Roth J, Kobinger GP, Kobasa D, Haller O, Staeheli P, von Messling V. Intranasal administration of alpha interferon reduces seasonal influenza A virus morbidity in ferrets. *J Virol* 2009;83:3843–51.
233. Chan M, Cheung C, Chui W, Tsao S, Nicholls J, Chan Y, CHan R, Long H, Poon L, Guan Y, Peiris JSM. Proinflammatory cytokine responses induced by influenza A (H5N1) viruses in primary human alveolar and bronchial epithelial cells. *Respir Res* 2005;6:1–13.
234. Kim HM, Lee Y-W, Lee K-J, Kim HS, Cho SW, van Rooijen N, Guan Y, Seo SH. Alveolar macrophages are indispensable for controlling influenza viruses in lungs of pigs. *J Virol* 2008;82:4265–74.
235. Walsh KB, Teijaro JR, Wilker PR, Jatzek A, Fremgen DM, Das SC, Watanabe T, Hatta M, Shinya K, Suresh M, Kawaoka Y, Rosen H, Oldstone MBA. Suppression of cytokine storm with a sphingosine analog provides protection against pathogenic influenza virus. *Proc Natl Acad Sci U S A* 2011;108:12018–23.
236. To KK, Hung IFN, Li IWS, Lee K-L, Koo C-K, Yan W-W, Liu R, Ho K-Y, Chu K-H, Watt C-L, Luk W-K, Lai K-Y, Chow F-L, Mok T, Buckley T, Chan JFW, Wong SSY, Zheng B, Chen H, Lau CCY, Tse H, Cheng VCC, Chan K-H, Yuen K-Y. Delayed clearance of viral load and marked cytokine activation in severe cases of pandemic H1N1 2009 influenza virus infection. *Clin Infect Dis* 2010;50:850–9.

237. Baritaki S, Katsman A, Chatterjee D, Yeung KC, Spandidos DA, Bonavida B. Regulation of tumor cell sensitivity to TRAIL-induced apoptosis by the metastatic suppressor Raf kinase inhibitor protein via Yin Yang 1 inhibition and death receptor 5 up-regulation. *J Immunol* 2007;179:5441–53.
238. Song K, Benhaga N, Anderson RL, Khosravi-Far R. Transduction of tumor necrosis factor-related apoptosis-inducing ligand into hematopoietic cells leads to inhibition of syngeneic tumor growth in vivo. *Cancer Res* 2006;66:6304–11.
239. Liu C, Liang B, Wang Q, Wu J, Zou M-H. Activation of AMP-activated protein kinase alpha1 alleviates endothelial cell apoptosis by increasing the expression of anti-apoptotic proteins Bcl-2 and survivin. *J Biol Chem* 2010;285:15346–55.
240. Hardie DG, Scott JW, Pan DA, Hudson ER. Management of cellular energy by the AMP-activated protein kinase system. *FEBS Lett* 2003;546:113–20.
241. Herrero-Martín G, Høyer-Hansen M, García-García C, Fumarola C, Farkas T, López-Rivas A, Jäättelä M. TAK1 activates AMPK-dependent cytoprotective autophagy in TRAIL-treated epithelial cells. *EMBO J* 2009;28:677–85.
242. Moseley CE, Webster RG, Aldridge JR. Peroxisome proliferator-activated receptor and AMP-activated protein kinase agonists protect against lethal influenza virus challenge in mice. *Influenza Other Respi Viruses* 2010;4:307–11.
243. Dawson TC, Beck MA, Kuziel WA, Henderson F, Maeda N. Contrasting effects of CCR5 and CCR2 deficiency in the pulmonary inflammatory response to influenza A virus. *Am J Pathol* 2000;156:1951–9.
244. Winter C, Taut K, Srivastava M, Länger F, Mack M, Briles DE, Paton JC, Maus R, Welte T, Gunn MD, Maus UA. Lung-specific overexpression of CC chemokine ligand (CCL) 2 enhances the host defense to *Streptococcus pneumoniae* infection in mice: role of the CCL2-CCR2 axis. *J Immunol* 2007;178:5828–38.
245. Brincks EL, Katewa A, Kucaba TA, Griffith TS, Legge KL. CD8 T cells utilize TRAIL to control influenza virus infection. *J Immunol* 2008;181:4918–25.
246. Wang L, Tassiulas I, Park-Min K-H, Reid AC, Gil-Henn H, Schlessinger J, Baron R, Zhang JJ, Ivashkiv LB. “Tuning” of type I interferon-induced Jak-STAT1 signaling by calcium-dependent kinases in macrophages. *Nat Immunol* 2008;9:186–93.
247. Hoffmann H-H, Palese P, Shaw ML. Modulation of influenza virus replication by alteration of sodium ion transport and protein kinase C activity. *Antiviral Res* 2008;80:124–34.
248. Burkard C, Verheij MH, Haagmans BL, van Kuppeveld FJ, Rottier PJM, Bosch B-J, de Haan CAM. ATP1A1-Mediated Src Signaling Inhibits Coronavirus Entry into Host Cells. In: Perlman S, editor. *J Virol* 2015;89:4434–4448.

References

249. Wu C-Y, Yeh Y-C, Yang Y-C, Chou C, Liu M-T, Wu H-S, Chan J-T, Hsiao P-W. Mammalian expression of virus-like particles for advanced mimicry of authentic influenza virus. *PLoS One* 2010;5:e9784.

9. Supplement

9.1. List of Figures

Figure 1-1 Schematic overview of pathological changes to alveolar compartment during the acute phase of ARDS, adapted from Matthay and Zeman, 2011 (2).	7
Figure 1-2 Origin and dynamics of murine macrophages, adapted from Hussel and Bell, 2014 (19).	8
Figure 1-3 Schematic presentation of the alveolar barrier, adapted from (64).	11
Figure 1-4 Schematic presentation of Na,K-ATPase protein, adapted from Geering, 2008 (78).	12
Figure 1-5 PURED pathway mediated degradation of plasma membrane Na,K-ATPase, adapted from Lecuona, Trejo and Sznajder, 2007 (101).	15
Figure 1-6 Schematic depiction of an influenza A virus particle, taken from Subbarao and Joseph, 2007 (141).	17
Figure 1-7 Influenza A virus replication cycle (153).	18
Figure 1-8 Host immune responses to IAV infection, adapted from (197).	21
Figure 1-9 IFN- β dependent TRAIL-mediated pro-apoptotic AM-AEC cross-talk in IAV-induced lung injury (204).	23
Figure 4-1 Murine PR8 infection promotes formation of alveolar edema.	40
Figure 4-2 Na,K-ATPase subunit mRNA expression in murine (m-) AEC 6 hours and 24 hours post infection (hpi).	41
Figure 4-3 Total abundance of NKA α 1 protein is decreased in AEC after PR8 infection.	42
Figure 4-4 Plasma membrane expressed NKA α 1 is decreased upon IAV infection <i>ex vivo</i> and <i>in vivo</i> .	43
Figure 4-5 Plasma membrane expressed NKA α 1 is decreased by paracrine cross-talk elicited by infected epithelial cells.	44
Figure 4-6 Na,K-ATPase subunit mRNA expression in murine (m-) AEC co-cultured with AM 6 hours and 24 hours post infection (hpi).	45
Figure 4-7 Total and plasma membrane expressed NKA α 1 is decreased in presence of infected macrophages.	46
Figure 4-8 Cytokine expression in cell culture supernatants 24h after IAV infection.	47

Figure 4-9 PR8-induced loss of Na,K-ATPase surface expression is dependent on an IFN-TRAIL signaling loop involving epithelial IFN α and type I IFN-induced macrophage TRAIL.	48
Figure 4-10 IAV-induced loss of Na,K-ATPase a1 subunit surface expression is mediated by activation of AMPK.	50
Figure 4-11 Calcium-dependent activation of CaMKK β is upstream of IAV-induced AMPK activation and subsequent loss of Na,K-ATPase a1 subunit surface expression.	51
Figure 4-12 IAV-induced reduction of epithelial NKA α 1 surface expression and AFC capacity require the presence of IFNAR and TRAIL as well as macrophage recruitment and are mediated by AMPK <i>in vivo</i> .	53
4-13 IAV replication is impaired in presence of ouabain.	54
Figure 4-14 NKA α 1 is relocalized to the apical cell membrane after IAV infection.	55
Figure 4-15 Localization of the junctional proteins occluding and ZO-1 is not altered after IAV infection.	56
Figure 4-16 NKA α 1 is relocalized to the apical cell membrane after IAV infection <i>in vivo</i> .	56
Figure 4-17 Heat-inactivated IAV does not induce relocalization of NKA α 1.	57
Figure 4-18 Expression of the viral M segment is sufficient to induce relocalization of NKA α 1.	58
Figure 4-19 NKA α 1 and M2 do co-immunoprecipitate.	59
Figure 4-20 NKA α 1 and M2 colocalize upon coexpression in A549 cells.	59
Figure 6-1 Model of type I IFN-mediated loss of Na,K-ATPase-mediated edema clearance in IAV infection.	74

9.2. Materials

9.2.1. Chemicals And Consumables

2-Propanol	Sigma-Aldrich, Taufkirchen (GER)
Ampicillin	Sigma-Aldrich, Taufkirchen (GER)
Amphotericin	Sigma-Aldrich, Taufkirchen (GER)
Atropin	B.Braun, Melsungen (GER)
Avicel	AMC Biopolymers, Brüssel (BEL)
BSA (bovine serum albumin)	Sigma-Aldrich, Taufkirchen (GER)
Calciumchloride	Sigma-Aldrich, Taufkirchen (GER)
dNTP's (desoxynucleoside triphosphate)	Thermo Scientific, Waltham (USA)

DMSO (Dimethyl sulfoxide)	Sigma-Aldrich, Taufkirchen (GER)
EDTA (Ethylenediaminetetraacetic acid)	Roth, Karlsruhe (GER)
EGTA (ethylene glycol tetraacetic acid)	Sigma-Aldrich, Taufkirchen (GER)
Ethanol	Sigma-Aldrich, Taufkirchen (GER)
Evans Blue	Sigma-Aldrich, Taufkirchen (GER)
EZ-link Sulfo-NHS-SS-Biotin	Thermo Scientific, Waltham (USA)
FCS (fetal calf serum)	Life Technologies, Carlsbad (USA)
Ficoll	GE Healthcare, Chalfont St Giles (UK)
FITC-Dextran (70kDa)	Sigma-Aldrich, Taufkirchen (GER)
Glycin	Roth, Karlsruhe (GER)
HEPES	Merck Millipore, Darmstadt (GER)
ITS (Insulin-Transferrin-Selenium)	Biozym Scientific, Hessisch Oldendorf (GER)
Ketaminhydrochloride (Ketavet)	Pharmaci & Upjohn, Peapack (USA)
L-Glutamin [200mM]	Gibco BRL, Karlsruhe (GER)
Lipofectamine 2000	Life Technologies, Carlsbad (USA)
Low melting Agarose	Sigma-Aldrich, Taufkirchen (GER)
Magnesium sulfate	Sigma-Aldrich, Taufkirchen (GER)
β-Mercaptoethanol	Sigma-Aldrich, Taufkirchen (GER)
Methanol	Roth, Karlsruhe (GER)
Milk powder	BD Biosciences, San Jose (USA)
NHS (Normal Horse Serum)	Sigma-Aldrich, Taufkirchen (GER)
NP40	Thermo Scientific, Waltham (USA)
Peqlgold protein marker V	Peqlab, Erlangern (GER)
PBS	Life Technologies, Carlsbad (USA)
PBS ⁺⁺ (containing MgCl ₂)	PAN-Biotech, Aidenbach (GER)
Parafilm	American National, Greenwich (USA)
Paraformaldehyde (PFA)	Merck, Darmstadt (GER)
Penicillin/Streptomycin [5000 U/ml]	Gibco BRL, Karlsruhe (GER)
Phosphatase inhibitor (100x)	Cell Signaling, Cambridge (UK)
Potassium chloride	Sigma-Aldrich, Taufkirchen (GER)
Protease inhibitor cocktail	Roche, Basel (CH)
Protein A/G Plus-agarose beads	Santa Cruz Biotechnology, Dallas (USA)
PVDF-Membran (Hybond™)	Amersham Biosciences, (UK)
Sandoglobulin	Novartis, Basel (CH)
Saponine	Merck Millipore, Darmstadt (GER)
SDS (Sodiumdodecylsulfate)	Roth, Karlsruhe (GER)

Sodiumchloride	Roth, Karlsruhe (GER)
Sodiumhydrogencarbonate	Sigma-Aldrich, Taufkirchen (GER)
Sodiumdihydrogencarbonate	Sigma-Aldrich, Taufkirchen (GER)
Sodium orthovanadate	Sigma-Aldrich, Taufkirchen (GER)
Streptavidin Agarose Resin	Thermo Scientific, Waltham (USA)
SYBR Green I	Life Technologies, Carlsbad (USA)
TissueTek	Sakura, Alphen aan den Rijn (NL)
Tris (Trishydroxymethylaminomethane)	Acros Organics, New Jersey (USA)
Triton-X-100	Roth, Karlsruhe (GER)
True Blue™ Peroxidase Substrate	PKL, Gaithersburg (USA)
Tween 80	Sigma-Aldrich, Taufkirchen (GER)
Vectashield Mounting Medium (DAPI)	Vector Laboratories, Burlingame (USA)
Xylazine hydrochloride, Rompun	Bayer AG, Leverkusen (GER)
Biotin-binder magnetic beads	Life Technologies, Carlsbad (USA)
Cell culture flasks 75cm ²	Greiner, Nürtingen (GER)
Cell culture plates, single- and multi-well	Greiner, Nürtingen (GER)
Cell scaper, 28cm and 40cm handle	Greiner, Nürtingen (GER)
Cell strainer filters 40, 70 and 100µm	BD Biosciences, San Jose (USA)
Cell nylon filters 20µM	Merck Millipore, Darmstadt (GER)
GentleMACS C tubes	Miltenyi Biotec, Bergisch Gladbach (GER)
Minigel protean TGX	Bio-Rad, Hercules (USA)
Polystyrene tubes, 15ml and 50ml	Greiner, Nürtingen (GER)
Polystyrene round-bottom tubes 5ml	BD Biosciences, San Jose (USA)
Reaction tubes 0.5ml and 1.5ml	Eppendorf, Hamburg (GER)
Syringe 1ml, 10ml and 20ml	B.Braun, Melsungen (GER)
Transwell permeable supports	Corning Life Sciences, Tewksbury (USA)

9.2.2. Enzymes, Recombinant Proteins And Inhibitors

Dispase	Corning Life Sciences, Tewksbury (USA)
Dispase II	Böhringer, Ingelheim am Rhein (GER)
DNase	Serva, Heidelberg (GER)
MLV-RT	Life Technologies, Carlsbad (USA)
Trypsin-EDTA	Merck Millipore, Darmstadt (GER)
Trypsin-TPCK	Worthington Biochemical, Lakewood (USA)
mouse recombinant GM-CSF	R&D Systems, Minneapolis (USA)
mouse recombinant interferon-α	pbl interferon source, Logan (USA)

mouse recombinant interferon-β	pbl interferon source, Logan (USA)
mouse recombinant TRAIL	R&D Systems, Minneapolis (USA)
(5Z)-7-Oxozeanol (Curvularia sp.)	Merck Millipore, Darmstadt (GER)
AICA-Riboside	Merck Millipore, Darmstadt (GER)
BAPTA-AM	Life Technologies, Carlsbad (USA)
Compound C (Dorsomorphin)	Merck Millipore, Darmstadt (GER)
STO-609	Merck Millipore, Darmstadt (GER)

9.2.3. Antibodies

β-Actin Ply6221	Biolegend, San Diego (USA)
AMPK α 40H9	Cell Signaling, Cambridge (UK)
CaMKIIβ C-20	Cell Signaling, Cambridge (UK)
CD74 ln-1	BD Biosciences, San Jose (USA)
CD326 (Ep-CAM) G8.8 APC/Cy7	Biolegend, San Diego (USA)
Glucose transporter 1 (Glut1), polyclonal	Merck Millipore, Darmstadt (GER)
Influenza A Virus Nucleoprotein	Abcam, Cambridge (UK)
Influenza A Matrix Protein 1, polyclonal	Bio-Rad, Hercules (USA)
Influenza A Matrix Protein 2, MA1-082	Thermo Scientific, Waltham (USA)
Influenza A Virus, polyclonal	Abcam, Cambridge (UK)
IgG Alexa Fluor 488, mouse	Merck Millipore, Darmstadt (GER)
Na,K-ATPase α1 Alexa Fluor 488 C464.6	Merck Millipore, Darmstadt (GER)
Occludin, polyclonal	Abcam, Cambridge (UK)
phospho-ACC S79	Cell Signaling, Cambridge (UK)
Podoplanin 8.1.1 PE/Cy7	Biolegend, San Diego (USA)
Rb-X Hu pro-SP-C	Merck Millipore, Darmstadt (GER)
ZO-1, polyclonal	Abcam, Cambridge (UK)
secondary goat APC	Life Technologies, Carlsbad (USA)
secondary goat Alexa Fluor 488	Life Technologies, Carlsbad (USA)
secondary rabbit APC	Life Technologies, Carlsbad (USA)
secondary rat PE	Life Technologies, Carlsbad (USA)
secondary mouse HRP	Cell Signaling, Cambridge (UK)
secondary rabbit HRP	Cell Signaling, Cambridge (UK)
biotinylated rat anti-mouse CD16/32	BD Biosciences, San Jose (USA)
biotinylated rat anti-mouse CD31	BD Biosciences, San Jose (USA)
biotinylated rat anti-mouse CD45	BD Biosciences, San Jose (USA)
mouse anti-human CD45 magentic beads	Miltenyi Biotec, Bergisch Gladbach (GER)

9.2.4. ELISA and CBA Kits

ELISA

mouse TRAIL, detection limit 1.8 pg/ml	R&D Systems, Minneapolis (USA)
mouse TNF- α , detection limit 2 pg/ml	R&D Systems, Minneapolis (USA)
mouse TGF- β , detection limit 4.6 pg/ml	R&D Systems, Minneapolis (USA)
mouse interferon α , detection limit 12.5pg/ml	pbl interferon source, Logan (USA)

Cytometric Bead Array (CBA)

mouse MCP-1, detection limit 2.7 pg/ml	BD Biosciences, San Jose (USA)
mouse KC, detection limit 0.1 pg/ml	BD Biosciences, San Jose (USA)
mouse IL-1 α , detection limit 0.8 pg/ml	BD Biosciences, San Jose (USA)
mouse RANTES, detection limit 3.3 pg/ml	BD Biosciences, San Jose (USA)

9.2. List of Abbreviations

A	Ampere
ACC	Acetyl-CoA carboxylase
Ad-Null	Adenovirus, expressing no contract
Ad-DN-AMPK	Adenovirus, expressing dominant negative AMPK
AEC	Alveolar epithelial cells
AFC	Alveolar fluid clearance
AICAR	AICA-Riboside
Al	altera
AM	Alveolar macrophage
AMP	Adenosine monophosphate
AMPK	AMP-dependent kinase
APC	allophycocyanin
BMM	Bone marrow-derived macrophage
BALF	Bronchoalveolar lavage fluid
BSA	bovine serum albumin
°C	Celsius
CaMKK β	Calcium/Calmodulin kinase kinase beta
CBA	Cytometric bead array
CCR2	C-C chemokine receptor type 2
CD	Cluster of differentiation
cDNA	Complementary DNA
Cl	Chloride
CO ₂	Carbon dioxide
C-Terminus	Carboxyterminus
dH ₂ O	Deionized water
DMEM	Dulbecco's modified Eagle's medium
DMSO	Dimethylsulfoxide
DNA	Desoxyribonucleic Acid
dNTP	Desoxynucleosidtriphosphate

DR5	Death receptor 5
DTT	Dithiotreitol
EDTA	Ethylenedinitrilotetraacetic acid
EGTA	Ethylene glycol tetraacetic acid
ELISA	Enzyme Linked Immunosorbent Assay
EpCAM	Epithelial cell adhesion molecule
FACS	Fluorescence activated cell sorting, flow cytometry
FCS	Fetal calf serum
FP	Forward primer
g	Gramms
GFP	Green fluorescent protein
Glut1	Glucose transporter 1
GM-CSF	Granulocyte macrophage colony-stimulating factor
h	Hours
HA	Hemagglutinin
HA	Hemagglutinin
HCl	Hydrochloric acid
HRP	Horseradish peroxidase
IFN	Type I interferon
IFN α	Interferon alpha
IFN β	Interferon beta
IFNAR	Interferon-alpha/beta receptor
IL-1 α	Interleukin 1 alpha
Ig	Immunglobuline
ITS	Insulin-Transferrin-Selenium
IAV	Influenza A virus
IVC	Individually ventilated cages, conventional
k	Kilo
K	Potassium
KC	Mouse keratinocyte-derived cytokine
kDa	Kilodalton
l	Liter
K	Potassium
m	Milli
M	Molar
mAEC	Murine alveolar epithelial cells
M1	Matrixprotein 1
M2	Matrixprotein 2
MCP-1	Monocyte chemotactic protein 1
MCDK	Madin Darbey Canine Kidney
MEM	Minimal Essential Medium
min	Minute
MLE-12	Mouse lung epithelium clone 12
mol	Mol

MOI	Multiplicity of infection
mRNA	Messenger RNA
μ	Micro
n	Nano
NA	Neuraminidase
Na	Sodium
NHS	Normal horse serum
NKA α 1	Sodium, Potassium ATPase alpha 1 subunit
NP	Nukleoprotein
nt	Nucleotide
N-Terminus	Amino-terminus
Osm	Osmolar
PA	Polymeraseprotein, acidic
PAGE	Polyacrylamideelectrophoresis
PB1	Polymeraseprotein basic 1
PB2	Polymeraseprotein basic 2
PBS	Phosphate buffered saline
pACC	Phospho-Acetyl-CoA carboxylase
pCO ₂	Partial pressure carbon dioxide
PCR	Polymerase chain reaction
PE	Phycoerythrin
PFA	Paraformaldehyde
pfu	Plaque forming units
pH	Potentia hydrogenii
Pol	Polymerase
pO ₂	Partial pressure oxygen
proSP-C	Pro-surfactant protein C
PR8	Influenza virus A/Puerto Rico/8/34 (H1N1)
qRT-PCR	Quantitative real time polymerase chain reaction
RANTES	Regulated on activation, normal T cell expressed and secreted
RP	Reverse primer
RNA	Ribonucleic acid
RNP	Ribonucleoprotein
rpm	Rounds per minute
RT	Room temperatue
s	Seconds
SA	Sialic acid
SDS	Natriumdodecylsulfate
siRNA	Small interfering ribonucleic acid
SPF	Specific pathogen-free
TGF- β	Transforming growth factor beta
TNF- α	Tumor necrosis factor alpha
TRAIL	TNF-related apoptosis-inducing ligand

Supplement

Tris	Trishydroxymethylaminomethane
U	Unit
Udorn	Influenza virus A/Udorn/1972 (H3N2)
V	Volt
wt	Wildtype

9.3. Affirmation - Eidesstattliche Erklärung

Ich erkläre:

Ich habe die vorgelegte Thesis selbständig, ohne unerlaubte fremde Hilfe und nur mit den Hilfen angefertigt, die ich in der Thesis angegeben habe. Alle Textstellen, die wörtlich oder sinngemäß aus veröffentlichten oder nicht veröffentlichten Schriften entnommen sind, und alle Angaben, die auf mündlichen Auskünften beruhen, sind als solche kenntlich gemacht. Bei den von mir durchgeführten und in der Thesis erwähnten Untersuchungen habe ich die Grundsätze guter wissenschaftlicher Praxis, wie sie in der Satzung der Justus-Liebig-Universität Gießen zur Sicherung guter wissenschaftlicher Praxis' niedergelegt sind, eingehalten.

Christin Becker